

Scenario set-up and forcing data for impact model evaluation and impact attribution within the third round of the Inter-Sectoral Model Intercomparison Project (ISIMIP3a)

Katja Frieler¹, Jan Volkholz¹, Stefan Lange¹, Jacob Schewe¹, Matthias Mengel¹, María del Rocío Rivas López¹, Christian Otto¹, Christopher P.O. Reyer¹, Dirk Nikolaus Karger², Johanna T. Malle², Simon Treu¹, Christoph Menz¹, Julia L. Blanchard³, Cheryl S. Harrison⁴, Colleen M. Petrik⁵, Tyler D. Eddy⁶, Kelly Ortega-Cisneros⁷, Camilla Novaglio³, Yannick Rousseau³, Reg A. Watson³, Charles Stock⁸, Xiao Liu⁹, Ryan Heneghan¹⁰, Derek Tittensor¹¹, Olivier Maury¹², Matthias Büchner¹, Thomas Vogt¹, Tingting Wang¹³, Fubao Sun¹³, Inga J. Sauer^{1,14}, Johannes Koch¹, Inne Vanderkelen^{15,16,17}, Jonas Jägermeyr^{1,18,19}, Christoph Müller¹, [Sam Rabin](#)²⁰, Jochen Klar¹, Iliusi D. Vega del Valle¹, Gitta Lasslop²¹, Sarah Chadburn²², Eleanor Burke²³, Angela Gallego-Sala²⁴, Noah Smith²², Jinfeng Chang²⁵, Stijn Hantson²⁶, Chantelle Burton²³, Anne Gädeke¹, Fang Li²⁷, Simon N. Gosling²⁸, Hannes Müller Schmied^{21,29}, Fred Hattermann¹, Jida Wang³⁰, Fangfang Yao³¹, Thomas Hickler²¹, Rafael Marcé^{32,33}, Don Pierson³⁴, Wim Thiery¹⁵, Daniel Mercado-Bettín³², [Robert Ladwig](#)³⁵, [Ana I. Ayala](#)³⁴, Matthew Forrest²¹, Michel Bechtold³⁶

Affiliations:

¹Potsdam Institute for Climate Impact Research, 14473 Potsdam, Germany

²Swiss Federal Research Institute WSL, Zürcherstrasse 111, 8903 Birmensdorf, Switzerland

³Institute for Marine and Antarctic Studies, University of Tasmania, Hobart, Tasmania, Australia

⁴Department of Ocean and Coastal Science and Center for Computation and Technology, Louisiana State University, Baton Rouge, Louisiana, USA

⁵Scripps Institution of Oceanography, University of California San Diego, CA, USA

⁶Centre for Fisheries Ecosystems Research, Fisheries & Marine Institute, Memorial University, St. John's, NL, Canada

⁷Department of Biological Sciences, University of Cape Town, Rondebosch, Cape Town, 7701, South Africa

⁸NOAA/OAR/Geophysical Fluid Dynamics Laboratory, Princeton, NJ, United States

⁹SAIC@NOAA/NWS/NCEP Environmental Modeling Center, 5830 University Research Court, College Park, MD 20740

¹⁰School of Mathematical Sciences, Queensland University of Technology, Brisbane, QLD, Australia

¹¹Department of Biology, Dalhousie University, Halifax, Nova Scotia, Canada, B3H 4R2

¹²Institute for Research for Development, UMR 248 MARBEC, France.

¹³Key Laboratory of Water Cycle and Related Land Surface Processes, Institute of Geographic Sciences and Natural Resources Research, Chinese Academy of Sciences, Beijing 100101, China

¹⁴Institute for Environmental Decisions, ETH Zurich, Zurich, Switzerland

¹⁵Vrije Universiteit Brussel, Department of Hydrology and Hydraulic Engineering, Brussels, Belgium

¹⁶Wyss Academy for Nature, University of Bern, Bern, Switzerland

¹⁷Climate and Environmental Physics and Oeschger Center for Climate Change Research, University of Bern, Bern, Switzerland

¹⁸NASA Goddard Institute for Space Studies, New York, NY 10025, USA

¹⁹Columbia University, Climate School, New York, NY 10025, USA

47 [20Climate and Global Dynamics Laboratory National Center for Atmospheric Research Boulder, CO](#)
48 [80302, USA](#)

49 ²¹Senckenberg Leibniz Biodiversity and Climate Research Centre (SBIK-F), Frankfurt am Main,
50 Germany.

51 ²²Department of Mathematics, University of Exeter, Exeter UK

52 ²³Met Office Hadley Centre, Fitzroy Road, Exeter, UK

53 ²⁴Geography Department, University of Exeter, Exeter, UK

54 ²⁵College of Environmental and Resource Sciences, Zhejiang University, Hangzhou, China

55 ²⁶Faculty of Natural Sciences, Universidad del Rosario, Bogotá, Colombia

56 ²⁷International Center for Climate and Environment Sciences, Institute of Atmospheric Physics, Chinese
57 Academy of Sciences, Beijing, China

58 ²⁸School of Geography, University of Nottingham, Nottingham, UK

59 ²⁹Institute of Physical Geography, Goethe University Frankfurt, Frankfurt am Main, Germany

60 ³⁰Department of Geography and Geospatial Sciences, Kansas State University, Manhattan, Kansas,
61 USA

62 ³¹Environmental Resilience Institute, University of Virginia, Charlottesville, Virginia 22903, USA

63 ³²Catalan Institute for Water Research (ICRA), 17003 Girona, Spain

64 ³³Universitat de Girona, Girona, Spain ¶

65 ³⁴Uppsala University, Norbyvägen 18 D, 752 36 Uppsala, Sweden ¶

66 ³⁵[Center for Limnology, University of Wisconsin-Madison, Madison, Wisconsin 53706, USA](#)

67 ³⁶KU Leuven, Department of Earth and Environmental Sciences, Leuven, Belgium ¶

68 [36Center for Limnology, University of Wisconsin-Madison, Madison, Wisconsin 53706, USA](#) ¶

69 ¶

70 *Correspondence to:* Katja Frieler (katja.frieler@pik-potsdam.de)

71

72 **Abstract.** This paper describes the rationale and the protocol of the first component of the third
73 simulation round of the Inter-Sectoral Impact Model Intercomparison Project (ISIMIP3a,
74 www.isimip.org) and the associated set of climate-related and direct human forcing data (CRF and
75 DHF, respectively). The observation-based climate-related forcings for the first time include high-
76 resolution observational climate forcings derived by orographic downscaling, monthly to hourly coastal
77 water levels, and wind fields associated with historical tropical cyclones. The DHFs include land use
78 patterns, population densities, information about water and agricultural management, and fishing
79 intensities. The ISIMIP3a impact model simulations driven by these observation-based climate-related
80 and direct human forcings are designed to test to what degree the impact models can explain observed
81 changes in natural and human systems. In a second set of ISIMIP3a experiments the participating
82 impact models are forced by the same DHFs but a counterfactual set of atmospheric forcings and
83 coastal water levels where observed trends have been removed. These experiments are designed to
84 allow for the attribution of observed changes in natural, human and managed systems to climate
85 change, rising CH₄ and CO₂ concentrations, and sea level rise according to the definition of the Working
86 Group II contribution to the IPCC AR6.

87

88 **1 Introduction**

89 The Inter-Sectoral Impact Model Intercomparison Project ISIMIP (www.isimip.org) provides a common
90 scenario framework for cross-sectorally consistent climate impact simulations currently covering the
91 following sectors: agriculture (global; in cooperation with AgMIP's Global Gridded Crop Model
92 Intercomparison Project (GGCMI)), water (global and regional), lakes (global and regional), biomes

93 (global), forest (regional), fisheries and marine ecosystems (global and regional), terrestrial biodiversity
94 (global), fire (global), permafrost (global), peat (global), coastal systems (global), energy (global), health
95 (temperature-related mortality; water-borne diseases; vector-borne diseases; and food security and
96 nutrition) (global and local), and labour productivity (global and local). The impact model simulations
97 are made freely available, allowing for all types of follow-up analysis. The consistent design of the
98 simulations does allow for the comparison of climate impact simulations within each sector. However,
99 it also enables the bottom-up integration of impacts across sectors. Thus, it provides a unique basis for
100 the estimation of the effects of climate change on, e.g., the economy, displacement and migration,
101 health, or water quality resolving the mechanisms along different impact channels and fully exploiting
102 the process-understanding represented in the biophysical impact models.

103

104 Initialised in 2012, [ISIMIP is organised in individual modelling rounds. The decision about their design](#)
105 [and the development of the associated simulation protocols has been developed into an iterative](#)
106 [process between stakeholders and users of ISIMIP data, the sectoral coordinators representing](#)
107 [participating modelling teams, the Scientific Advisory Board, and the Cross-Sectoral and Coordination](#)
108 [Team at PIK \(ISIMIP Coordination Team, Sectoral Coordinators, Scientific Advisory Board, 2018\).](#)
109 [Since its second round the ISIMIP protocols comprise an ‘a’ part describing impact model simulations](#)
110 [that cover the historical period forced by observational climate-related and direct human forcings](#)
111 [\(evaluation set-up\), and a ‘b’ part dedicated to impact simulations based on simulated climate-related](#)
112 [forcings including future projections. This paper describes the ISIMIP3a simulation framework only](#)
113 [where the DHF described here are also used for the historical simulations within ISIMIP3b. Compared](#)
114 [to ISIMIP2a the evaluation set-up based on observational forcing data has been extended to now](#)
115 [include additional years up to 2021 and sensitivity experiments using high resolution historical climate](#)
116 [forcing data to quantify associated improvements of impact simulations \(see section 3.1\). Besides, the](#)
117 [set of historical observation-based direct human forcings has been updated compared to previous](#)
118 [ISIMIP simulation rounds \(see Table 1\).](#) For the first time, and closely connected to the evaluation set-
119 up, ISIMIP3a now also includes an ‘impact attribution’ scenario set-up designed to address the question
120 “To what degree have observed changes in the climate-related systems contributed to observed
121 changes in natural, human or managed systems compared to direct human influences?” Here, changes
122 in climate-related systems mean climate change itself, changes in atmospheric CO₂ and CH₄
123 concentration, and sea level changes. The attribution question can both refer to [the impacts of individual](#)
124 [events \(e.g. to what extent has long-term climate change contributed to the observed extent of a specific](#)
125 [river flood?\) and to long-term changes \(e.g. to what extent have long-term climate change and](#)
126 [increasing CO₂ fertilisation contributed to an observed change in crop yields?\). The IPCC AR5 \(Cramer](#)
127 [et al., 2014\) and AR6 \(\(O’Neill et al., 2022; Hope et al., 2022\) have established a framework for impact](#)
128 [attribution according to which an ‘observed impact of climate change or change in any other climate-](#)
129 [related system’ is defined as the difference between the observed state of the human, natural or](#)
130 [managed system and a counterfactual baseline that characterises the system’s behaviour in the](#)
131 [absence of changes in the climate-related systems. This counterfactual baseline may be stationary or](#)
132 [vary in response to direct human influences such as changes in land use patterns, agricultural or water](#)

133 [management or population distribution and economic development affecting exposure and vulnerability](#)
134 [to weather-related hazards. While the definition is established for about a decade at least, the number](#)
135 [of studies addressing impact attribution based on this basic definition is still relatively small compared](#)
136 [to the number of studies addressing climate attribution, i.e. the question to what degree anthropogenic](#)
137 [emissions of climate forcers, in particular greenhouse gases, have induced changes in the climate-](#)
138 [related systems. While climate attribution is mainly confronted by the challenge of separating the](#)
139 [anthropogenically forced changes from the internal variability of the climate-related systems, the focus](#)
140 [of climate impact attribution is on separating the impacts of observed changes in these climate-related](#)
141 [systems from the effects of other direct \(human\) drivers of changes in the considered natural, human](#)
142 [or managed systems. 'Observed changes in the climate-related systems' does not necessarily imply](#)
143 ['changes induced by anthropogenic climate forcing', but only means 'any long-term trend' in line with](#)
144 [the IPCC definition of climate change \(see Glossary of the AR5 \(IPCC, 2014\) and AR6 \(Matthews et](#)
145 [al., 2021\)\).¶](#)

146 [Impact attribution studies usually face the problem that the counterfactual baseline assuming no long-](#)
147 [term changes in the climate-related systems cannot be observed \(see \(Hansen et al., 2016\) for](#)
148 [examples\). However, impact models such as the ones participating in ISIMIP are well suited to simulate](#)
149 [this baseline. As the impact models usually account not only for the changes in climate or the climate-](#)
150 [related systems but also for direct human forcings such as land use and irrigation changes, changes in](#)
151 [water and agricultural management, population distributions etc. \(see **Table 1** for a comprehensive list](#)
152 [of direct human forcings provided within ISIMIP3a\) they are ideal tools to address the attribution](#)
153 [question: In line with the IPCC definition it requires the comparison of a factual simulation based on the](#)
154 [observed variations in the climate-related and direct human drivers to a counterfactual simulations](#)
155 [where only the climate-related forcings are replaced by counterfactual versions where long-term trends](#)
156 [have been removed. While the factual simulations correspond to the evaluation runs within ISIMIP3a](#)
157 [\(see section 2.1\), the protocol now also includes the counterfactual simulations based on the newly](#)
158 [generated counterfactual data sets derived from observational data of climate and coastal water levels](#)
159 [\(see sections 2.2 for the associated concept and scenario design and **Table 3** for a comprehensive list](#)
160 [of the counterfactual climate and sea level forcing data that are described in more detail in section 3.1](#)
161 [and 3.3, respectively\). To allow for an attribution of 'observed changes in natural, human, and managed](#)
162 [systems' in contrast to an attribution of simulated changes it has to be demonstrated that the processes](#)
163 [represented in the impact model can explain the observed changes in the affected system, i.e. it has to](#)
164 [be shown that the model forced by observed changes in the climate-related systems and accounting](#)
165 [for the historical development of direct \(human\) forcings is able to reproduce the observed changes in](#)
166 [the affected system. In this way the attribution exercise is closely linked to the ISIMIP3a evaluation](#)
167 [exercise. Thereby, models can either explicitly represent known changes in non-climate drivers such](#)
168 [as known adjustments of fertiliser input or growing seasons \(explicit accounting for non-climate drivers\)](#)
169 [or implicitly account for their potential contributions by e.g., allowing for non-climate related temporal](#)
170 [trends in empirical models as often done in empirical approaches \(implicit accounting for non-climate](#)
171 [drivers\).¶](#)

172 [While the default attribution experiment in ISIMIP3a is designed for the attribution of observed changes](#)
173 [in human, natural, and managed systems to observed change in the climate-related systems in](#)
174 [combination \(in the current ISIMIP3a setting this is changes in atmospheric climate forcing in](#)
175 [combination with changes in atmospheric CO2 and CH4 concentrations, see Table 3\), the protocol also](#)
176 [includes a sensitivity experiments that allow for the quantification of the influence of increasing CO2](#)
177 [concentrations separately and for an attribution of observed changes in natural, human and managed](#)
178 [systems to historical changes in atmospheric CO2 concentrations only \(see section 2.1\). Here, we](#)
179 [consistently define ‘an observed impact of a change in any component of the historical forcing as the](#)
180 [difference between the observed state of the system to a counterfactual world where only this specific](#)
181 [component of the forcing has not changed. So the ‘observed impact of increasing CO2 concentrations’](#)
182 [is approximated by the difference between a full forcing run and a run where CO2 concentrations are](#)
183 [held constant. This is different from the ‘CO2 only’ experiment considered within TRENDY \(Trends in](#)
184 [the land carbon cycle, \(Sitch et al., 2015, Protocol - TRENDY, 2023\)\) where the pure effect of increasing](#)
185 [CO2 concentrations on the terrestrial carbon cycle \(e.g. net biome production\) is estimated by](#)
186 [simulations where the Dynamic Global Vegetation Models \(as participating in the biomes sector of](#)
187 [ISIMIP\) are forced by the observed increases in CO2 concentrations but a time-invariant “pre-industrial”](#)
188 [climate and land use mask. In the above sense, other ISIMIP3a experiments can also be considered](#)
189 [counterfactual baseline experiments that allow for the attribution of observed changes in human,](#)
190 [natural, or managed systems to changes in the direct human forcings as a whole \(DHF set to zero or](#)
191 [fixed at 1901 and 2015 levels\) or to changes in individual components such as changes in water](#)
192 [management, irrigation patterns, and riverine influx of nutrients into the ocean \(see section 2.1 and](#)
193 [Table 2\). The attribution to changes in direct human forcings is e.g. similar to the comparison of the full](#)
194 [forcing run within TRENDY to the ‘CO2 and climate only’ run where climate change and atmospheric](#)
195 [CO2 concentrations are prescribed according to observations but land use changes are held constant](#)
196 [to quantify the contribution of this direct human forcing to observed changes in the carbon cycle for the](#)
197 [annual report of the Global Carbon Project \(e.g. \(Friedlingstein et al., 2022\)\). However, in this paper](#)
198 [the term ‘impact attribution’ is used as a short form of ‘attribution of observed changes in natural, human](#)
199 [and managed systems to observed changes in the climate-related systems’ which is the focus of the](#)
200 [ISIMIP3a experiments. In other cases the driver to which the changes are attributed is explicitly named.](#)
201 [In addition to ISIMIP3a, there are other model intercomparison projects that address different kinds of](#)
202 [attribution questions such as Land Use Model Intercomparison Project \(LUMIP, \(Lawrence et al., 2016\)\)](#)
203 [and Detection and Attribution Model Intercomparison Project \(DAMIP, \(Gillett et al., 2016\)\) embedded](#)
204 [into the sixth phase of the Coupled Model Intercomparison Project \(CMIP6\). While the phase 2 LUMIP](#)
205 [experiments include historical climate model simulations to quantify the contribution of historical land](#)
206 [use changes to observed climate change, the AMIP protocol include a counterfactual ‘no anthropogenic](#)
207 [climate forcing’ baseline to attribute observed changes in climate to anthropogenic climate forcings.](#)

¶

208
209 The development of the ~~ISIMIP3~~ protocol was coordinated by the ISIMIP-Cross-Sectoral Science
210 Team (CSST) at the Potsdam Institute for Climate Impact Research (PIK) and involved the sectoral
211 coordinators, participating ~~modelling~~ teams, and the Scientific Advisory Board. The process

212 was initiated by a proposal for the main research questions to be addressed and an associated scenario
213 set-up accounting for suggestions collected in a stakeholder engagement process (Lejeune et al.,
214 2018). Following ISIMIP's mission and implementation document (ISIMIP Coordination Team, Sectoral
215 Coordinators, Scientific Advisory Board, 2018), the basic proposal was approved by the ISIMIP strategy
216 group at the cross-sectoral ISIMIP workshop in Potsdam, September 2018 (Outcomes of the ISIMIP
217 Strategy Group Meeting, 2023). Thereby the CSST and the sectoral coordinators were tasked to
218 translate the decisions into a cross-sectorally consistent simulation protocol and to generate, pre-
219 process or collect the required climate-related and direct human forcing data. [The provided forcing data
220 sets \(e.g. the climate variables or components of atmospheric composition or types of land use\) is very
221 much demand driven. The data we describe here represent a core set that is sufficient for the range of
222 models participating so far \(see ISIMIP output data table \(ISIMIP Output Data Table, 2023\) that also
223 provides information about the input data used by the individual models\) but may be extended if there
224 were further demands.](#) This paper presents the results of this process and the motivation and reasoning
225 behind the individual steps for ISIMIP3a, while a ~~follow-up~~^{rather} paper ~~will~~ provides the same
226 information for ISIMIP3b dedicated to ~~future~~-impact projections based on climate model simulations
227 (Frieler, submitted 2023). It provides the point of reference for ~~modelling~~^{modelling} teams interested in
228 participating in ISIMIP3a but also for users of the impact simulation data, which become freely
229 accessible according to the ISIMIP terms of use (ISIMIP terms of use, 2023). The paper is accompanied
230 by a simulation protocol (ISIMIP3 simulation protocol, 2023) providing all technical details such as file
231 and variable naming conventions and sector-specific lists of output variables to be reported by the
232 participating modelling teams. The ISIMIP3 simulation round was officially started on 21st February
233 2020¹ with the release of the associated protocol. Since then, the protocol has already received some
234 updates through the addition of output variables, correction of errors, and inclusion of new sectors. This
235 paper refers to the protocol version of 14th January 2023. However, the protocol may still receive
236 updates similar to the ones mentioned above. Impact ~~modellers~~ interested in contributing to ISIMIP
237 should therefore refer to (ISIMIP3 simulation protocol, 2023) for the most up to date ~~version~~^{version} for planned
238 impact model simulations. [The protocol landing page \(protocol.isimip.org\)](#) includes a unique version
239 identifier ~~(the commit hash) that links to the latest protocol version on github~~ for traceability.

240
241 In the second round of ISIMIP the observation-based model evaluation part (ISIMIP2a) was temporally
242 separate from the climate model-based second part (ISIMIP2b, (Frieler et al., 2017). This has led to
243 inconsistencies in the models and model versions contributing to ISIMIP2a and ISIMIP2b. Also, not all
244 models providing future projections within ISIMIP2b also provided model evaluation runs for ISIMIP2a.
245 To avoid this problem and ensure that each model's set of future projections is accompanied by
246 associated historical simulations allowing for model evaluation, in the third simulation round (~~ISIMIP3~~),
247 the ISMIP3a and ISIMIP3b protocols were released together and participating in ISIMIP3 means
248 contributing to ISIMIP3a and ISIMIP3b using the same impact model versions.
249

¹ announced via email to the ISIMIP mailing list from 21st February 2020

250 In [the following section 2 of this paper](#), we [provide the comprehensive list of all ISIMIP3a model](#)
251 [evaluation and sensitivity experiments \(see Table 2 within section 2.1\) and the counterfactual ‘no](#)
252 [climate change’ experiments \(see Table 4 within section 2.2\)](#) describe the rationale behind the scenario
253 set-ups. Detailed description of the climate-related forcing data sets (see CRF section of **Table 1 in**
254 [section 2.1 and Table 3 in section 2.2](#)) are provided in the third section: atmospheric climate data
255 ([see section 3.1](#)); tropical cyclone data ([see section 3.2](#)); coastal water levels ([see section 3.3](#)), and the
256 ocean data ([see section 3.4](#)). Section 4 presents the ISIMIP3a direct human forcing data sets (see DHF
257 section of **Table 1**), comprising population data ([see section 4.1](#)), gross domestic product ([see section](#)
258 **4.2**), land use and irrigation patterns ([see section 4.3](#)), fertiliser inputs ([see section 4.4](#)), land
259 transformations ([see section 4.5](#)), nitrogen deposition ([see section 4.6](#)), crop calendar ([see section](#)
260 **4.7**), dams and reservoirs ([see section 4.8](#)), fishing intensities ([see section 4.9](#)), regional forest
261 management ([see section 4.10](#)), and desalination ([see section 4.11](#)).¶

262

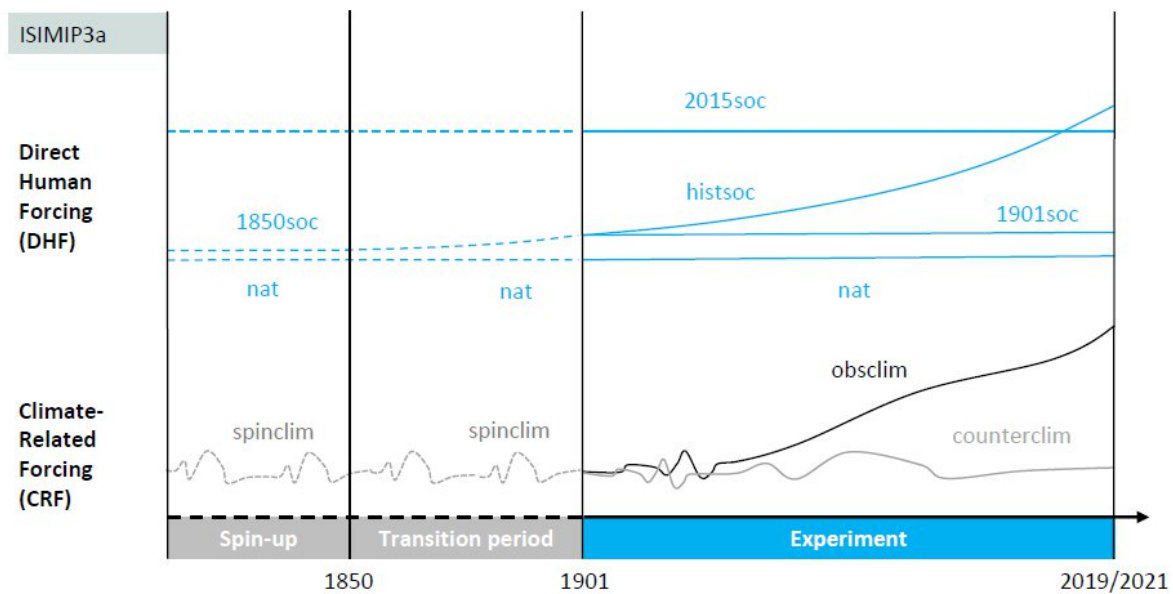
263

264 **2 Experiments and underlying rationale**

265

266 [ISIMIP3a includes a core \(‘default’\) set of experiments that are specified by a specific set of](#) underlying
267 climate-related forcings and direct human forcings [that have to be indicated in the file names when](#)
268 [submitting simulation data to the ISIMIP repository](#). In the following [we first](#) introduce [these default](#)
269 [experiments](#) by [defining](#) the combination of both types of forcing data sets. [In the subheadings naming](#)
270 [the experiments the associated CRF and DHF](#) specifiers to be used in the file names [are indicated in](#)
271 brackets [where the third sensitivity specifier is set to ‘default’](#) (CRF specifier + DHF specifier, [default](#)).
272 The different combinations of the default sets of ISIMIP3a CRFs (‘obsclim’, ‘counterclim’) and DHFs
273 (‘histsoc’, ‘2015soc’, ‘1901soc’, ‘1850soc’, ‘nat’) are sketched in **Figure 1** and [defined](#) in more detail
274 below ([see Table 1 for the default ‘obsclim’ CRF and the default DHFs and Table 3 for the ‘counterclim’](#)
275 [CRF](#)). Some of the forcing data sets are mandatory: i.e. if impact models account for the forcing, the
276 specified dataset must be used; if an alternative input data set is used instead, the run cannot be
277 considered an ISIMIP simulation. We also provide ‘optional’ forcing data that could be used but are not
278 ‘mandatory’ in the above sense (see [second column of Table 1 and Table 3](#)). In addition, the protocol
279 includes a set of sensitivity experiments that are described as deviations from the default runs and
280 labelled by the baseline CRF and DHF settings and [the](#) third specifier [then](#) indicating the deviation from
281 this default setting [instead of being set to ‘default’](#). The ISIMIP3a sensitivity runs include experiments
282 with high-resolution climate forcing (‘30arcsec’, ‘90arcsec’, ‘300arcsec’, or ‘1800arcsec’), fixed levels
283 of atmospheric CO₂ concentrations (‘1901co2’), a scenario assuming no water management
284 (‘nowatermgt’), simulations excluding the occurrence of wildfires (‘nofire’), keeping irrigation patterns at
285 1901 levels (‘1901irr’), and assuming fixed 1955 riverine inputs of freshwater and nutrients into the
286 ocean (‘1955-riverine-input’) (see **Table 2**). [Table 2 and Table 4 providing the comprehensive list of all](#)
287 [‘obsclim’ and ‘counterclim’-based experiments, respectively, also indicate the priority of the experiments](#)
288 [where ‘1st priority’ means that modellers should focus on this set of experiments if their capacities were](#)
289 [limited and they wanted to limit the set of experiments. However, this is just an indication trying to ensure](#)

290 [the generation of a small set of experiments that is covered by as many impact models as possible. If](#)
 291 [an impact modeller can only do part of the first priority set-up or has to start from second priority](#)
 292 [simulations these fragmented data sets can also be submitted to the ISIMIP3a repository.](#)
 293
 294



295
 296 **Figure 1: ISIMIP3a scenario design:** Illustration of the default ISIMIP3a forcing data sets. Each experiment is
 297 defined by a combination of a CRF data set with a DHF data set. The considered combinations are listed in **Table**
 298 **2** and **Table 4** and the underlying rationale is described in section 2.1 (evaluation runs based on 'obsclim' defined
 299 in **Table 1**) and section 2.2 (attribution runs based on 'counterclim' defined in **Table 3**). **Table 1** also lists all data
 300 sets defining the 'histsoc' DHF. Solid lines indicate the part of the experiments that should be reported while the
 301 dashed lines illustrate the different spin-up procedures for the models that require a spin-up. Note that the oceanic
 302 climate-related forcing for the *marine ecosystems and fisheries* sector is only available for 'obsclim' and the period
 303 1961-2010, i.e. the actual experiments only start from the year 1961. The associated spin-up procedure and the
 304 simulations set-up for a transition period are not illustrated in the Figure but described below for the 'obsclim +
 305 histsoc, default', 'obsclim + nat, default', 'obsclim + histsoc, 60arcmin', and 'obsclim + nat, 60arcmin' experiments
 306 considered in this sector.
 307

308 **2.1 Model evaluation and sensitivity experiments based on observed CRFs ('obsclim')**

309 [The experiments described in this section are all based on observational \(factual\) climate data, coastal](#)
 310 [water levels, and atmospheric CO2 as well as CH4 concentrations including observed trends. The only](#)
 311 [exception are the sensitivity experiments where CO2 concentrations are fixed at 1901 levels](#)
 312 [\('1901co2'\). However, as these experiments only deviate in this one aspect from the factual CRF they](#)
 313 [are also described by the 'obsclim' CRF specifier but the '1901co2' sensitivity specifier to indicate the](#)
 314 [deviation. So all experiments described in this section share the common 'obsclim' CRF specifier in the](#)
 315 [file names. In contrast, all experiments described in section 2.2 can be identified by the 'counterclim'](#)
 316 [specifier in the names of the output files containing the impact model simulations. ¶](#)

317 ¶

318 **2.1.1 Default evaluation experiments based on observed CRFs ('obsclim')¶**

319 [In this first part of section 2.1 we describe the default ISIMIP3a experiments \(sensitivity specifier in the](#)
 320 [file names set to 'default'\) that are based on the standard observed climate-related forcings \('obsclim',](#)

321 see CRF part of **Table 1**) [in combination with](#) different assumptions regarding direct human forcings
 322 ('histsoc', '2015soc', '1901soc', and 'nat') [illustrated in Figure 1](#).

323

324 **Standard evaluation experiment ~~using observed variations of direct human forcings (obsclim +~~**
 325 **histsoc; default)**. The first set of observation-based simulations is dedicated to impact model
 326 evaluation, i.e., to test our ability to reproduce and explain observed long-term changes or variations in
 327 impact indicators such as crop yields, river discharge, changes in natural vegetation carbon, vegetation
 328 types, and peatland moisture conditions. To this end, we provide the climate-related ('obsclim'), direct
 329 human ('histsoc'), and static geographical forcings listed in **Table 1**. [They are](#) ~~and~~ described in more
 330 detail in sections **3** and **4**.

331

332 For impact model simulations that require a spin-up to e.g. balance carbon stocks, 100 years of climate
 333 data ('spinclim') are provided that represent stable 1900 climate conditions. The spinclim data is
 334 equivalent to the first 100 years of the counterfactual climate data that are described in section **3.1**. If
 335 more than 100 years of spin-up are needed, the spinclim data can be repeated as often as needed. For
 336 the spin-up, CO₂ concentrations and direct human forcing should be kept constant at 1850 levels. To
 337 get to the historical reporting period starting in 1901, modellers should simulate a transition period from
 338 1850 to 1900 using spinclim climate data and the observed increase in CO₂ concentrations and
 339 historical changes in socioeconomic forcings (from 1850-1900).

340

341 The temporal coverage of the evaluation experiment is limited to 1961-2010 in the *marine ecosystems*
 342 *and fisheries* sector due to the availability of reanalysis-based oceanic forcing data (Liu et al., 2021).
 343 As spin-up + transition period for the 'obsclim + histsoc, default' experiments starting in 1961 the models
 344 should be run through six cycles of 1961-1980 '1955-riverine-input' CRFs (120 years, see **Table 1**)
 345 assuming reconstructed fishing efforts from 1861-1960 and constant 1861 levels before during 1841-
 346 1860 (see **Table 1** and **Figure 3** in section **4.9**). If more years of spin-up are required, additional cycles
 347 of the 1961-1980 '1955-riverine-input' CRFs should be added, assuming constant 1861 fishing efforts.

348

349 **Table 1: Climate-related, direct human, and static geographic forcing data provided for the model**
 350 **evaluation and sensitivity experiments within ISIMIP3a**. The CRFs are grouped according to the definition of
 351 the default 'obsclim' CRF ([30 arcmin for the atmospheric data and 15 arcmin for the oceanic data](#)), the higher
 352 resolution '30arcsec', '90arcsec', '300arcsec', '1800arcsec' atmospheric CRF, the lower resolution '60arcmin'
 353 oceanic CRF, and the '1955-riverine-input' oceanic CRF for the sensitivity experiments. The listed set of DHFs
 354 defines the 'histsoc' set-up.

Forcing	Status	Source, description
Climate-Related Forcings ('obsclim')		
Atmospheric forcings		
Standard observation-based	mandatory	GSWP3-W5E5, 20CRv3-W5E5, 20CRv3-ERA5, 20CRv3, see section 3.1

atmospheric climate forcing		
Local atmospheric climate forcing for lake locations	mandatory	Atmospheric data extracted from the data sets above for 72 lakes that have been identified within the <i>lake</i> sector as locations (grid cells of the ISIMIP 0.5° grid) where models can be calibrated based on observed temperature profiles and hypsometry (Golub et al., 2022, https://www.isimip.org/gettingstarted/input-data-bias-adjustment/isimip3-local-lake-sites/).
Tropical cyclone tracks, <u>as well as and</u> wind <u>and precipitation</u> fields	mandatory	Tracks from IBTrACS database (period 1950 1841-2021; (Knapp et al., 2010). Wind <u>and precipitation</u> fields calculated by Holland model (Holland, 1980, 2008), see section 3.2
Lightning	mandatory	Satellite-based (1995-2014) climatology of monthly flash rates (number of strokes km ⁻² d ⁻¹ on 0.5° grid (Cecil, 2006)
Oceanic forcings		
Standard observation-based oceanic forcing data	mandatory	GFDL MOM6/COBALTv2 simulations driven by reanalysis-based atmospheric forcing (Liu et al., 2021); see section 3.4
Regional oceanic climate forcing for regional <i>marine ecosystems</i> and <i>fisheries</i> sector	mandatory	Extraction from data set above for 21 regional marine ecosystems <u>associated with the interests identified by the modelling groups</u> (https://www.isimip.org/gettingstarted/input-data-bias-adjustment/isimip3-ocean-regions/). The extraction has been done for individual layers (ocean surface or bottom) and a subset of the variables that have been integrated along the ocean column (see Table 8).
Coastal water levels		
Coastal water levels	mandatory	Hourly coastal water levels with long-term trends <u>for impact attribution</u> , see section 3.3
Atmospheric composition		
Atmospheric CO ₂	mandatory	1850-2005: (Meinshausen et al., 2011); 2006-2021: Global

concentration		annual CO ₂ from NOAA Global Monthly Mean CO ₂ ; (Lan et al., 2023; Büchner and Reyer, 2022)
Atmospheric CH ₄ concentration	mandatory	1850-2014: (Meinshausen et al., 2017); 2015-2021: (Büchner and Reyer, 2022; Lan et al., 2023)
Climate-Related Forcings for sensitivity experiments (30arcsec, 90arcsec, 300arcsec, 1800arcsec, 60arcmin, and 1955-riverine-input), identical to 'obsclim' except for:		
Atmospheric forcings (30arcsec, 90arcsec, 300arcsec, 1800arcsec)		
High resolution observation-based atmospheric forcing data	mandatory	see section 3.1 for a description of the CHELSA method applied to downscale the W5E5 observation-based atmospheric data to 30". The data is then upscaled to 90" (~3 km), 300" (~10 km) and 1800" = 0.5° (~60 km) to provide the forcings for additional sensitivity experiments.
Oceanic forcings (60arcmin)		
Low resolution observation-based oceanic forcing data	mandatory	GFDL MOM6/COBALTv2 simulations (1961 - 2010) driven by reanalysis-based atmospheric forcing (Liu et al., 2021) upscaled to 1°, see section 3.4
Oceanic forcings (1955-riverine-input)		
Observation-based oceanic forcing data but assuming climatological 1951 to 1958 levels of riverine input	mandatory	GFDL MOM6/COBALTv2 simulations (1961 - 2010) driven by reanalysis-based atmospheric forcing (Liu et al., 2021), but fixed climatological 1951 to 1958 levels of freshwater input and input of nutrients inputsand pollutants , see section 3.4
Direct Human Forcing ('histsoc')		
Population data	mandatory	see section 4.1
GDP data	mandatory	see section 4.2
Land use and irrigation	mandatory	HYDE-based irrigated and rainfed cropland downscaled to up to 15 crops, managed pasture and grassland, and urban areas, see section 4.3
N-fertiliser inputs	mandatory	see section 4.4

Wood harvest	optional	Historical annual country-level wood harvesting data based on the LUH2 v2h Harmonization Data Set (del Valle et al., 2022; Hurtt et al., 2011, 2020, Land use harmonization, 2023), see section 4.5
Land transformation	mandatory	Historical annual land-use transformation data, based on the LUH v2h Harmonization Data Set (Hurtt et al., 2011, 2020, Land use harmonization, 2023), see section 4.5
N-fertiliser inputs	mandatory	see section 4.4
N-deposition	optional	(Yang and Tian, 2020; Tian et al., 2018); see section 3.6
Crop calendar	optional	Observation-based representation of recent average planting and maturity dates not accounting for changes over time (Jägermeyr et al., 2021a), see section 4.7
Dams and reservoirs	optional	see section 4.8
Lake and reservoir surface area	optional	Total lake and reservoir area fractions (percentage of grid cell) calculated from the HydroLAKES v1.0 (Messenger et al., 2016) and GRanDv1.3 databases (Lehner et al., 2011b) mapped to 0.5 degrees resolution. Areas increase with time because of the increasing number of reservoirs documented in GRanDv1.3. Reservoirs from 2017 onwards are kept constant. This data set differs from the lake surface areas provided as static geographic forcing (see below) which describe the surface area of one representative lake per grid cell and does not change over time.
Water abstraction	optional	For modelling groups that do not have their own representation, we provide files containing the multi-model mean of domestic and industrial water withdrawal and consumption generated by the WaterGAP, PCR-GLOBWB, and H08 models (1850-2021). This data is based on ISIMIP2a ‘varsoc’ simulations for 1901-2005 and extended by SSP2-based RCP6.0 simulations from the Water Futures and Solutions project up to 2021 (Wada et al., 2016b). Years before 1901 have been filled with the value for year 1901.
Marine fishing effort	mandatory	Observation-based reconstruction of fishing effort spanning

		<p>1841-2010 (Rousseau et al., 2022) based on (Rousseau et al., submitted 2023); see section 4.9</p> <p>The climate-related forcing for the <i>marine ecosystems and fisheries</i> sector is only available for 1961-2010, but the spin-up procedure also requires fishing efforts for the earlier years (see description of the procedure for the ‘obsclim + histsoc; default’ scenario above).</p>
Dams and reservoirs	optional	see section 4.8
Water abstraction	optional	<p>For modelling groups that do not have their own representation, we provide files containing the multi-model mean of domestic and industrial water withdrawal and consumption generated by the WaterGAP, PCR-GLOBWB, and H08 models (1850-2021). This data is based on ISIMIP2a ‘varsoc’ simulations for 1901-2005 and extended by SSP2-basedRCP6.0 simulations from the Water Futures and Solutions project up to 2021 (Wada et al., 2016b). Years before 1901 have been filled with the value for year 1901.</p>
Lake and reservoir surface area	optional	<p>Total lake and reservoir area fractions (percentage of grid cell) calculated from the HydroLAKES v1.0 (Messenger et al., 2016) and GRanDv1.3 databases (Lehner et al., 2011b) mapped to 0.5 degrees resolution. Areas increase with time because of the increasing number of reservoirs documented in GRanDv1.3. Reservoirs from 2017 onwards are kept constant. This data set differs from the lake surface areas provided as static geographic forcing (see below) which describe the surface area of one representative lake per grid cell and does not change over time.</p>
Forest management	mandatory	<p>Observed stem numbers, thinning type, planting numbers from and common management practices for 9 forest sites in Europe (Reyer et al., 2020b),(Reyer et al., 2023), see section 4.10</p>
Population data	mandatory	see section 4.1
GDP data	mandatory	see section 4.2

Static geographic forcing		
Lake volume at different depths	optional	The gridded data set describes the volume at different depths of one hypothetical lake representing the typical characteristics of all real lakes in the grid cell according to the GLOBathy (Khazaei et al., 2022; Messenger et al., 2016) and HydroLAKES v1.0 (Khazaei et al., 2022; Messenger et al., 2016) datasets (Golub et al., 2022). Each hypsographic curve consists of 11 data pairs. Level refers to the depth of the lake taking the lake bottom as the reference. Volume is the volume at the corresponding level.
Lake area at different depths	optional	The gridded data set describes the lake area at different depths of one hypothetical lake representing the typical characteristics of all real lakes in the grid cell according to the GLOBathy (Khazaei et al., 2022; Messenger et al., 2016) and HydroLAKES (Khazaei et al., 2022; Messenger et al., 2016) datasets (Golub et al., 2022). Each hypsographic curve consists of 11 data pairs. Level refers to the depth of the lake taking the lake bottom as the reference.
Lake elevation	optional	The gridded data set provides the elevation above sea level for the representative lakes described above. The information is derived from HydroLAKES v1.0 (Messenger et al., 2016).
Maximum lake depth	optional	Gridded data set that provides the maximum depth for the representative lakes described above and derived from GLOBathy (Khazaei et al., 2022). We recommend using the area or volume hypsographic curves described above as inputs for your lake model. Use this file only if your lake model does not accept a full hypsographic curve as an input.
Lake depth	optional	Gridded data set that provides the mean depth for the representative lakes as calculated from GLOBathy and HydroLAKES v1.0 (Khazaei et al., 2022; Messenger et al., 2016). We recommend using the area or volume hypsographic curves described above as inputs for your lake model. Use this file only if your lake model does not accept a full hypsographic curve as an input.

Lake volume	optional	Gridded data set of volume (km ³) for representative lakes described above as calculated from GLOBathy and HydroLAKES v1.0 (Khazaei et al., 2022; Messenger et al., 2016). We recommend using the area or volume hypsographic curves described above as inputs for your lake model. Use this file only if your lake model does not accept a full hypsographic curve as an input.
Lake surface area	optional	Gridded data set of surface area for the representative lakes described above as calculated from GLOBathy and HydroLAKES v1.0 (Khazaei et al., 2022; Messenger et al., 2016). As opposed to the “Lake and reservoir surface area” listed above under “Direct human forcing”, this data set refers to one specific lake associated with each grid cell, and the corresponding surface area does not change over time. We recommend using the area or volume hypsographic curves described above as inputs for your lake model. Use this file only if your lake model does not accept a full hypsographic curve as an input.
HydroLAKES ID	optional	HydroLAKES reference to relate HydroLAKES and GLOBathy database fields to the representative lakes described above. This dataset contains IDs of the 41449 representative lakes used in ISIMIP, which are a subset of the about 1.4 million lakes contained in the HydroLAKES and GLOBathy database.
HydroLAKES IDs for big lakes	optional	This dataset is analogous to the one above, but only contains IDs of 93 large lakes. It can be used to produce global plots with conspicuous large lakes. To be used together with the file storing the big lakes mask.
Big lakes mask	optional	This dataset indicates the 0.5° grid cells actually occupied by each of the 93 large lakes, which can be larger than a single grid cell. It can be used to produce global plots with conspicuous large lakes. To be used together with the big lakes IDs in the dataset above.
Drainage direction map for river routing	optional	Includes for each grid cell a basin number, flow direction, and slope. Source: ISIMIPddm30 (Müller Schmied, 2022)

		based on DDM30 (Döll and Lehner, 2002)
Soil data	optional	<p>Gridded soil characteristics have been generated within the Global Soil Wetness Project (GSWP3) (Dirmeyer et al., 2006; van den Hurk et al., 2016, Global soil wetness project phase 3 — GSWP3 documentation, 2023) and have already been provided within ISIMIP2a.</p> <p>Alternatively, we also provide maps of the dominant soil types (i.e., the type covering the largest fraction of the cell of the topmost soil layer) within each ISIMIP grid cell and the dominant soil types on the agricultural land within each ISIMIP grid cell. Both maps were derived from the Harmonized World Soil Database (HWSD Version 1.1, 2009) assuming that soil types are evenly distributed within the ISIMIP grid cells. We have used version 1.12 of the HWSD data at high resolution (30 arcsec). Information about the fraction of agricultural land within each ISIMIP 0.5°×0.5° grid cell was taken from MIRCA2000 (Portmann et al., 2010). If there is no soil information for an ISIMIP grid cell, e.g. due to differing land-sea-masks, the information from neighbouring cells is used. For further details please see GGCM-HWSD (2023).</p>
Land-sea mask	optional	<p>We provide the binary land-sea mask of the W5E5 dataset. It is a conservative land mask where grid cells that in reality cover both land and ocean are counted as ocean. Thus, climate conditions over the land grid cells of this land-sea mask can be safely assumed to represent climate conditions over land rather than a mix of climate conditions over land and ocean. This refers to all climate datasets based on W5E5, i.e. GSWP3-W5E5 and 20CRv3-W5E5 of ISIMIP3a and the ISIMIP3b climate forcing that has been bias-adjusted using W5E5. The mask is also provided in a version without Antarctica. In addition, the generic land-sea mask from ISIMIP2b is provided to be used for global water simulations in ISIMIP3. It marks more grid cells as land than the main mask described above (Lange and Büchner, 2020).</p>

Sea floor depth	optional	Grid cell level ocean depth in metres of GFDL-MOM6-COBALT2 data in 0.25 and 1° horizontal resolution
Binary country mask	optional	Binary country map on a 0.5° x 0.5° latitude-longitude grid
Fractional country mask	optional	Fractional country map on the ISIMIP 0.5° x 0.5° grid. This is the map that has been used to calculate the national data for ISlpedia (isipedia.org) and to e.g. prepare the national population and GDP data provided within ISIMIP3 (see sections 4.1 and 4.2).
Large Marine Ecosystem masks	mandatory	Binary masks available at 0.25°, 0.5°, and 1° resolution (Sherman, 2017).
Regional Marine Ecosystem masks	optional	Binary masks describing the 21 ocean regions for the regional modelling activities in the fisheries and marine ecosystems available at 0.25° and 1° resolution. These masks have been used for the ocean forcing data extractions (see CRF part of this table).

355

356 **Fixed 2015 direct human forcing (obsclim + 2015soc; default).** To allow for the quantification of the
357 effect of historical changes in direct human forcings, ISIMIP3a also contains an experiment where all
358 direct human forcings are held constant at year 2015 levels. The difference between the evaluation run
359 described above and this baseline simulation can be considered the impact of changes in direct human
360 forcings. [In this sense the experiment allows for the attribution of observed changes in the natural,
361 human, and managed systems to changes in DHF after 2015.](#) In addition, the simulated changes in
362 models' output variables can be considered the 'pure effects of climate-related forcings', conditional on
363 present-day socio-economic conditions. The experiment is also introduced because not all impact
364 models can account for varying direct human forcings but rather assume fixed 'present day' conditions.
365 All modelling teams are asked to do this experiment even if they are able to account for varying direct
366 human forcings to generate one set of impact simulations that can be integrated across all participating
367 models from different sectors or where all simulations from one sector can be compared. If a spin-up is
368 required, it should be based on the 'spincim' data as described above but fixed 2015 direct human
369 forcings.

370 ¶

371 ¶

372 **Impact of historical changes in direct human forcings – Fixed 1901 direct human forcing baseline**
373 **(obsclim + 1901soc; default).** Fixing direct human forcings at 1901 levels is an alternative approach
374 to quantify i) the effects of direct human forcings when comparing these baseline simulations to the
375 evaluation run and ii) the 'pure effect of observed change in climate-related systems', conditional on
376 socio-economic conditions observed before the onset of this change. [As such the experiment is the](#)

377 [counterfactual baseline when aiming for the attribution of observed changes in natural, human, and](#)
378 [managed systems to observed changes in direct human forcings instead of the attribution to observed](#)
379 [changes in the climate-related systems based on the analogous ‘counterfactual + histsoc, default’](#)
380 [experiment described in section 2.2. Both experiments consider changes in direct human forcings or](#)
381 [climate-related systems from 1901 levels, respectively.](#) Because of the low levels of direct human
382 forcings in 1901, this experiment is similar to the sector-specific ‘nat’ experiment that includes no direct
383 human forcings whatsoever (see below). However, while the fully naturalised ‘nat’ run is suitable for the
384 dynamic vegetation models from the *biomes* sector that simulate land cover by vegetation on their own,
385 models in other sectors need land cover as an input. As this information is not available for pristine
386 conditions, we introduce the 1901soc scenario such that models in the *water* sector can use land cover
387 data approximately representative of 1901 conditions to describe a situation with minor human
388 influences. If a spin-up is required, it should be based on the ‘spinclim’ data as described above but
389 fixed 1901 direct human forcings.

390
391 **Impact of direct human forcings—No direct human forcing baseline (obsclim + nat; default).** To
392 estimate the full effect of 2015 levels of DHF we also introduce a baseline ‘nat’ experiment that does
393 not consider any DHFs but a natural state of the world. Then the difference to the ‘obsclim + 2015soc,
394 default’ experiment can be considered the effect of 2015 levels of DHF. [The comparison to the ‘obsclim](#)
395 [+ histsoc, default’ experiment allows for the attribution of observed changes in the natural, human, and](#)
396 [managed systems to historical changes in the DHF.](#) ~~In addition,~~ trends in the ‘obsclim + nat; default’
397 run only represent the impacts historical changes in the climate-related forcings would have had on an
398 otherwise natural state of the world. While the ‘1901soc’ conditions may be similar to ‘nat’ conditions,
399 trends in the ‘obsclim + 1901soc; default’ run may not only be induced by historical changes in the CRFs
400 but could also represent lagged responses to changes in DHFs during the transition period. The ‘nat’
401 experiment can also be used to quantify the natural carbon sequestration potential of natural vegetation
402 without any management or land-use as an important counterfactual [baselinedata-set](#) to assess the
403 additionality of carbon sequestration measures. The ‘nat’ experiment is sector-specific for the *biomes*,
404 *peat* and *marine ecosystems and fisheries* sectors. If a spin-up is required in the *biomes* and *peat*
405 sector, it should be based on the ‘spinclim’ data as described above but assuming no direct human
406 forcings. In the *marine ecosystems and fisheries* sector the spin-up should be based on the ‘1955
407 riverine input’ CRF as described for ‘obsclim + histsoc, default’ section but assuming no DHF, i.e. no
408 fishing efforts.

409
410 [2.1.2 Sensitivity experiments based on observed CRFs \(‘obsclim’\)](#)
411 [This second part of section 2.1 is dedicated to the different sensitivity experiments described as](#)
412 [deviations from the default cases described in section 2.1.1. Instead of the ‘default’ specifier, all](#)
413 [experiments described here are labelled by a sensitivity specifiers indicating their deviation from the](#)
414 [default cases. The experiments listed here are not explicitly depicted in Figure 1.](#) ¶

415 ¶

416 **High and low resolution sensitivity experiments (obsclim + histsoc; 30arcsec, 90arcsec,**
417 **300arcsec, 1800arcsec, and 60arcmin).** To test whether high resolution atmospheric climate data
418 improve the climate impact model simulations, we also provide observational atmospheric forcing data
419 at 30" ('30arcsec'), 90" ('90arcsec'), and 300" ('300arcsec') resolution as well as atmospheric forcings
420 at the original 1800" resolution but derived from the 30" (~1 km) data ('1800arcsec'). In addition, the
421 oceanic data (original resolution of 0.25°) is upscaled to 1° to also test the sensitivity of the impact
422 simulations to this modification ('60arcmin').

423 The 30" atmospheric data (1979-2016) is derived from ~~by~~ a topographic downscaling of the
424 observational W5E5 data (resolution of 0.5°) that particularly corrects for systematic effects induced by
425 orographic details not represented in global reanalyses (CHELSA-W5E5, see section 3.1). The data
426 set comprises daily mean precipitation, daily mean surface downwelling shortwave radiation, daily
427 mean near-surface air temperature, daily maximum near surface air temperature, daily minimum near
428 surface air temperature (see Table 5). We additionally provide simple approaches to downscale surface
429 downwelling longwave radiation, near-surface relative humidity, air pressure and near-surface wind
430 speed (see section 3.1). Given the considerable storage capacities required by daily 1 km x 1 km data
431 and constraints on data handling and download, we also aggregate the CHELSA-W5E5 data to 90" (~3
432 km), 300" (~10 km) and 1800" = 0.5° (~60 km) to determine which resolution is required to improve the
433 impact model simulations compared to observed impact indicators. The evaluation of these historical
434 sensitivity experiments will inform future downscaling activities for the GCM climate forcing data
435 including future projections. The '1800arcsec' experiment is included as a reference, as the aggregated
436 CHELSA-W5E5 data differ from the standard W5E5 data at the same resolution (see section 3.1). So
437 far the experiments have been added to the agriculture, lakes, global and regional water, regional
438 forests, terrestrial biodiversity, and labour protocol. However, they may be added to other sectors, too.
439 The inclusion of the experiment is only constrained by the restricted set of variables included in
440 CHELSA-W5E5. We do not provide spin-up data for the experiments. This means that models requiring
441 a spin-up currently cannot perform the experiments. We will work on a solution on demand.

442 In contrast to the experiment testing the sensitivity of the impact simulations to a higher resolution of
443 the atmospheric CRFs, the associated sensitivity experiment for the *marine ecosystems and fisheries*
444 sector is not based on higher but on lower resolution oceanic data. While the default 'obsclim' oceanic
445 forcing data is derived by interpolating the observation-based historical ocean simulations from a tri-
446 polar 0.25° grid to a regular 0.25° grid (see section 3.4), the CRFs for the sensitivity experiment are
447 derived by aggregating the default 'obsclim' data to a regular 1.0° grid ('60arcmin'). Evaluating the 1.0°
448 resolution is of interest because this is the resolution of the oceanic forcing data in ISIMIP3b. The low
449 resolution simulations could either start from the end of the simulations of the transition period of the
450 associated higher resolution runs ('obsclim + histsoc; default') or starting conditions could be newly
451 generated by following the 'spin-up + transition' procedure of 'obsclim + histsoc; default' experiment but
452 using the low-resolution '1955-riverine-input' CRF from the years 1961-1980.

453

454 **Low resolution sensitivity experiment (obsclim + nat; 60arcmin).** This sensitivity experiment for
455 the *marine ecosystems and fisheries* sector is analogous to the 'obsclim + nat; default' experiment

456 described further above, but using the lower-resolution oceanic CRF ('60arcmin'). The difference
457 between this experiment and the 'obsclim + histsoc; 60arcmin' sensitivity experiment can be considered
458 the effect of [the historical changes in 2015 levels of DHF](#) as estimated using lower-resolution CRF, and
459 comparison with the same difference in the default experiments then indicates how the estimate of this
460 effect depends on the resolution of the oceanic forcing. The simulations could either start from the end
461 of the simulations of the transition period of the associated higher resolution runs ('obsclim + nat;
462 default') or starting conditions could be newly generated by following the 'spin-up + transition' procedure
463 of 'obsclim + nat, default' experiment but using the low-resolution '1955-riverine-input' CRF from the
464 years 1961-1980.

465

466 **CO₂ sensitivity experiments (obsclim + histsoc, obsclim + 2015soc, or obsclim + 1901soc;
467 1901co2).** To quantify the pure effect of the historical increase in atmospheric CO₂ concentrations on
468 vegetation leaf gas exchange and follow-on effects on carbon stocks, water use efficiency, vegetation
469 distribution etc., we introduced three sensitivity experiments where atmospheric CO₂ concentrations
470 are held constant at 1901 levels (= 296.13 ppm) in contrast to the default 'obsclim + histsoc', 'obsclim
471 + 2015soc', or 'obsclim + 1901soc' experiments, respectively, where atmospheric CO₂ concentrations
472 are assumed to increase according to observations. The effect is known as CO₂ fertilisation through an
473 increase of the photosynthesis rate of plants and limited leaf transpiration (increase in water use
474 efficiency) enabling a more efficient uptake of carbon by the plants. [Comparing the 'obsclim + histsoc,
475 default' experiment to the 'obsclim + histsoc, 1901soc' experiment can be considered as attributing
476 historical changes in natural, human, and managed systems to historical changes in CO₂
477 concentrations as a single component of the changes in climate-related systems.](#) The experiment is
478 included into the protocols of the *agriculture, terrestrial biodiversity, biomes, fire, lakes (global and
479 local), permafrost, peat and water (global and regional)* sector. A potentially required spin-up should be
480 identical to the spin-up for the associated default experiments using the transition period 1850-1900 to
481 reach the 1901 CO₂ level.

482

483 **Water management sensitivity experiment (obsclim + histsoc, obsclim + 2015soc; nowatermgt).**
484 In this "no water management" experiment, models are run assuming [no irrigation](#), no human water
485 abstraction, no dams or reservoirs, and no seawater desalination, while other direct human forcings
486 such as land use changes are considered according to 'histsoc' or '2015soc'. By comparison to the
487 default experiments, the simulations allow for a quantification of the pure effects of dedicated water
488 management measures on, e.g., discharge. [When comparing 'obsclim + histsoc, nowatermgt' to
489 'obsclim + histsoc, default' this can be considered attributing observed changes in natural, human, or
490 managed systems to \(changes in\) water management.](#) The sensitivity experiment has been introduced
491 into the *global and regional water* sector protocols. If a spin-up is required, it should be done similar to
492 the spin-up for the associated default experiments but assuming "no water management".

493

494 **Irrigation sensitivity experiment (obsclim + histsoc, 1901irr).** In this "no irrigation expansion"
495 experiment, models are run assuming irrigation extent and irrigation water use efficiencies fixed at the

496 year 1901, while other direct human forcings such as land use changes and water management
497 categories are considered according to 'histsoc' or '2015soc'. By comparison to the default experiments,
498 the simulations allow for a quantification of the pure effects of historical irrigation expansion [\(i.e. the](#)
499 [attribution of historical changes in natural, human, or managed systems to changes in irrigation](#)
500 [compared to 1091\)](#). The sensitivity experiment has been introduced into the *global water and biome*
501 sector protocols. If a spin-up is required, it should be done similar to the spin-up for the associated
502 default experiments but assuming "no irrigation expansion". This experiment is designed such that its
503 outcomes are comparable to those of the Irrigation Impacts Model Intercomparison Project (IRRMIIP;
504 <https://hydr.vub.be/projects/irrmip>), in which Earth System Models simulate irrigation influences on the
505 Earth system.

506

507 **No-fire sensitivity experiment (obsclim + histsoc; nofire).** In this 'nofire' experiment, fire is switched
508 off in the model simulations. In comparison to the default 'obsclim + histsoc' simulations, the historical
509 effects of fires on, e.g., carbon fluxes and vegetation distributions can be determined. The sensitivity
510 experiment has been introduced into the *fire, biomes, permafrost, and peat* protocols. The required
511 spin-up should be done similar to the spin-up for the associated default experiments but assuming no
512 fire activities.¶

513 ¶

514 [Fixed 1955 riverine input into the ocean sensitivity experiment \(obsclim + histsoc; obsclim + nat; 1955-](#)
515 [riverine-input\)](#). In this '1955-riverine-input' experiment, riverine input into the ocean (amount of
516 [freshwater and nutrients\)](#) is held constant at 1955 levels. In comparison to the default 'obsclim + histsoc'
517 [simulation, the experiment allows for the quantification of the impacts of historical climate-induced](#)
518 [variations in freshwater influx in combination with the climate and directly human induced changes in](#)
519 [nutrient inputs \(attribution of observed changes in marine ecosystems and fisheries to long term](#)
520 [changes in riverine freshwater and nutrient inputs\)](#). The riverine inputs in the 'obsclim + nat; 1955-
521 [riverine-input' experiment are identical to the ones in the 'obsclim + histsoc; 1955-riverine-input', i.e.](#)
522 [the riverine inputs also account for the human contribution to the nutrient influx due to land use changes](#)
523 [and fertiliser inputs and are not 'naturalized'. Instead the 'nat' specifier in the marine ecosystems and](#)
524 [fisheries sector only means 'no fishing efforts'. Thus, the comparison to the naturalised default](#)
525 [experiment \(obsclim + nat; default\) not accounting for any fishing efforts to the 'obsclim + nat; 1955-](#)
526 [riverine-input' experiment allows for a quantification of the contribution of climate-induced changes in](#)
527 [freshwater-influx to the overall impacts of climate change in combination with the contribution of the](#)
528 [effect of the human contribution to nutrient inputs at 1955 levels. The sensitivity experiment has been](#)
529 [introduced into the marine ecosystems and fisheries protocol. A potentially required spin-up should be](#)
530 [done similar to the spin-up for the associated default experiments but assuming riverine inputs fixed at](#)
531 [1955 levels.](#)¶

532

533 **Table 2: ISIMIP3a evaluation and sensitivity experiments**

Experiment	Short description	Period: Historical 1901-2019
model evaluation histsoc	CRF: Observed climate change, CO ₂ and CH ₄ levels, and coastal water levels	obsclim
1st priority	DHF: Varying direct human influences according to observations	histsoc
model evaluation 2015soc	CRF: Observed climate change, CO ₂ and CH ₄ levels, and coastal water levels	obsclim
1st priority	DHF: Fixed 2015 levels of direct human forcing for the entire time period	2015soc
model evaluation 1901soc	CRF: Observed climate change, CO ₂ and CH ₄ levels, and coastal water levels	obsclim
2nd priority	DHF: Fixed 1901 levels of direct human forcing for the entire time period	1901soc
model evaluation nat	CRF: Observed climate change, CO ₂ and CH ₄ levels, and coastal water levels	obsclim
2nd priority	DHF: No direct human influences	nat
CO₂ sensitivity histsoc	CRF: Observed climate change, CH ₄ concentrations and coastal water levels, fixed CO ₂ concentration at 1901 level	obsclim Sensitivity experiment: 1901co2
2nd priority	DHF: Varying direct human influences according to observations	histsoc
CO₂ sensitivity 2015soc	CF: Observed climate change, CH ₄ concentrations and coastal water levels, fixed CO ₂ concentration at 1901 level	obsclim Sensitivity experiment: 1901co2

2nd priority	DHF: Fixed 2015 levels of direct human forcing for the entire time period	2015soc
CO₂ sensitivity 1901soc 2nd priority	CRF: Observed climate change, CH ₄ concentrations and coastal water levels, fixed CO ₂ concentration at 1901 level	obsclim Sensitivity experiment: 1901co2
	DHF: Fixed 1901 levels of direct human forcing for the entire time period	1901soc
Water management sensitivity histsoc 2nd priority	CRF: Observed climate change, coastal water levels, and CO ₂ and CH ₄ concentrations	obsclim
	DHF: No accounting for water management but representation of other direct human influences such as land use changes according to "histsoc"	histsoc Sensitivity experiment: nowatermgt
Water management sensitivity 2015soc 2nd priority	CRF: Observed climate change, coastal water levels, and CO ₂ and CH ₄ concentrations	obsclim
	DHF: No accounting for water management but representation of other direct human influences such as land use patterns according to "2015soc"	2015soc Sensitivity experiment: nowatermgt
Irrigation sensitivity histsoc 2nd priority	CRF: Observed climate change, coastal water levels, and CO ₂ and CH ₄ concentrations	obsclim
	DHF: Fixed year-1901 irrigation areas and water use efficiencies but representation of other direct human influences such as land use changes according to "histsoc"	histsoc Sensitivity experiment: 1901irr
No-fire sensitivity	CRF: Observed climate change, coastal water levels, CO ₂ and CH ₄ concentrations	obsclim

<p>histsoc</p> <p>2nd4st priority</p>	<p>DHF: Varying direct human influences according to observations</p>	<p>histsoc</p> <p>Sensitivity experiment: nofire</p>
<p>Riverine influx sensitivity</p> <p>histsoc</p> <p>2nd4st priority</p>	<p>CRF: Observation-based oceanic forcing data, but with constant riverine nutrient and freshwater influx.</p>	<p>obsclim</p> <p>Sensitivity experiment: 1955-riverine-input</p>
	<p>DHF: Varying direct human influences according to observations</p>	<p>histsoc</p>
<p>Riverine influx sensitivity</p> <p>nat</p> <p>2nd4st priority</p>	<p>CRF: Observation-based oceanic forcing data, but with constant riverine nutrient and freshwater influx.</p>	<p>obsclim</p> <p>Sensitivity experiment: 1955-riverine-input</p>
	<p>DHF: No direct human influences</p>	<p>nat</p>
<p>High-resolution sensitivity, 1km</p> <p>histsoc</p> <p>2nd priority</p>	<p>CRF: Observed high-resolution climate forcing (30"), coastal water levels, and CO₂ and CH₄ concentrations. For this experiment only 1979-2016 is covered</p>	<p>obsclim</p> <p>Sensitivity experiment: 30arcsec</p>
	<p>DHF: Varying direct human influences according to observations</p>	<p>histsoc</p>
<p>High-resolution sensitivity, 3km</p> <p>histsoc</p> <p>2nd priority</p>	<p>CRF: Observed high-resolution climate forcing (90"), coastal water levels, and CO₂ and CH₄ concentrations. For this experiment only 1979-2016 is covered</p>	<p>obsclim</p> <p>Sensitivity experiment: 90arcsec</p>
	<p>DHF: Varying direct human influences according to observations</p>	<p>histsoc</p>
<p>High-resolution sensitivity, 12km</p>	<p>CRF: Observed high-resolution climate forcing (360"), coastal water levels, and CO₂ and CH₄ concentrations. For this experiment only 1979-</p>	<p>obsclim</p> <p>Sensitivity</p>

histsoc 2nd priority	2016 is covered	experiment: 360arcsec
	DHF: Varying direct human influences according to observations	histsoc
High-resolution sensitivity, 60km histsoc 2nd priority	CRF: Observed climate forcings aggregated from high-resolution data, coastal water levels, CO ₂ and CH ₄ concentrations. For this experiment only 1979-2016 is covered	obsclim Sensitivity experiment: 1800arcsec
	DHF: Varying direct human influences according to observations	histsoc
Low-resolution sensitivity, 1° in the ocean histsoc 2nd priority	CRF: Observation-based oceanic forcing data	obsclim Sensitivity experiment: 60arcmin
	DHF: Varying direct human influences according to observations	histsoc
Low-resolution sensitivity, 1° in the ocean nat 2nd priority	CRF: Observation-based oceanic forcing data	obsclim Sensitivity experiment: 60arcmin
	DHF: No direct human influences	nat

534

535 **2.2 Counterfactual baseline simulations for impact attribution ('counterclim')**

536

537 The second set of impact model simulations within ISIMIP3a is dedicated to the attribution of historical
 538 changes in natural, managed, and human systems to long-term changes in climate-related systems,
 539 i.e. the atmosphere, ocean and cryosphere as physical or chemical systems ([see section 1](#)). In
 540 ISIMIP3a, we address attribution to changes in the climate-related systems itself, e.g., trends in
 541 atmospheric temperature and precipitation, [and changes in](#), coastal water levels, and atmospheric CO₂
 542 concentrations. The provided counterfactual forcing data comprises daily atmospheric climate derived
 543 from the ISIMIP observational climate datasets (see section 3.1); daily counterfactual coastal water

544 levels derived from the ISIMIP historical coastal water level dataset (see section 3.3); and constant
 545 1901 atmospheric CO₂ and CH₄ concentrations (see **Table 3**). So far, we do not address attribution to
 546 long-term changes in i) the ocean (e.g. temperature or ocean acidification changes), ii) the cryosphere
 547 (e.g. glacier mass loss), and iii) tropical cyclone characteristics (e.g. trends in associated heavy
 548 precipitation or wind speeds) other than the effects mediated through sea level rise. **Table 3** lists the
 549 climate-related forcings defining the ‘counterclim’ experiments. The ‘counterclim’ climate-related
 550 forcings are combined with the observed direct human forcing to facilitate the attribution experiments
 551 listed in **Table 4** [and explained below](#).

552
 553

Table 3: ISIMIP3a counterfactual climate-related forcings (‘counterclim’)

Forcing	Status	Source, description
Climate-related forcings (counterclim)		
Atmospheric forcings		
Counterfactual ‘no-climate change’ atmospheric climate forcing	mandatory	Detrended versions of the GSWP3-W5E5, 20CRv3-W5E5, 20CRv3-ERA5, 20CRv3 data sets derived by the Attrici method, see section 3.1
Local atmospheric climate forcing for lake location	mandatory	Atmospheric data extracted from the data sets above for 72 lakes that have been identified within the <i>lake</i> sector as locations (grid cells of the ISIMIP 0.5° grid) where models can be calibrated based on observed temperature profiles and hypsometry (depth and area).
Tropical cyclone tracks and windfields	mandatory	We do not provide ‘no climate change’ TC tracks and windfields but the original tracks from the IBTrACS database (Knapp et al., 2010); period 1841-2021) windfields calculated by Holland model (Holland, 2008, 1980) should be used in combination with the counterfactual water levels to estimate the impacts of sea level rise on TC induced damages, losses or replacement, see section 3.2
Lightning	mandatory	We do not provide ‘no climate change’ lightning data. Instead the original Flash Rate Monthly Climatology (Cecil, 2006) should be used in the

		'counterclim' set-up.
Oceanic forcings		
Oceanic forcing data	-	We do not provide any counterfactual oceanic forcings, i.e. there is no 'no climate change' experiment proposed for the <i>marine ecosystems and fisheries</i> sector.
Coastal water levels^α		
Coastal water levels^α	mandatory^α	Counterfactual monthly (1901 - 1978) and hourly (1979 - 2015) coastal water levels where long-term trends have been removed, see section 3.3^α
Atmospheric composition or fluxes		
Atmospheric CO ₂ concentration	mandatory	1901 levels ([CO ₂] = 296.13 ppm) of observed atmospheric CO ₂ concentrations according to (Meinshausen et al., 2011)
Atmospheric CH ₄ concentration	mandatory	1901 levels of atmospheric CH ₄ concentrations ([CH ₄] = 928.80 ppb), according to (Meinshausen et al., 2017)

554

555 ~~The attribution question “To what degree have observed changes in the climate-related systems~~
556 ~~contributed to observed changes in natural, human or managed systems?” could refer to individual~~
557 ~~events (e.g. to what extent has long term climate change contributed to the observed extent of a specific~~
558 ~~river flood?) or long term changes (e.g. to what extent have long term climate change and increasing~~
559 ~~CO₂ fertilisation contributed to an observed change in crop yields?). In line with IPCC-WG2-AR6, chapter~~
560 ~~16 ((O’Neill et al., 2022)), an observed impact of climate change or any other change in a climate-~~
561 ~~related system is defined as the difference between the observed state of the human, natural or~~
562 ~~managed system and a counterfactual baseline that characterises the system’s behaviour in the~~
563 ~~absence of changes in the climate-related systems. This counterfactual baseline may be stationary or~~
564 ~~vary in response to direct human influences such as changes in land-use patterns, agricultural or water~~
565 ~~management or population distribution and economic development affecting exposure and vulnerability~~
566 ~~to weather-related hazards.^{¶¶}~~

567 ¶¶

568 ~~While the definition is quite straightforward, the number of studies addressing impact attribution based~~
569 ~~on this basic definition is still relatively small compared to the number of studies addressing climate~~
570 ~~attribution, i.e. the question to what degree anthropogenic emissions of climate forcers, in particular~~

571 greenhouse gases, have induced changes in the climate-related systems. While climate attribution is
572 confronted by the challenge of separating the anthropogenically forced changes from the internal
573 variability of the climate-related systems, climate impact attribution is about separating the impacts of
574 observed changes in these climate-related systems from the effects of other direct (human) drivers of
575 changes in the considered natural, human or managed systems. Despite this difference, both climate
576 and climate impact attribution share the feature that they rely on the comparison of the observed
577 situation to a counterfactual situation that cannot be observed but simulated by either climate models
578 (climate attribution) or climate impact models (impact attribution). In the case of impact attribution, that
579 means simulations of the considered natural, human or managed system in the absence of climate
580 change, sea level rise, and changes in CO₂ concentrations. These simulations are now part of the
581 ISIMIP3a protocol. ¶

582 Impact attribution relies on a high explanatory power of impact models for historical observations. As
583 a first step, it has to be demonstrated that the processes represented in the impact model can explain
584 the observed changes in the affected system, i.e. it has to be shown that the model forced by observed
585 changes in the climate-related systems ('obsclim') and accounting for the historical development of
586 direct (human) forcings is able to reproduce the observed changes in the affected system (ISIMIP3a
587 evaluation experiments, see section 2.1). Thereby, models can either explicitly represent known
588 changes in non-climate drivers such as known adjustments of fertiliser input or growing seasons (explicit
589 accounting for non-climate drivers) or implicitly account for their potential contributions by e.g., allowing
590 for non-climate related temporal trends in empirical models as often done in empirical approaches
591 (implicit accounting for non-climate drivers). In a second step, the impact model can be used to describe
592 the counterfactual world without long-term changes in the climate-related systems by forcing it with the
593 observed changes in direct human influences as in the evaluation experiments (see section 2.1) but by
594 a counterfactual, stationary state of the climate-related systems (see Table 3). Attribution of climate
595 impacts to anthropogenic forcing would need an additional step separating anthropogenic climate
596 forcing from other sources of climate trends, which is not covered by the ISIMIP3a attribution setup.
597 Here, we describe the reasoning behind the individual experiments. Potentially required spin-up should
598 be identical to the corresponding 'obsclim' experiments mentioned in each description.

599 **Standard attribution experiment using counterfactual climate-related forcings and observed**
600 **variations of direct human forcings (counterclim + histsoc; default).** This is the twin experiment to
601 the default 'obsclim+histsoc' evaluation experiment. It uses the 'counterclim' climate-related forcings
602 as described in Table 3 while all direct human forcings are the same as the ones used in the evaluation
603 experiment ('histsoc'). As the corresponding evaluation experiment aims to ensure that impact models
604 can fully capture the historical variations including its long-term trends, this experiment is best suited
605 for impact attribution. It is therefore the standard impact attribution experiment that each sector should
606 strive to follow.

607
608 **Fixed 2015 direct human forcing attribution experiment (counterclim + 2015soc; default).** This
609 is the twin experiment to the 'obsclim+2015soc' experiment. It uses the 'counterclim' climate-related

610 forcings as described in **Table 3** and constant direct human forcings at 2015 levels ('2015soc'). Impact
 611 attribution using this experiment has caveats because the twin 'obsclim+2015soc' experiment is not
 612 built to fully explain the historical observations including its trends. Impact attribution building on this
 613 experiment therefore needs to find other means to ensure that the impact model correctly captures the
 614 response to changes in the climate-related systems. It may e.g. build on the assumption that fixed direct
 615 human forcings do not change the models' sensitivity to historical climate change. The impact models
 616 that cannot account for varying historical direct human forcings can take up the attribution task through
 617 this experiment.

618
 619 **Fixed 1901 direct human forcing attribution experiment (counterclim + 1901soc; default).** This is
 620 the twin experiment to the 'obsclim+1901soc' experiment. It allows for a quantification of the combined
 621 effect of changes in all forcings (climate-related and direct human) during the historical period when
 622 compared to the default evaluation experiment ('obsclim+histsoc'). It also allows for a quantification of
 623 the effect of varying direct human drivers when compared to the 'counterclim+histsoc' experiment and
 624 the effect of the 2015 to 1901 difference in direct human forcing if compared to the
 625 'counterclim+2015soc' experiment, conditional on counterclim climate-related forcings.

626
 627 **No direct human forcing attribution experiment (counterclim + nat; default)** This is the twin
 628 experiment to the default 'obsclim+nat' experiment. It allows for a quantification of the effect of climate
 629 change under conditions of absent direct human forcings but a natural state of the world. The 'nat'
 630 experiment is included in the *biomes* sector protocol.

631
 632 **Table 4: ISIMIP3a attribution experiments**

Experiment	Short description	Period: Historical 1901-2019
counterfactual climate	CRF: Detrended observational atmospheric climate forcing, detrended observed coastal water level forcings, and other CRF as listed in Table 3	counterclim
histsoc 1st priority	DHF: Varying direct human influences according to observations	histsoc
counterfactual climate 2015soc	CRF: Detrended observational atmospheric climate forcing, detrended observed coastal water level forcings, and other CRF as listed in Table 3	counterclim

1st priority	DHF: Fixed 2015 levels of direct human forcing for the entire time period	2015soc
counterfactual climate 1901soc	CRF: Detrended observational atmospheric climate forcing, detrended observed coastal water level forcings, and other CRF as listed in Table 3	counterclim
2nd priority	DHF: Fixed 1901 levels of direct human forcing for the entire time period	1901soc
counterfactual climate nat	CRF: Detrended observational atmospheric climate forcing, detrended observed coastal water level forcings, and other CRF as listed in Table 3	counterclim
2nd priority	DHF: No direct human influences	nat

633

634 3 Climate-related forcing data

635

636 3.1 Observational atmospheric climate forcing data (factual + counterfactual)

637

638 [The data sets described in this section all contain the variables listed in Table 5 at the resolution](#)
639 [indicated there. While section 3.1.1 described the standard atmospheric climate forcing as one](#)
640 [component of the default ‘obsclim’ CRF used within the evaluation experiments \(see section 2.1.1\).](#)
641 [section 3.1.2 describes the derivation of the high resolution data used within the ‘obsclim’-based](#)
642 [sensitivity experiments \(see section 2.1.2\), and section 3.1.3 provides a description of the basic](#)
643 [approach and the references for the derivation of the counterfactual atmospheric climate forcings](#)
644 [used for the ‘counterclim’ experiments described in section 2.2. ¶](#)

645 ¶

646 **Table 5:** Atmospheric climate variables provided as part of the climate-related forcing

Variable	Variable specifier	Unit	Resolutio n	Datasets
Near-Surface Relative Humidity	hurs	%	0.5° grid, daily	GSWP3-W5E5 (factual and counterfactual, 1901-2019), 20CRv3-W5E5 (factual and counterfactual, 1901-2019), 20CRv3-ERA5 (factual and counterfactual, 1901-2021), 20CRv3 (factual and counterfactual, 1901-2015)

Near-Surface Specific Humidity	huss	kg kg-1	0.5° grid, daily	GSWP3-W5E5 (factual and counterfactual, 1901-2019), 20CRv3-W5E5 (factual and counterfactual, 1901-2019), 20CRv3-ERA5 (factual and counterfactual, 1901-2021), 20CRv3 (factual and counterfactual, 1901-2015)
Precipitation (including snowfall)	pr	kg m-2 s-1	0.5° grid, daily	GSWP3-W5E5 (factual and counterfactual, 1901-2019), 20CRv3-W5E5 (factual and counterfactual, 1901-2019), 20CRv3-ERA5 (factual and counterfactual, 1901-2021), 20CRv3 (factual and counterfactual, 1901-2015)
			30" grid, 90" grid, 300" grid, 1800" grid; daily	CHELSA-W5E5 (factual, 1979-2016)
Snowfall	prsn	kg m-2 s-1	0.5° grid, daily	GSWP3-W5E5 (factual only, 1901-2019, 0.5°)
Surface Air Pressure	ps	Pa	0.5° grid, daily	GSWP3-W5E5 (factual and counterfactual, 1901-2019), 20CRv3-W5E5 (factual and counterfactual, 1901-2019), 20CRv3-ERA5 (factual and counterfactual, 1901-2021), 20CRv3 (factual and counterfactual, 1901-2015)
Surface Downwelling Longwave Radiation	rlds	W m-2	0.5° grid, daily	GSWP3-W5E5 (factual and counterfactual, 1901-2019), 20CRv3-W5E5 (factual and counterfactual, 1901-2019), 20CRv3-ERA5 (factual and counterfactual, 1901-2021), 20CRv3 (factual and counterfactual, 1901-2015)
Surface Downwelling Shortwave Radiation	rlds	W m-2	0.5° grid, daily	GSWP3-W5E5 (factual and counterfactual, 1901-2019), 20CRv3-W5E5 (factual and counterfactual, 1901-2019), 20CRv3-ERA5 (factual and counterfactual, 1901-2021),

				20CRv3 (factual and counterfactual, 1901-2015)
			30" grid, 90" grid, 300" grid, 1800" grid; daily	CHELSA-W5E5 (1979-2016)
Near-Surface Wind Speed	sfcwind	m s-1	0.5° grid, daily	GSWP3-W5E5 (factual and counterfactual, 1901-2019), 20CRv3-W5E5 (factual and counterfactual, 1901-2019), 20CRv3-ERA5 (factual and counterfactual, 1901-2021), 20CRv3 (factual and counterfactual, 1901-2015)
Near-Surface Air Temperature	tas	K	0.5° grid, daily	GSWP3-W5E5 (factual and counterfactual, 1901-2019), 20CRv3-W5E5 (factual and counterfactual, 1901-2019), 20CRv3-ERA5 (factual and counterfactual, 1901-2021), 20CRv3 (factual and counterfactual, 1901-2015)
			30" grid, 90" grid, 300" grid, 1800" grid; daily	CHELSA-W5E5 (1979-2016)
Daily Maximum Near-Surface Air Temperature	tasmax	K	0.5° grid, daily	GSWP3-W5E5 (factual and counterfactual, 1901-2019), 20CRv3-W5E5 (factual and counterfactual, 1901-2019), 20CRv3-ERA5 (factual and counterfactual, 1901-2021), 20CRv3 (factual and counterfactual, 1901-2015)
			30" grid, 90" grid, 300" grid, 1800" grid; daily	CHELSA-W5E5 (factual and counterfactual, 1979-2016)

Daily Minimum Near-Surface Air Temperature	tasmin	K	0.5° grid, daily	GSWP3-W5E5 (factual and counterfactual, 1901-2019), 20CRv3-W5E5 (factual and counterfactual, 1901-2019), 20CRv3-ERA5 (factual and counterfactual, 1901-2021), 20CRv3 (factual and counterfactual, 1901-2015)
			30" grid, 90" grid, 300" grid, 1800" grid; daily	CHELSA-W5E5 (1979-2016)

647

648 ¶

649 **3.1.1 Default factual data:** ¶

650 **As one component of the default ‘obsclim’ CRFs, we** provide four observational datasets specifically
651 generated for the evaluation experiments of ISIMIP3a: GSWP3-W5E5, 20CRv3-W5E5, 20CRv3-ERA5,
652 and 20CRv3. All four datasets have daily temporal and 0.5° spatial resolution [and cover the variables](#)
653 [listed in Table 5](#). Their temporal coverage varies, with GSWP3-W5E5 and 20CRv3-W5E5 covering
654 1901-2019, while 20CRv3-ERA5 covers 1901-2021 and 20CRv3 covers 1901-2015. Instead of
655 excluding datasets that do not cover the most recent years, we focused on including datasets that
656 start in 1901, to allow for a common spin-up procedure (described in section 2.1 for the ‘obsclim +
657 histsoc; default’ experiment), in order to support models that need to spin up, e.g., their carbon pools
658 under stable climate-related and direct human forcings before they can do the actual experiments.

659

660 The GSWP3-W5E5 dataset is based on W5E5 v2.0 (Lange et al., 2021), which is also used as the
661 observational reference dataset for the bias adjustment of climate input data for ISIMIP3b [that will be](#)
662 [described in an ISIMIP3b protocol paper](#)(Frieler, submitted 2023). W5E5 v2.0 combines WFDE5 v2.0
663 ~~(WATCH Forcing Data methodology applied to ERA5 reanalysis data over land;~~(Cucchi et al., 2020)
664 with data from the latest version of the European Reanalysis (ERA5; (Hersbach et al., 2020) over the
665 ocean. ~~WFDE5 v2.0 is generated with the WATCH Forcing Data methodology that includes bias~~
666 [adjustment of all variables \(Cucchi et al., 2020\)](#). Since W5E5 v2.0 only covers the years 1979 to 2019,
667 it was extended backward in time to the year 1901. For this extension, we used version 1.09 of the
668 Global Soil Wetness Project phase 3 (GSWP3) dataset (Kim, 2017), bias-adjusted to W5E5 v2.0 in
669 order to reduce discontinuities at the 1978–1979 transition. The method used for this bias adjustment
670 was ISIMIP3BASD v2.5 (Lange, 2019, 2021). The GSWP3 dataset is a dynamically downscaled and
671 bias-adjusted version of the Twentieth Century Reanalysis version 2 (20CRv2; (Compo et al., 2011)).
672 For a detailed description of the GSWP3-W5E5 dataset and its constituents, see (Mengel et al., 2021).

673

674 Unfortunately, for some variables, GSWP3 shows discontinuities at every turn of the month. The month-
675 by-month bias adjustment applied in its creation is responsible for this artefact (Rust et al., 2015). In
676 order to overcome this issue, which also affects GSWP3-W5E5, we additionally provide 20CRv3-
677 W5E5, a dataset where W5E5 v2.0 is backward-extended using ensemble member 1 of the Twentieth
678 Century Reanalysis version 3 (20CRv3; (Slivinski et al., 2019, 2021), interpolated to 0.5° and then bias-
679 adjusted to W5E5 v2.0 using ISIMIP3BASD v2.5. The 20CRv3-W5E5 data are continuous at every turn
680 of the month thanks to the application of ISIMIP3BASD v2.5 in running-window mode (see section 3.1).
681 Since GSWP3 is based on 20CRv2, the 20CRv3-W5E5 dataset can be considered an update of
682 GSWP3-W5E5.

683

684 Two more climate input datasets are provided in ISIMIP3a in order to facilitate climate input data-related
685 quantifications of uncertainty in the associated impact assessments. Those datasets are not based on
686 W5E5 to account for trend and variability artefacts in W5E5 that are related to the climatological infilling
687 procedures used to deal with gaps in the station observations employed for the bias adjustment of
688 ERA5 for the production of WFDE5 (for a detailed description of this caveat see
689 <https://data.isimip.org/caveats/20/>). The first of the additional ISIMIP3a climate input datasets is
690 20CRv3-ERA5, which was created in the same way as 20CRv3-W5E5, but using ERA5 instead of
691 W5E5 for the time period 1979-2021, and also as the bias adjustment target for the time period 1901-
692 1978. Finally, we also provide the ‘raw’ 20CRv3 data, i.e., ensemble member 1 of 20CRv3, interpolated
693 to 0.5° but not bias-adjusted to any other dataset. This dataset is included since it was generated with
694 only one method and did not need to be combined with another dataset to fully cover the 20th century.

695

696 **3.1.2 Default counterfactual data.** ¶

697 ~~To simulate the baseline ‘no climate change’ state of a human or natural system that is required for~~
698 ~~impact attribution, we provide a detrended version of the observational factual forcing data using the~~
699 ~~ATTRICI approach (ATTRibuting Climate Impacts, (Mengel et al., 2021). The method identifies the~~
700 ~~long-term shifts in the factual daily climate variables that are correlated to global mean temperature~~
701 ~~change assuming a smooth annual cycle of the associated scaling coefficients for each day of the year.~~
702 ~~The observed trends since 1901 are then removed from the observational data by projecting the~~
703 ~~observed data onto the estimated distributions assuming a fixed 1901 level of global warming. The~~
704 ~~projection is done through quantile mapping, a method borrowed from the bias adjustment literature. In~~
705 ~~this way we preserve the internal variability of the observed data in the sense that factual and~~
706 ~~counterfactual data for a given day have the same rank in their respective statistical distributions. The~~
707 ~~impact model simulations forced by the counterfactual climate inputs therefore allow for quantifying the~~
708 ~~contribution of the observed climate change (no matter from where the trends originate) to observed~~
709 ~~long-term changes in impact indicators but also for quantifying the contribution of the observed trend in~~
710 ~~climate to the magnitude of individual impact events.~~ ¶

711

712 **3.1.2 High resolution atmospheric factual data (CHELSA-W5E5)** ¶

713 This dataset is provided to facilitate the high resolution sensitivity experiment described in section [2.1.2](#).
714 It covers the global land area at 30'' (~1 km) horizontal and daily temporal resolution from 1979 to 2016
715 for the variables precipitation (pr), surface downwelling shortwave radiation (rsds), and daily mean,
716 minimum and maximum near-surface air temperature (tas, tasmin, tasmax). CHELSA-W5E5 v1.0
717 (Karger et al., 2022b) is a downscaled version of the W5E5 v1.0 dataset, where the downscaling is
718 done with the Climatologies at High resolution for the Earth's Land Surface Areas (CHELSA) v2.0
719 algorithm (Karger et al., 2017, 2021, 2022a).

720

721 This algorithm applies topographic adjustments based on surface altitude (orog) information from the
722 Global Multi-resolution Terrain Elevation Data 2010 (GMTED2010; (Danielson and Gesch, 2011)). The
723 algorithm is applied day by day. CHELSA-W5E5 tas is obtained by applying a lapse rate adjustment to
724 W5E5 tas, using differences between CHELSA-W5E5 orog and W5E5 orog in combination with
725 temperature lapse rates from ERA5. Those lapse rates are calculated based on atmospheric
726 temperature, T , at 950 hPa and 850 hPa, and the geopotential height, z , of those pressure levels. The
727 lapse rate used for the adjustment is calculated as the daily mean of hourly values of $(T_{850} - T_{950}) /$
728 $(z_{850} - z_{950})$. The variables tasmax and tasmin are downscaled in the same way, using the same
729 lapse rate value.

730 Precipitation downscaling uses daily mean zonal and meridional wind components from ERA5 to
731 approximate the orographic wind effect on small-scale precipitation patterns (differences between
732 windward and leeward precipitation rates) and combines that with the height of the planetary boundary
733 layer to estimate the total orographic effect on precipitation intensity. Using that, precipitation from
734 W5E5 is downscaled such that precipitation fluxes are preserved at the original 0.5° resolution of W5E5.
735 More details are given in (Karger et al., 2021).

736 Surface downwelling shortwave radiation, rsds, at 30 arcsec resolution is strongly influenced by
737 topographic features such as aspect or terrain shadows, which are less pronounced at 0.5° resolution.
738 The downscaling algorithm combines such geometric effects with orographic effects on cloud cover for
739 an orographic adjustment of rsds. Geometric effects are considered by computing 30'' clear-sky
740 radiation estimates using the method described in (Karger et al., 2022a) and a simplified, uniform
741 atmospheric transmittance of 80%. These effects include shadowing from surrounding terrain, diffuse
742 radiation, and terrain aspect. To include how orographic effects on cloud cover influence rsds, the clear-
743 sky radiation estimates are adjusted using downscaled ERA5 total cloud cover. The cloud cover
744 downscaling uses ERA5 cloud cover at all pressure levels and the orographic wind field following the
745 methods described in (Brun et al., 2022b). Finally, the clear-sky radiation estimates adjusted for cloud
746 cover are rescaled such that they match W5E5 rsds, B-spline interpolated to 30''.

747 We provide the original CHELSA-W5E5 data with a horizontal resolution of 30'' = 0.5' (~1 km) as well
748 as spatially aggregated versions with resolutions of 1.5' (~3 km, aggregation factor 3), 5.0' (~10 km,
749 aggregation factor 10) and 30.0' = 0.5° (~60 km, aggregation factor 60). The aggregation to 0.5° is
750 necessary since the aggregated CHELSA-W5E5 data differ from the default GSWP3-W5E5 and

751 20CRv3-W5E5 data provided in the ‘obsclim’ set-up for 1979-2016. This has two reasons. First, the
 752 downscaled data are based on W5E5 v1.0 whereas GSWP3-W5E5 and 20CRv3-W5E5 are based on
 753 W5E5 v2.0. Secondly, for all variables except pr, the CHELSA downscaling algorithm produces data
 754 that differs from the original data when it is upscaled (spatially aggregated) back to the original
 755 resolution.

756

757 We do not provide a counterfactual version of the high resolution climate forcing.

758

759 The CHELSA method is not yet available for all variables included in the standard forcing data. Relative
 760 humidity, surface wind, air pressure, and longwave radiation can not yet be downscaled by the
 761 approach. To allow modellers to start the sensitivity experiments already now, we provide an alternative
 762 downscaling approach as described below. We use observational data with the required higher spatial
 763 resolution but lower temporal resolution to generate the high resolution daily relative humidity and
 764 surface wind speeds. Air pressure is derived by on orographic correction of the linearly interpolated sea
 765 level pressure and surface downwelling longwave radiation is derived from high-resolution
 766 temperatures derived by CHELSA and relative humidity. The code required to generate the data is
 767 freely available (Malle, 2023).

768

769 For daily mean near-surface relative humidity (hurs) the provided downscaling algorithm combines
 770 monthly 30” CHELSA-BIOCLIM+ data (Brun et al., 2022b, a) with daily W5E5 data. In a first step we
 771 regrid daily 0.5° W5E5 hurs to the target grid (30”) by bilinear interpolation. We assume relative humidity
 772 to follow a beta-distribution and logit-transform both regrided monthly-averaged W5E5 ($hurs_{mon}^{W5E5}$) and
 773 monthly CHELSA-BIOCLIM+ ($hurs_{mon}^{CHELSA}$) relative humidity data. The difference ($\Delta hurs_{mon}$) is then
 774 added to daily regrided and logit-transformed W5E5 hurs of the respective month, and the final raster
 775 is obtained by back-transforming the sum:

776
$$hurs_{dly} = \frac{1}{(1+exp^{-h})} , (1)$$

777 where

778
$$h = \log\left(\frac{hurs_{dly}^{W5E5}}{1-hurs_{dly}^{W5E5}}\right) + \Delta hurs_{mon} , (2)$$

779
$$\Delta hurs_{mon} = \log\left(\frac{hurs_{mon}^{CHELSA}}{1-hurs_{mon}^{CHELSA}}\right) - \log\left(\frac{hurs_{mon}^{W5E5}}{1-hurs_{mon}^{W5E5}}\right) . (3)$$

780 To include orographic effects into daily mean near-surface wind speed (*sfcwind*) we follow the approach
 781 of (Brun et al., 2022b), and use an aggregation of the Global Wind Atlas 3.0 data (Badger et al.,
 782 n.d.) Technical University of Denmark (Badger et al., n.d.) in combination with daily 0.5° sfcwind from
 783 W5E5. We first regrid both the Global Wind Atlas data and the W5E5 sfcwind data to the target grid of
 784 30” using bilinear interpolation. The Global Wind Atlas data product ($sfcWind_{cli}^{GWA}$) represents average

785 wind speeds for 2008 to 2017. We therefore average daily regrided W5E5 data over this time period
 786 ($sfcWind_{cli}^{W5E5}$). We assume surface wind speeds follows a Weibull distribution and log-transform both
 787 datasets before computing the difference $\Delta sfcWind_{cli}$, whereby a small positive constant (c) was added
 788 to all data points before applying the transformation to avoid the problem that $\log(0)$ is undefined. We
 789 add this difference layer ($\Delta sfcWind_{cli}$) to each log-transformed daily W5E5 raster, and back-transform
 790 the sum to obtain the final daily mean near-surface wind speed raster:

$$791 \quad sfcWind_{dly} = \exp^{(\log(sfcWind_{dly}^{W5E5} + c) + \Delta sfcWind_{cli}) - c}, \quad (4)$$

792 where

$$793 \quad \Delta sfcWind_{cli} = \log(sfcWind_{cli}^{GWA} + c) - \log(sfcWind_{cli}^{W5E5} + c). \quad (5)$$

794

795 Daily mean surface air pressure (ps) is calculated using the barometric formula:

$$796 \quad ps_{dly} = psl_{dly}^{W5E5} \times \exp^{-(g \times orog \times M)/(T_0 \times R)}, \quad (6)$$

797 with psl_{dly}^{W5E5} being the regrided 0.5° W5E5 daily mean sea-level pressure (bilinear interpolation to 30"),
 798 g the gravitational acceleration constant (9.80665 m/s²), $orog$ the altitude at which air pressure is
 799 calculated (CHELSA-W5E5 orog, m), M the molar mass of dry air (0.02896968 kg/mol), R the universal
 800 gas constant (8.314462618 J/(mol K)) and T_0 the sea level standard temperature (288.16 K).

801

802 For Surface Downwelling Longwave Radiation ($rlds$) we follow (Fiddes and Gruber, 2014) as well as
 803 (Konzelmann et al., 1994), and account for orographic effects by reducing the clear-sky component of
 804 all-sky emissivity with elevation. We assume cloud emissivity remains unchanged when moving from
 805 coarse to fine resolution. First, we compute clear-sky emissivity components both for the 0.5° W5E5
 806 grid and the target 30" grid (ϵ_{clear}^{W5E5} , $\epsilon_{clear}^{highres}$ respectively):

$$807 \quad \epsilon_{clear}^{highres/W5E5} = 0.23 + x1(pV_{dly}^{highres/W5E5} / tas_{dly}^{highres/W5E5})^{1/x2}, \quad (7)$$

808 where $x1 = 0.43$ and $x2 = 5.7$ and $pV_{dly}^{highres/W5E5}$ is water vapour pressure as a function of relative
 809 humidity at the respective resolution (see (Fiddes and Gruber, 2014)). By using 0.5° W5E5 $rlds$ and tas
 810 data and inverting the Stefan-Boltzmann equation we obtain all-sky emissivity:

$$811 \quad \epsilon_{allsky}^{W5E5} = rlds_{dly}^{W5E5} / (\sigma \times (tas_{dly}^{W5E5})^4), \quad (8)$$

812 with σ being the Stefan-Boltzmann constant (5.67 x 10⁻⁸ Js⁻¹ m⁻² K⁻⁴). In a next step, the cloud-based
 813 component of emissivity ($\Delta \epsilon_{dly}^{W5E5}$) can be estimated as the difference between all-sky and clear-sky
 814 emissivity, which is then regrided to the target grid via bilinear interpolation.

815
$$\Delta\epsilon_{dly}^{W5E5} = \epsilon_{allsky}^{W5E5} - \epsilon_{clear}^{W5E5} \quad (9)$$

816 In a last step we obtain elevation-corrected longwave radiation ($rlds_{dly}$) by adding $\Delta\epsilon_{dly}^{W5E5}$ to the high-
 817 resolution clear-sky emissivity ($\epsilon_{clear}^{highres}$) and applying the Stefan-Boltzmann law again:

818
$$rlds_{dly} = (\epsilon_{clear}^{highres} + \Delta\epsilon_{dly}^{W5E5}) \times \sigma \times (tas_{dly}^{highres})^4 \quad (10)$$

819 As soon as the CHELSA approach is extended to also cover the missing variable we plan to also provide
 820 these data and test for the sensitivity of the impact simulations to these two alternative downscaling
 821 methods. ¶

822 ¶

823 [3.1.3 Default counterfactual data.](#) ¶

824 [To simulate the baseline ‘no climate change’ state of a human or natural system that is required for](#)
 825 [impact attribution, we provide a detrended version of the observational factual forcing data using the](#)
 826 [ATTRICI approach \(ATTRibuting Climate Impacts, Mengel et al., 2021\). The method identifies the long-](#)
 827 [term shifts in the factual daily climate variables that are correlated to global mean temperature change](#)
 828 [assuming a smooth annual cycle of the associated scaling coefficients for each day of the year. The](#)
 829 [observed trends since 1901 are then removed from the observational data by projecting the observed](#)
 830 [data onto the estimated distributions assuming a fixed 1901 level of global warming. The projection is](#)
 831 [done through quantile mapping, a method borrowed from the bias adjustment literature. In this way we](#)
 832 [preserve the internal variability of the observed data in the sense that factual and counterfactual data](#)
 833 [for a given day have the same rank in their respective statistical distributions. The impact model](#)
 834 [simulations forced by the counterfactual climate inputs therefore allow for quantifying the contribution](#)
 835 [of the observed climate change \(no matter from where the trends originate\) to observed long-term](#)
 836 [changes in impact indicators but also for quantifying the contribution of the observed trend in climate to](#)
 837 [the magnitude of individual impact events.](#) ¶

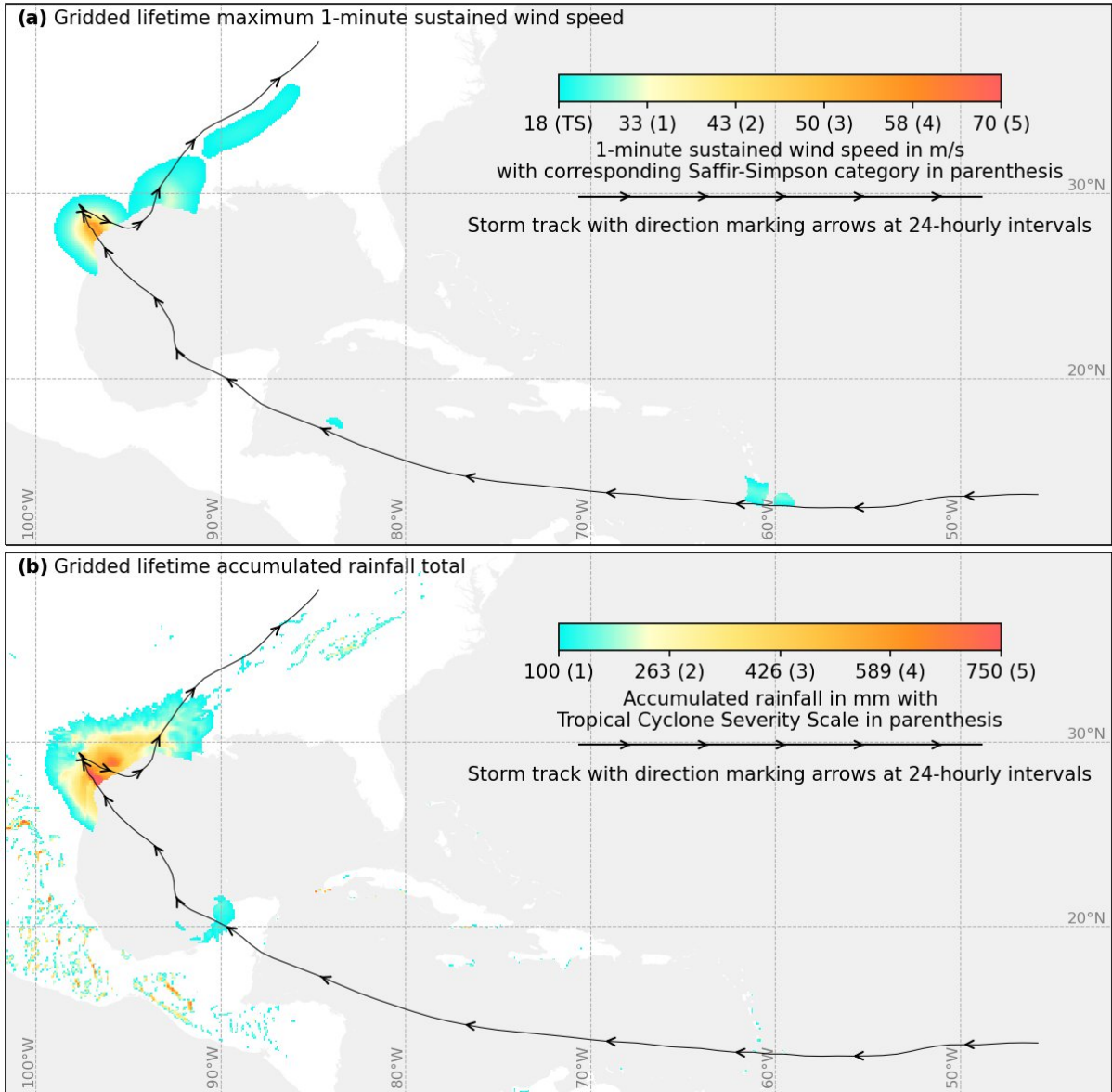
838

839

840 **3.2 Tropical cyclone (TC) data (factual)**

841

Hurricane Harvey (2017)



842
843
844
845
846
847
848
849
850

Figure 2: Tropical cyclone storm track (a and b, line with arrows), and derived maximum wind speeds (a, coloured shades) and accumulated rainfall totals (b, coloured shades), according to the Holland wind profile, (Holland, 1980, 2008) of Hurricane Harvey major hurricane Laura that made landfall in Texas Louisiana (USA) in August 2017. The wind speeds are according to the Holland wind profile (Holland, 1980, 2008), and the rainfall is according to the TCR model (Zhu et al., 2013). The colouring in (b) follows the “Tropical Cyclone Severity Scale” (Bloemendaal et al., 2021).

Table 6: Tropical cyclone information provided as part of the ISIMIP3a climate-related forcing

Variable	Variable specifier	Unit	Resolution	Datasets
Time associated with a given location of the storm centre	time	hours since 1950-01-01 00:00	along-track, at least 3-hourly	IBTrACS (1950-2021, postprocessed)

Latitudinal/ longitudinal coordinate of storm centre (as defined by the reporting agencies)	lat lon	degrees north/ east	along-track, at least 3-hourly	IBTrACS (1950-2021, postprocessed)
Longitudinal coordinate of storm centre (as defined by the reporting agencies)	lon	degrees east	along-track, at least 3-hourly	IBTrACS (1950-2021, postprocessed)
Ocean basin: NA/SA (North/South Atlantic), EP/WP/SP (East/West/South Pacific), NI/SI (North/South Indian Ocean)	basin	two-letter abbreviation	along-track, at least 3-hourly	IBTrACS (1950-2021, postprocessed)
Central pressure	pres	hPa	along-track, at least 3-hourly	IBTrACS (1950-2021, postprocessed)
Environmental pressure (pressure of the outermost closed isobar)	penv	mbar	along-track, at least 3-hourly	IBTrACS (1950-2021, postprocessed)
Maximum 1-minute sustained wind speed	wind spatial max	knots	along-track, at least 3-hourly	IBTrACS (1950-2021, postprocessed)
Radius of maximum wind speeds	rmw	nautical miles	along-track, at least 3-hourly	IBTrACS (1950-2021, postprocessed)
Radius of the outermost closed isobar	roci	nautical miles	along-track, at least 3-hourly	IBTrACS (1950-2021, postprocessed)
Wind speed on the 850 hPa pressure level	u850 v850	ms ⁻¹	along-track, at least 3-hourly	IBTrACS (1950-2021, postprocessed)
Temperature on the 600 hPa pressure level	T t600	K	along-track, at least 3-hourly	IBTrACS (1950-2021, postprocessed)

1-minute sustained wind speed	wind	ms ⁻¹	along-track, at least 3-hourly on a 300 arc-seconds (~10 km) grid	according to the Holland wind profile (Holland, 1980, 2008) and the Emanuel-Rotunno wind profile (Emanuel and Rotunno, 2011)
Gridded lifetime Maximum 1-minute sustained wind speed during the whole storm duration	max_windlif etimemax	ms ⁻¹	per stormfor each TC on a 300 arc-seconds (~10 km) grid	according to the Holland wind profile (Holland, 1980, 2008) and the Emanuel-Rotunno wind profile (Emanuel and Rotunno, 2011)
National territory exposed to wind speeds of at least 34, 48, 64, 96 knots	34kn_area 48kn_area 64kn_area 96kn_area	km ²	per stormfor each TC and country	according to the Holland- wind profile (Holland, 1980, 2008) and to the Emanuel-Rotunno wind profile (Emanuel and Rotunno, 2011)
Number of people exposed to wind speeds of at least 34, 48, 64, 96 knots	34kn_pop 48kn_pop 64kn_pop 96kn_pop	count	per stormfor each TC and country	according to the Holland wind profile (Holland, 1980, 2008) and to the Emanuel-Rotunno wind profile (Emanuel and Rotunno, 2011) and assuming temporally varying (histsoc) or fixed 2015 (2015soc) population distributions (see section 4.1).
Economic assets exposed to wind speeds of at least 34, 48, 64, 96 knots	34kn_asset s 48kn_asset s	Int\$ PPP 2005	per stormfor each TC and country	Windfields according to the Holland wind profile (Holland, 1980, 2008) and Emanuel-Rotunno

	64kn_assets 96kn_assets			wind profile (Emanuel and Rotunno, 2011) and assuming temporally varying (histsoc) or fixed 2015 (2015soc) asset distributions (see section 4.2).
<u>Total</u> rainfall	rain	mm	along track, at least 3-hourly on a 300 arc-seconds (~10 km) grid	according to the Holland wind profile (Holland, 1980, 2008) and to the Emanuel-Rotunno wind profile (Emanuel and Rotunno, 2011)
Maximum 24-hourly rainfall <u>total</u> during the whole storm duration	max_rain	mm	per storm for each TC on a 300 arc-seconds (~10 km) grid	according to the Holland wind profile (Holland, 1980, 2008) and to the Emanuel-Rotunno wind profile (Emanuel and Rotunno, 2011)

851 As additional CRF, we provide historical TC tracks (information about the observed location of minimal
852 pressure), with associated gridded wind and rain fields ([see variable names and units in Table 6 and](#)
853 [the maps of maximum wind speed and accumulated rainfall totals for the example of hurricane Harvey](#)
854 [in Figure 2](#)). In addition to this purely CRF, we also provide wind exposure in terms of (i) shares of
855 national territory affected by extreme winds speeds, (ii) national shares of people exposed to extreme
856 winds speeds, and (iii) national shares of economic assets affected by extreme winds speeds as derived
857 from the estimated wind fields and historical population and GDP distributions (see below). [Table 6](#)
858 [provides a comprehensive list of all variables, their meaning and resolution as well as their source.](#)

859

860 **TC Tracks (position of storm centre, central pressure, environmental pressure, radius of**
861 **maximum wind speed and the outermost closed isobar)**. We provide processed track information
862 of historical TCs from 1950 to 2021. The information is derived from IBTrACS, the most comprehensive
863 global dataset of historical TC activity (Knapp et al., 2010) that provides information about the location
864 of the storm centre, the pressure at the centre and at the outermost closed isobar as well as the
865 maximum 1-minute sustained wind speed as reported by the WMO Regional Specialised Meteorological

866 Centers (RSMCs) and by agencies in Shanghai and Hong Kong. For recent events and most reporting
867 agencies, IBTrACS also contains observational information about the radius from the centre where
868 maximum wind speed is attained and the radius of the outermost closed isobar. Information is provided
869 in at least 6-hourly time steps. Usually temporal resolution reaches three hours or even less. The latest
870 version (v04r00) of IBTrACS is continuously updated with near real time data taken from regional
871 meteorological agencies. The data is marked as provisional before it is replaced by so-called best track
872 data one-up to two years after the events. IBTrACS contains data from 1842 to present, but coverage
873 by the WMO RSMCs starts much later for some of the basins (around 1850 for the North Atlantic and
874 South Indian, in 1905 for the South Pacific, in 1950 for the North Pacific, and in 1990 for the Northern
875 Indian basin). Data quality is globally consistent starting from the mid 1970s when satellite observations
876 became available.

877 The data set we provide uses best track data from 1950 to 2021. For each TC in IBTrACS, we merge
878 the data of different reporting agencies into a single track data set with information about the following
879 variables: time, location of the storm centre, ocean basin, central pressure, maximum 1-minute
880 sustained wind speed, environmental pressure, radius of maximum wind speeds, and radius of the
881 outermost closed isobar (see Table 8). Several processing steps are applied to ensure consistency and
882 completeness of the data: For each storm, the variables that are not reported by the officially responsible
883 WMO RSMC for this storm are taken from the next agency in the following list that did report this variable
884 for this storm: the US agencies (NHC, JTWC, CPHC), Japanese Meteorological Agency, Indian
885 Meteorological Department, MeteoFrance (La Reunion), Bureau of Meteorology (Australia), Fiji
886 Meteorological Service, New Zealand MetService, Chinese Meteorological Administration, Hong Kong
887 Observatory. Thus, for different storms, the same variable might be taken from different agencies. As
888 sustained wind speeds are reported at different averaging intervals by different agencies, we use
889 multiplicative factors to rescale all wind speeds to 1-minute sustained winds (Knapp and Kruk, 2010).
890 All variables are extracted at the highest temporal resolution where time and location information is
891 available in IBTrACS. Temporal reporting gaps within a variable are linearly interpolated so that the
892 temporal resolution is at least 3-hourly. After interpolation, time steps where neither central pressure
893 nor maximum wind speeds are available, are discarded. Tracks with less than two valid time steps are
894 discarded. If at least one of central pressure or maximum wind speed is available, one variable is
895 estimated from the other using statistical wind-pressure relationships. Missing RMW and ROCI values
896 are estimated from the central pressure using statistical relationships. Finally, missing environmental
897 pressure values are filled with basin-specific defaults (1010 hPa for the Atlantic and Eastern Pacific,
898 1005 hPa for the Indian Ocean and Western Pacific, and 1004 hPa for the South Pacific).

899 We provide two additional along-track variables that are taken from the European Reanalysis (ERA5;
900 Hersbach et al., 2020), and that are needed for the computation of precipitation (see below): The
901 temperature at the storm centre on the 600 hPa pressure level, and the wind speed on the 850 hPa
902 pressure level, averaged over the 200-500 km annulus around the storm centre.

903 **Gridded maps of (maximum) wind speeds.** We derive two different gridded wind field products from
904 an extrapolation of the observed TC track information to gridded estimates of surface wind speeds (1-

905 minute sustained winds at 10 metres above ground), at a spatial resolution of 300 arc-seconds
906 (approximately 10 km). The two products are based on circular wind fields from different radial wind
907 profiles. The first is a semiempirical model that estimates the full wind profile from the central pressure
908 variable based on the gradient wind balance assumption (Holland, 1980, 2008). The second, more
909 physics-based model uses the less-reliable maximum wind speed variable to derive the wind profile
910 from the boundary layer angular momentum balance (Emanuel and Rotunno, 2011). This wind profile
911 represents the storm's inner core very well, but tails off too sharply in the outer region (Chavas and Lin,
912 2016). However, for high-impact events, the core is the most relevant storm region, and outer wind
913 profiles are not analytically solvable, incurring considerable computational expense when applied to a
914 large track set.

915 In both cases, the circular wind fields are combined with translational wind vectors that arise from the
916 TC movement, assuming that the influence of translational wind decreases with distance from the TC
917 centre (Cyclone Database Manager, 2023). We use the highest available temporal resolution (up to 3-
918 hourly) provided in IBTrACS and interpolate it to 1-hourly resolution before applying the parametric
919 wind field models. In a postprocessing step, we also calculate the maximum value of wind speeds over
920 the duration of the TC event ('max_wind').

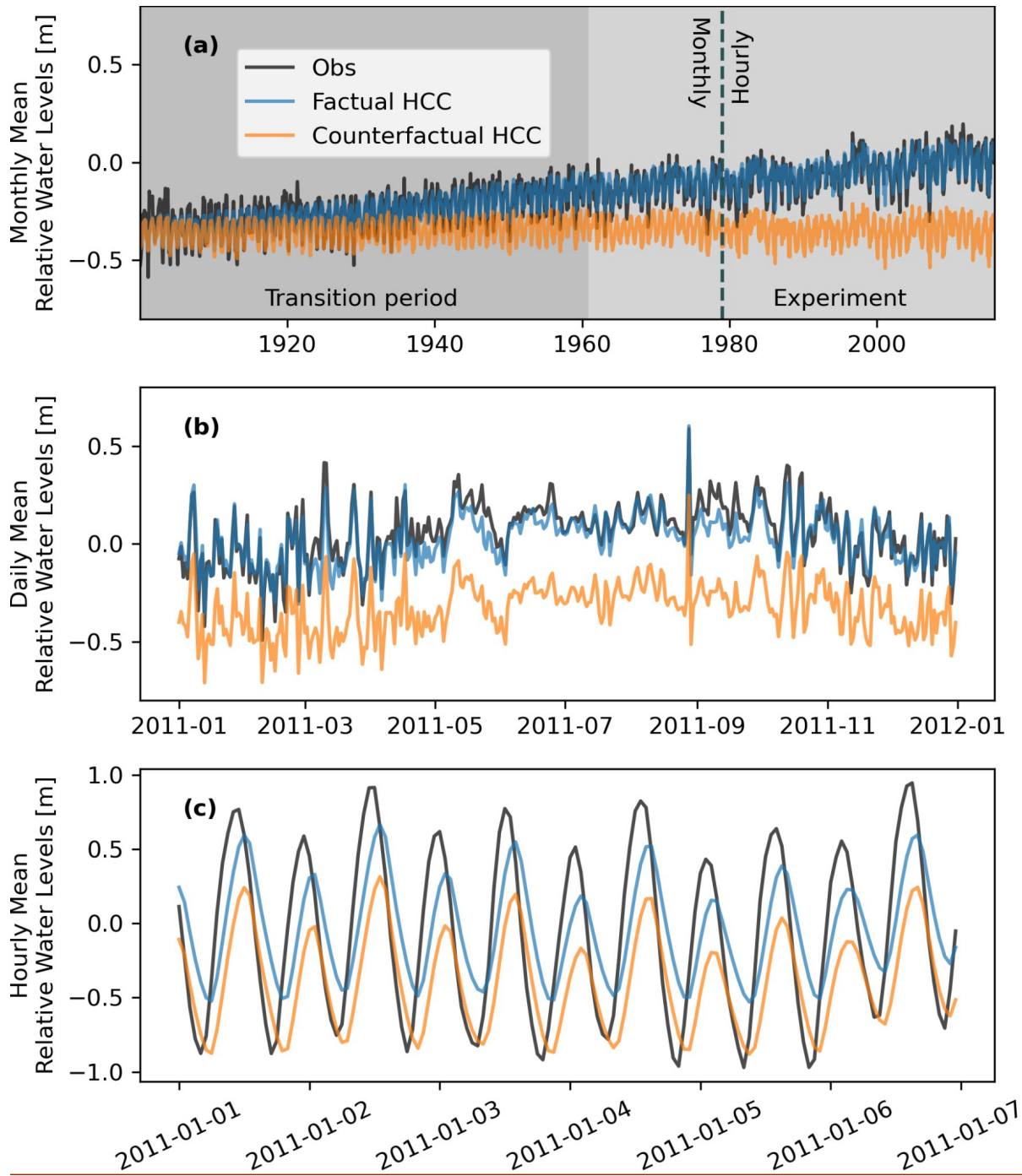
921 The approach by Holland has been successfully applied in socioeconomic risk and impact analyses
922 (Peduzzi et al., 2012; Geiger et al., 2018; Eberenz et al., 2021). The Emanuel-Rotunno approach has
923 been used for storm surge simulations (Krien et al., 2017; Marsooli et al., 2019; Gori et al., 2020; Yang
924 et al., 2021), and as the basis for the rain field model that we describe below (Feldmann et al., 2019).

925 **Wind Exposure.** As an extension of the tropical cyclone exposure data set TCE-DAT (Geiger et al.,
926 2018), we provide national shares of people and economic assets exposed to 1-minute sustained winds
927 above 34, 48, 64, and 96 knots for each storm. In addition to that, shares of national territory affected
928 by 1-minute sustained winds above 34, 48, 64, and 96 knots are provided. To estimate the exposed
929 population and assets we use the 'histsoc' population and GDP distributions described in section 4.1
930 and section 4.2, respectively. The GDP values are converted to assets by applying the decadal (2010-
931 2019) mean of national capital stock to GDP ratios from the Penn World Table version 10.0 (Feenstra
932 et al., 2015). We also provide exposed population and assets assuming fixed 2015 population and
933 asset distributions.

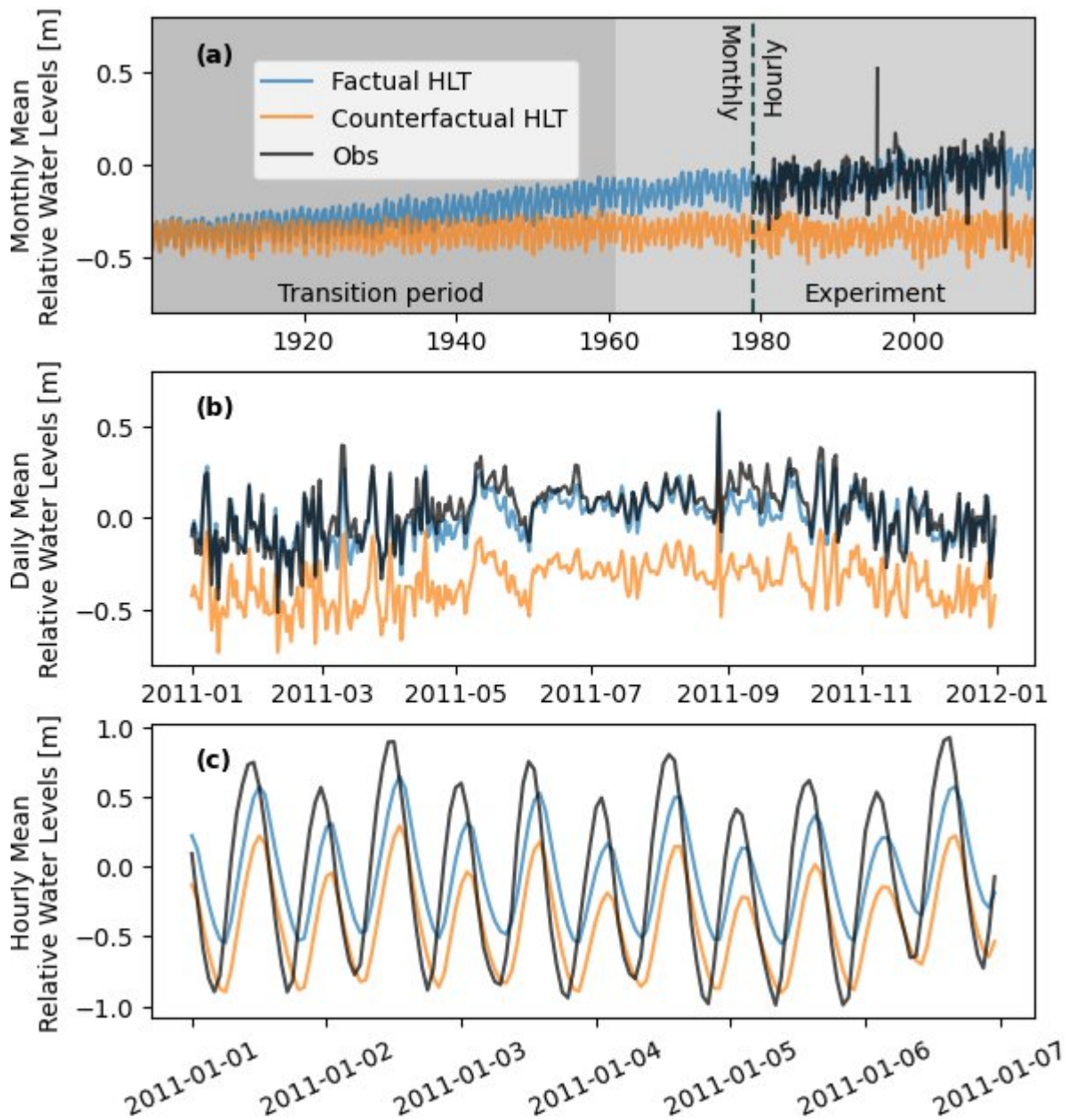
934 **Precipitation.** We are also planning to provide rainfall fields, following a physics-based model that
935 simulates convective TC rainfall by relating the precipitation rate to the total upward velocity within the
936 TC vortex (Zhu et al., 2013). The approach has been successfully applied in rainfall risk assessments
937 in the US (Feldmann et al., 2019; Gori et al., 2022). The rain rate will be simulated for all events in the
938 IBTrACS database at 0.5-hourly temporal and 300 arc-seconds (approximately 10 km) spatial resolution
939 within a 1500 km radius around the storm center ~~the storm extent defined by the ROCI storm~~
940 ~~track variable.~~ We provide the derived rainfall totals at hourly resolution as well as ~~We will also~~
941 ~~aggregate the result to~~ the maximum 24-hourly rainfall total during the entire storm duration since this
942 variable is frequently used for rainfall risk assessment studies (Fagnant et al., 2020).

943 Different TC wind profiles can be used as an input for the rain field model (Lu et al., 2018; Xi et al.,
944 2020). We will provide the rainfall fields for the two wind profile models by Holland and Emanuel-
945 Rotunno that we also use for the wind fields described above.

947 **3.3 Coastal water levels (factual + counterfactual)**
948



949



950

951

952 **Figure 3: Observed and reconstructed coastal relative water levels** at New York, USA. The counterfactual
 953 baseline represents water levels without long-term trend since 1900. Water levels are aggregated to monthly
 954 means in panel (a) and daily means in the year 2011 in panel (b) while panel c shows part of the data in hourly
 955 resolution. The reconstructed water levels are available as monthly mean values from 1901⁹ to 1978⁹ and as
 956 hourly mean values from 1979 to 2015.

957

958

Table 7: Information about coastal water levels provided as ISIMIP3a climate-related forcing.

Variable	Variable specifier	Unit	Resolution	Datasets
Coastal water levels	cwl	m	custom coastal grid; monthly from 1901 to 1978 and hourly from 1979 to 2015	HCCHLT obsclim and counterclim (Treu et al., submitted-2023)

959

960 To enable the quantification of impacts of historical relative sea level rise on coastal systems we provide
961 observation-based coastal water levels building on the [HCCHLT dataset](#) ([Hourly Coastal water levels](#)
962 [with Counterfactual Hourly sea level change with long-term trends for impact attribution](#); (Treu et al.,
963 [submitted-2023](#)). In contrast to absolute sea levels, relative sea levels are measured against a land-
964 based reference frame (tide gauge measurements). This means that they are not only determined by
965 thermal expansion, loss of land ice, or dynamical processes influenced by climate change, but also by
966 vertical land movements (Wöppelmann and Marcos, 2016) induced by, e.g., glacial isostatic
967 adjustments (Caron et al., 2018; Whitehouse, 2018) or human interventions such as ground water
968 abstraction (Wada et al., 2016a). [HCCHLT](#) encompasses factual and counterfactual coastal water
969 levels along global coastlines from 1901 to 1978 on monthly resolution and from 1979 to 2015 on hourly
970 resolution ([see Figure 3](#)). The counterfactual [coastal water levels](#) are derived from the factual dataset
971 by removing the trend in relative sea level since 1900. The detrending preserves the timing of historical
972 extreme sea-level events similar to the counterfactual atmospheric climate forcing described in section
973 [3.1](#) ([see Figure 3, panel B](#)). Hence, the data can be used for an event-based attribution of, e.g.,
974 observed flooding to observed relative sea-level rise with [pairstuples](#) of impact simulations driven with
975 the factual and counterfactual datasets. It is important to highlight that ‘attribution to observed changes
976 in relative water levels’ does not imply attribution to anthropogenic climate forcing because such
977 observed changes may include trends that are not driven by human greenhouse gas emissions.
978 Important sources for such trends are the ongoing adjustments of ice sheets, glaciers and the earth
979 crust to climate conditions before industrialization (Slangen et al. 2016) and the land subsidence due
980 to water, gas and oil extraction (Nicholls et al. 2021). In the following the derivation of the data is
981 described in more detail.

982
983 **Default factual data.** To capture the impacts of extreme water levels we provide hourly observation-
984 based coastal water levels as forcing data. To this end we combine the Coastal Dataset for the
985 Evaluation of Climate Impact (CoDEC) dataset (Muis et al., 2020) that describes high frequency
986 variation of sea level along global coastlines with a recent reconstruction of observed long-term sea-
987 level rise (Dangendorf et al., 2019). The CoDEC hourly data builds on a shallow-water model with fixed
988 ocean density driven by ERA5 wind and atmospheric pressure fields. The CoDEC data thus starts only
989 in the year 1979 and does not include variations due to ocean density changes and multi-year trends
990 from observed sea-level rise or vertical land movement. In contrast, the hybrid reconstructions (HR)
991 dataset from (Dangendorf et al., 2019) represents sea-level change since 1900 on a monthly timescale,
992 including density variations and multi-year trends. Long term sea-level change in HR is based on fitting
993 theoretically known and modelled spatial-temporal fields of individual contributing factors of sea level
994 change to a set of observations of sea level change from tide gauges. The individual contributing factors
995 are theoretically known cryospheric fingerprints from two ice sheets, 18 major glacier regions, glacial
996 isostatic adjustment from 161 Earth rheological models and dynamic changes of sea surface height
997 modelled by six global climate models. Short term sea-level variations are represented in HR by
998 extending the spatio-temporal patterns from satellite altimetry back to the year 1900 using tide gauge
999 records. We create the [HCCHLT](#) dataset by low-pass filtering the HR dataset and high-pass filtering

1000 the CoDEC dataset before summing them. [Vertical land motion is subsequently added to yield relative](#)
1001 [changes of water levels along global coastlines](#). [HCCHLT](#) shows improved agreement with tide gauge
1002 records on hourly to monthly time scales when compared to CoDEC due to the inclusion of density
1003 variations. This is most apparent for lower latitudes. The performance on interannual time scales is
1004 equal to (Dangendorf et al., 2019).

1005

1006 **Default counterfactual data.** To estimate the effects of historical sea-level rise on coastal systems,
1007 we provide a counterfactual sea-level dataset as forcing for coastal impact models (Treu et al.,
1008 [submitted-2023](#)). To this end the long term trend in the [HCCHLT](#) data (1900-2015) was identified by a
1009 simple quadratic model in time and subtracted from the factual [HCCHLT](#) data. The quadratic model
1010 assumes a constant acceleration of sea-level rise over time. Analysis of sea level rise acceleration
1011 shows variation throughout the last century with an acceleration phase in the early century followed by
1012 a deceleration and then again acceleration until today (Dangendorf et al., 2019). By design, this
1013 variation is not included in our quadratic trend estimate. In general, we expect our trend estimation to
1014 largely exclude natural variability from the trend due to the low dimensionality of the trend model and
1015 the long data period. This is a desired outcome and preserves the natural variability in the
1016 counterfactual. Extreme sea-level events have the same timing in the counterfactual and the factual
1017 dataset, facilitating event-based impact attribution.

1018

1019 **3.4 Ocean data (factual)**

1020

1021 **Default factual data.** For the fisheries and marine ecosystem models, we provide a number of physical
1022 and biogeochemical variables for the period 1961 to 2010 at different depth levels in the ocean (see
1023 [Table 810](#)). Since direct measurements of these variables are very scarce (Sarmiento and Gruber,
1024 2006, WOCE Atlas, 2023), the only way to obtain a globally (or even regionally) complete and consistent
1025 forcing dataset is to use numerical models. Global ocean models, which also serve as oceanic
1026 components of Earth System models, often simulate many or all of the required variables. To let
1027 observations at least indirectly enter the oceanic forcing data for ISIMIP3a, we provide outputs from an
1028 ocean model run that is forced by an observation-based reanalysis product of atmospheric forcing (Liu
1029 et al., 2021). Compared to the oceanic forcing (Stock et al., 2014) provided to generate the ISIMIP2a
1030 simulations for the *marine ecosystems and fisheries* sector (Tittensor et al., 2018), this new dataset is
1031 based on the latest GFDL-MOM6 and COBALTv2 physical and biogeochemical ocean models running
1032 on a tripolar 0.25° grid and using the JRA-55 reanalysis (Tsujino et al., 2018) as the surface forcing, in
1033 contrast to the inter-annual forcing dataset of (Large and Yeager, 2009), which was previously used to
1034 drive GFDL-MOM4. The simulations also account for dynamic, time-varying river freshwater and
1035 nitrogen inputs that were simulated based on GFDL's land-watershed model LM3-TAN (Land Model
1036 version 3 with Terrestrial and Aquatic Nitrogen; (Lee et al., 2019), adjusted using observations from the
1037 Global Nutrient Export from WaterSheds (NEWS) database (Seitzinger et al., 2006). To create the
1038 default 'obsclim' climate-related forcings for the fisheries and marine ecosystem models these ocean
1039 model simulation data have been interpolated to a regular 0.25° grid while vertical resolution is

1040 preserved. In contrast to the atmospheric data, oceanic CRF are provided at monthly temporal
 1041 resolution.

1042
 1043 **Low resolution factual data.** To test to what degree a lower spatial resolution of the climate-related
 1044 forcings affects the impact model simulations, the oceanic climate-related forcings have also been
 1045 aggregated to one degree resolution as input for the ‘obsclim + histsoc, 60arcmin’ sensitivity
 1046 experiment.

1047
 1048 **CRF for the ‘1955-riverine-input’ sensitivity experiment.** The ‘1955-riverine-inputs’ sensitivity
 1049 experiment builds on 0.25 degree GFDL-COBALT2 simulation forced by the JRA-55 reanalysis, but
 1050 without time-varying riverine inputs. Instead the influx of freshwater and nutrients are fixed at mean
 1051 1951 to 1958 levels as described in the “control run” introduced by (Liu et al., 2021). The data is
 1052 interpolated to a regular 0.25 degree grid in the same way as the default ‘obsclim’ CRFs.

1053
 1054 We currently do not provide counterfactual versions of the ocean data forcing, though options are being
 1055 explored.

1056
 1057 **Table 8: ISIMP3a oceanic climate-related forcing.** Variables with suffixes -bot, -surf, and -vint were obtained
 1058 from the seafloor, the top layer of the ocean, and vertical integration, respectively.

Variable	Variable specifier	Unit	Resolution	Datasets
Mass concentration of total phytoplankton expressed as chlorophyll	chl	kg m-3	0.25° and 1° grid, 35 levels (m from the surface), monthly	GFDL-COBALT2 simulation forced by the JRA-55 reanalysis, accounting for climate-driven changes in riverine inputs (‘default’) or assuming fixed levels of riverine inputs (‘1955-riverine-input’). Standard salt water density of 1035 kg m-3 applied when converting from mass to volumetric unit, i.e. µg kg-1 to kg m-3
Downward flux of organic particles expressed as organic carbon at ocean bottom	expc-bot	mol m-2 s-1	0.25° and 1° grid, monthly	GFDL-COBALT2 simulation forced by the JRA-55 reanalysis, accounting for climate-driven changes in riverine inputs (‘default’) or assuming fixed levels of riverine inputs (‘1955-riverine-input’). Derived from nitrogen

				<p>detritus flux at ocean bottom (fndet_btm) by multiplying with fixed N-C ratio of 6.625.</p> <p>Extractions for individual grid cells available in ASCII format for regional models (see Table 1).</p>
Particulate organic carbon content in the upper 100 m	intpoc	kg m ⁻²	0.25° and 1° grid, monthly	<p>GFDL-COBALT2 simulation forced by the JRA-55 reanalysis, accounting for climate-driven changes in riverine inputs ('default') or assuming fixed levels of riverine inputs ('1955-riverine-input'). Derived by aggregating bacterial, detritus, diazotroph, large+small phytoplankton, large+medium+small zooplankton nitrogen biomass and multiplying by a fixed N-C ratio of 6.625.</p> <p>Extractions for individual grid cells available in ASCII format for regional models (see Table 1).</p>
Net primary organic carbon production by all types of phytoplankton in grid cell column	intpp	mol m ⁻² s ⁻¹	0.25° and 1° grid, monthly	<p>GFDL-COBALT2 simulation forced by the JRA-55 reanalysis, both accounting for climate-driven changes in riverine inputs ('default') or assuming fixed levels of riverine inputs ('1955-riverine-input'). Derived by aggregating net primary productions by diatoms, diazotrophs and pico-phytoplankton and under the assumption of a fixed N-C ratio of 6.625.</p> <p>Extractions for individual grid cells available in ASCII format for</p>

				regional models (see Table 1).
Net primary organic carbon production by diatoms in grid cell column	intppdiat	mol m-2 s-1	0.25° and 1° grid, monthly	GFDL-COBALT2 simulation forced by the JRA-55 reanalysis, both accounting for climate-driven changes in riverine inputs ('default') or assuming fixed levels of riverine inputs ('1955-riverine-input'). Derived under the assumption of a fixed N-C ratio of 6.625. Extractions for individual grid cells available in ASCII format for regional models (see Table 1).
Net primary organic carbon production of carbon by diazotrophs in grid cell column	intppdiaz	mol m-2 s-1	0.25° and 1° grid, monthly	GFDL-COBALT2 simulation forced by the JRA-55 reanalysis, both accounting for climate-driven changes in riverine inputs ('default') or assuming fixed levels of riverine inputs ('1955-riverine-input'). Derived under the assumption of a fixed N-C ratio of 6.625. Extractions for individual grid cells available in ASCII format for regional models (see Table 1).
Net Primary Mole Productivity of Carbon by Picophytoplankton in grid cell column	intpppico	mol m-2 s-1	0.25° and 1° grid, monthly	GFDL-COBALT2 simulation forced by the JRA-55 reanalysis, both accounting for climate-driven changes in riverine inputs ('default') or assuming fixed levels of riverine inputs ('1955-riverine-input'). Derived under the

				assumption of a fixed N-C ratio of 6.625.
Mixed Layer Ocean Thickness defined by a Sigma Theta difference (= density difference) of 0.125 kg m ⁻³ compared to the surface	m1otst-0125	m	0.25° and 1° grid, monthly	GFDL-COBALT2 simulation forced by the JRA-55 reanalysis, both accounting for climate-driven changes in riverine inputs ('default') or assuming fixed levels of riverine inputs ('1955-riverine-input')
Dissolved oxygen concentration; vertically resolved, at the bottom or at the surface, respectively	o2, o2-bot, o2-surf	mol m ⁻³	0.25° and 1° grid, 35 levels (m from the surface), monthly	GFDL-COBALT2 simulation forced by the JRA-55 reanalysis, both accounting for climate-driven changes in riverine inputs ('default') or assuming fixed levels of riverine inputs ('1955-riverine-input'). Extractions for individual grid cells of the bottom and surface layer available in ASCII format for regional models (see Table 1).
pH; vertically resolved, at the bottom or at the surface, respectively	ph, ph-bot, ph-surf	1	0.25° and 1° grid, 35 levels (m from the surface), ocean bottom and surface fields, monthly	GFDL-COBALT2 simulation forced by the JRA-55 reanalysis, both accounting for climate-driven changes in riverine inputs ('default') or assuming fixed levels of riverine inputs ('1955-riverine-input') where pH is derived from ion concentrations H ⁺ as $pH = -\log_{10}(H^+)$. Extractions for individual grid cells of the bottom and surface layer available in ASCII format for regional models (see Table 1).

<p>Total phytoplankton carbon concentration; vertically resolved or integrated over the grid cell column, respectively</p>	<p>phyc, phyc-vint</p>	<p>mol m-3</p>	<p>0.25° and 1° grid, 35 levels (m from the surface) and vertically integrated, monthly</p>	<p>GFDL-COBALT2 simulation forced by the JRA-55 reanalysis, both accounting for climate-driven changes in riverine inputs ('default') or assuming fixed levels of riverine inputs ('1955-riverine-input'). Aggregated from diatom, diazotroph and pico-phytoplankton. Standard salt water density of 1035 kg m-3 and fixed N-C ratio of 6.625 applied when converting from mass to volumetric unit, i.e. mol kg-1 to mol m-3.</p> <p>Extractions for individual grid cells of the vertically integrated data set are available in ASCII format for regional models (see Table 1).</p>
<p>Concentration of diatoms expressed as carbon in sea water; vertically resolved or integrated over the grid cell column, respectively</p>	<p>phydiat, phydiat-vint</p>	<p>mol m-3</p>	<p>0.25° and 1° grid, 35 levels (m from the surface) and vertically integrated, monthly</p>	<p>GFDL-COBALT2 simulation forced by the JRA-55 reanalysis, both accounting for climate-driven changes in riverine inputs ('default') or assuming fixed levels of riverine inputs ('1955-riverine-input'). Standard salt water density of 1035 kg m-3 and fixed N-C ratio of 6.625 applied when converting from mass to volumetric unit, i.e. mol kg-1 to mol m-3.</p> <p>Extractions for individual grid cells of the vertically integrated data set are available in ASCII format for regional models (see Table 1).</p>

Concentration of diazotrophs expressed as carbon in sea water; vertically resolved or integrated over the grid cell column, respectively	phydiaz, phydiaz-vint	mol m-3	0.25° and 1° grid, 35 levels (m from the surface) and vertically integrated, monthly	GFDL-COBALT2 simulation forced by the JRA-55 reanalysis, both accounting for climate-driven changes in riverine inputs ('default') or assuming fixed levels of riverine inputs ('1955-riverine-input'). Standard salt water density of 1035 kg m-3 and fixed N-C ratio of 6.625 applied when converting from mass to volumetric unit, i.e. mol kg-1 to mol m-3.
Mole concentration of picophytoplankton expressed as carbon in sea water; vertically resolved or integrated over the grid cell column, respectively	phypico, phypico-vint	mol m-3	0.25° and 1° grid, 35 levels (m from the surface) and vertically integrated, monthly	GFDL-COBALT2 simulation forced by the JRA-55 reanalysis, both accounting for climate-driven changes in riverine inputs ('default') or assuming fixed levels of riverine inputs ('1955-riverine-input'). Standard salt water density of 1035 kg m-3 and fixed N-C ratio of 6.625 applied when converting from mass to volumetric unit, i.e. mol kg-1 to mol m-3.
Net downward shortwave radiation at sea water surface	rsntds	W m-2	0.25° and 1° grid, monthly	From JRA-55 reanalysis
Sea ice area fraction	siconc	%	0.25° and 1° grid, monthly	From JRA-55 reanalysis
Sea water salinity; vertically resolved, at the bottom, or at the surface, respectively	so, so-bot, so-surf	0.001	0.25° and 1° grid, 35 levels (m from the surface), ocean bottom and surface fields, monthly	GFDL-COBALT2 simulation forced by the JRA-55 reanalysis, both accounting for climate-driven changes in riverine inputs ('default') or assuming fixed levels of riverine inputs ('1955-riverine-input'). Extractions for individual grid cells of the surface and bottom layer are

				available in ASCII format for regional models (see Table 1).
Sea water potential temperature	thetao	°C	0.25° and 1° grid, 35 levels (m from the surface), monthly	GFDL-COBALT2 simulation forced by the JRA-55 reanalysis, both accounting for climate-driven changes in riverine inputs ('default') or assuming fixed levels of riverine inputs ('1955-riverine-input')
Ocean model cell thickness	thkcello	m	0.25° and 1° grid, 35 levels (m from the surface), constant	GFDL-COBALT2 simulation forced by the JRA-55 reanalysis, both accounting for climate-driven changes in riverine inputs ('default') or assuming fixed levels of riverine inputs ('1955-riverine-input')
Sea water potential temperature at sea floor (bottom)	tob	°C	0.25° and 1° grid, monthly	GFDL-COBALT2 simulation forced by the JRA-55 reanalysis, both accounting for climate-driven changes in riverine inputs ('default') or assuming fixed levels of riverine inputs ('1955-riverine-input'). Extractions for individual grid cells are available in ASCII format for regional models (see Table 1).
Sea surface temperature	tos	°C	0.25° and 1° grid, monthly	GFDL-COBALT2 simulation forced by the JRA-55 reanalysis, both accounting for climate-driven changes in riverine inputs ('default') or assuming fixed levels of riverine inputs ('1955-riverine-input'). Extracted from uppermost ocean layers potential

				temperatures. Extractions for individual grid cells are available in ASCII format for regional models (see Table 1).
Sea water zonal velocity	uo	m s ⁻¹	0.25° and 1° grid, 35 levels (m from the surface), monthly	GFDL-COBALT2 simulation forced by the JRA-55 reanalysis, both accounting for climate-driven changes in riverine inputs ('default') or assuming fixed levels of riverine inputs ('1955-riverine-input')
Sea water meridional velocity	vo	m s ⁻¹	0.25° and 1° grid, 35 levels (m from the surface), monthly	GFDL-COBALT2 simulation forced by the JRA-55 reanalysis, both accounting for climate-driven changes in riverine inputs ('default') or assuming fixed levels of riverine inputs ('1955-riverine-input')
Concentration of zooplankton of meso size expressed as carbon in seawater; vertically resolved or integrated over the grid cell column, respectively	zmeso, zmeso-vint	mol m ⁻³	0.25° and 1° grid, 35 levels (m from the surface) and vertically integrated, monthly	GFDL-COBALT2 simulation forced by the JRA-55 reanalysis, both accounting for climate-driven changes in riverine inputs ('default') or assuming fixed levels of riverine inputs ('1955-riverine-input'). Aggregated from large and medium zooplankton. Standard salt water density of 1035 kg m ⁻³ and fixed N-C ratio of 6.625 applied when converting from mass to volumetric unit, i.e. mol kg ⁻¹ to mol m ⁻³ . Extractions for individual grid cells of the vertically integrated data set are available in ASCII format for regional models (see Table 1).

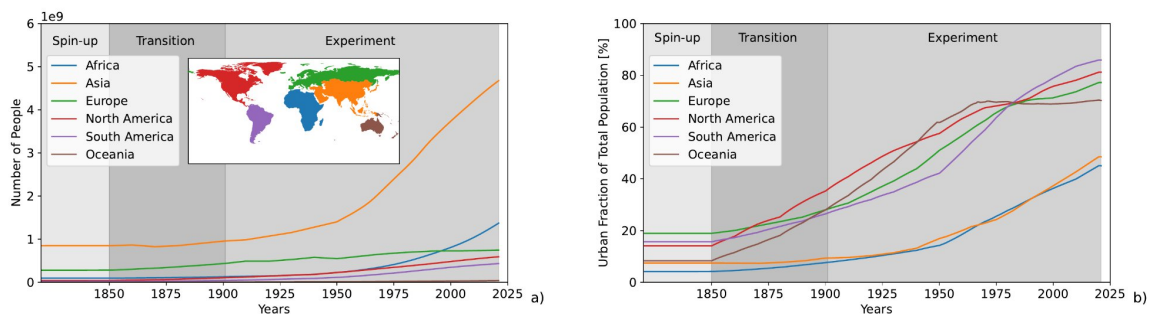
<p>Concentration of zooplankton of micro scale expressed as carbon in seawater; vertically resolved or integrated over the grid cell column, respectively.</p>	<p>zmicro, zmicro-vint</p>	<p>mol m-3</p>	<p>0.25° and 1° grid, 35 levels (m from the surface) and vertically integrated, monthly</p>	<p>GFDL-COBALT2 simulation forced by the JRA-55 reanalysis, both accounting for climate-driven changes in riverine inputs ('default') or assuming fixed levels of riverine inputs ('1955-riverine-input'). Standard salt water density of 1035 kg m-3 and fixed N-C ratio of 6.625 applied when converting from mass to volumetric unit, i.e. mol kg-1 to mol m-3.</p> <p>Extractions for individual grid cells of the vertically integrated data set are available in ASCII format for regional models (see Table 1).</p>
<p>Total Zooplankton Carbon Concentration; vertically resolved or integrated over the grid cell column, respectively</p>	<p>zooc, zooc-vint</p>	<p>mol m-3</p>	<p>0.25° and 1° grid, 35 levels (m from the surface) and vertically integrated, monthly</p>	<p>GFDL-COBALT2 simulation forced by the JRA-55 reanalysis, both accounting for climate-driven changes in riverine inputs ('default') or assuming fixed levels of riverine inputs ('1955-riverine-input'), aggregated from large, medium and micro zooplankton. Standard salt water density of 1035 kg m-3 and fixed N-C ratio of 6.625 applied when converting from mass to volumetric unit, i.e. mol kg-1 to mol m-3.</p> <p>Extractions for individual grid cells of the vertically integrated data set are available in ASCII format for regional models (see Table 1).</p>

1059
1060

1061 **4 Direct human forcings**

1062

1063 **4.1 Population data**



1064

1065 **Figure 4: Historical evaluation of population for different continents.** Total number of people living in the
 1066 region (panel a) and urban population as a fraction of the total population per region (panel b).
 1067

1068

Table 9: Population data provided as part of the ISIMIP3a direct human forcing.

Variable	Variable specifier	Unit	Resolution	Datasets
National population	pop	Number of people in millions	annual	UN 2019 WPP database (2023): census-based from 1950 to 2020 + “medium-variant” forecast provided for 2021
Gridded total population	total-population	Number of people	0.5°x 0.5°, annual	HYDE3.3 data for 1950-2020 constantly extended to 2021 and adjusted to match the national UN numbers described above (see text below)
Gridded rural population	rural-population	Number of people	0.5°x 0.5°, annual	HYDE3.3 data for 1950-2020 constantly extended to 2021 and rescaled by the same national scaling factors as the total population
Gridded urban population	urban-population	Number of people	0.5°x 0.5°, annual	HYDE3.3 data for 1950-2020 constantly extended to 2021 and rescaled by the same national scaling factors as the total population

1069

1070
1071
1072
1073
1074
1075
1076
1077
1078
1079
1080
1081
1082
1083
1084
1085
1086
1087
1088
1089
1090
1091
1092
1093
1094
1095
1096

1097
1098

[For ISIMIP3a we provide consistent gridded and national population data \(see Table 9\) by rescaling the gridded data to match the national aggregates. Figure 4 shows the temporal evolution of total and urban population for different continents.](#)

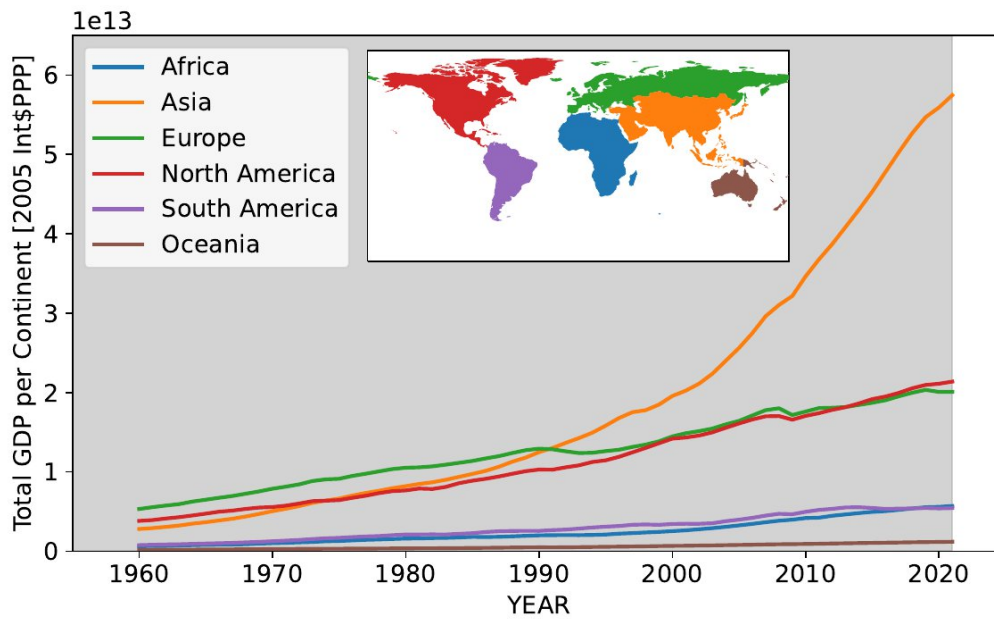
National data. Annual national population data are taken from the 2019 UN World Population Prospects (WPP) database for the period from 1950 – 2021 (United Nations, 2019). The 2019 revision of the WPP provides census-based population numbers from 1950 through 2020. For the year 2021, we use the “medium-variant” of the probabilistic forecast also provided by the WPP. The forecast accounts the past experience of each country, while reflecting uncertainty about future changes based on the past experience of other countries under similar conditions (see United Nations, 2019 for details). For countries not covered in the database, estimates are taken from the MissingIslands dataset (Arujo et al., 2021) to finally provide population data for 249 countries.

Gridded data. We provide gridded population data that is based on HYDE v3.3 (Klein Goldewijk, 2022). Just like the original dataset we provide total, rural and urban population per grid cell. The original HYDE 3.3 data was on a $1/12^\circ \times 1/12^\circ$ grid and has been interpolated to ISIMIP's $0.5^\circ \times 0.5^\circ$ grid. Furthermore, the land-sea distinction was modified to comply with the ISIMIP country mask (see **Table 1**). Before the year ~~1950~~2000 HYDE provides data every ten years, the intermediate years have been filled by linear interpolation. Also, the original HYDE data ends in 2020. So to cover the whole ISIMIP3a time frame the final year 2020 has been duplicated as 2021. In this way annual coverage of 1850 to 2021 has been achieved.

[Data for A](#)all grid cells of a country, as defined by the ISIMIP $0.5^\circ \times 0.5^\circ$ fractional country map (see **Table 1**), have been rescaled such that the country's total population matches the numbers provided in the national population data. Since the national data only starts in 1950, all years prior to 1950 have been rescaled by the national scaling factors of 1950. The urban and rural populations have been rescaled by the same national scaling factors as the total population.

1099 **4.2 Gross Domestic Product (GDP)**

1100



1101

1102 **Figure 5: Aggregated GDP (Int\$ PPP 2005) for different continents.**

1103

1104

Table 10: GDP data provided as part of the ISIMIP3a direct human forcing.

Variable	Variable specifier	Unit	Resolution	Datasets
National Gross Domestic Product	gdp	Int\$ PPP 2005	annual	World Bank’s World Development Indicator database (Anon, 2008)
Gridded Gross Domestic Product	gridded-gdp	Int\$ PPP 2005	annual	National GDP data downscaled to the 0.5° grid according to (Wang and Sun, 2022)

1105

1106 [Similar to the population data we also provide gridded and national GDP data \(see Table 10\). The](#)
 1107 [downscaling of the national numbers is based on population and nightlight data \(see below\). In contrast](#)
 1108 [to ISIMIP2a the gridded GDP and population data are now consistent such that previous artefacts in](#)
 1109 [the derived GDP per capita could be eliminated \(see below\). Figure 5 shows the historical increase in](#)
 1110 [GDP for different continents.](#)

1111 ¶

1112 **National GDP data.** Time series of per-capita GDP for the time period 1960-2021 are taken from the
 1113 World Bank’s World Development Indicator database ([WDI](#)) (Anon, 2008) and converted into constant
 1114 2005 Int\$PPP, using deflators and PPP conversion factors from WDI. For countries not covered in the

1115 WDI database, data from the MissingIslands dataset (Arujo et al., 2021) is used to allow covering 249
1116 countries. Following a method developed by (Koch and Leimbach, 2023); the values for the year 2021
1117 are derived from the IMF's World Economic Outlook short-term estimates of GDP per capita growth
1118 (International Monetary Fund, 2021) that comprise estimates of the growth impacts of the Covid-19
1119 shock.

1120

1121 **Gridded GDP data.** Gridded GDP data at 0.5 degree resolution are derived from the national GDP time
1122 series by applying the LitPop method (Zhao et al., 2017; Eberenz et al., 2019), which uses [the ISIMIP3a](#)
1123 gridded population [based on HYDE v.3.3](#) and nighttime light (NTL) data to downscale national GDP
1124 data [for the period 1960-2021 to the ISIMIP 0.5°×0.5° grid.](#) ~~For the GDP data provided here (Wang~~
1125 ~~and Sun, 2022), Here, the LitPop approach was applied using a combination of Hyde3.3-based gridded~~
1126 ~~population data and NTL images from both the NOAA's DMSP-OLS stale light database, version 4~~
1127 ~~(Earth observation group—defense meteorological satellite program, boulder) and the Suomi NPP~~
1128 ~~VIIRS Day/Night Band (DNB, (Elvidge et al., 2017). The Suomi NPP VIIRS data set is a newer product~~
1129 ~~that has a higher resolution of 15 arcseconds and features a wider radiometric detection range but it~~
1130 ~~was launched only in 2012. Using relations from the overlapping years allowed for improvements of the~~
1131 ~~longer running DMSP-OLS data. This way NTL data covering the years 2000-2020 was obtained. For~~
1132 ~~the earlier years from 1960 to 1999 the NTL data from 2000 was used, and in the same vein 2021 NTL~~
1133 ~~data was assumed to be identical to the 2020 values. Together with the Hyde3.3-based gridded~~
1134 ~~population data provided within ISIMIP3a, the annual time series of national GDP over 1960—2021~~
1135 ~~were disaggregated to the ISIMIP 0.5°×0.5° grid using the LitPop approach.~~

1136

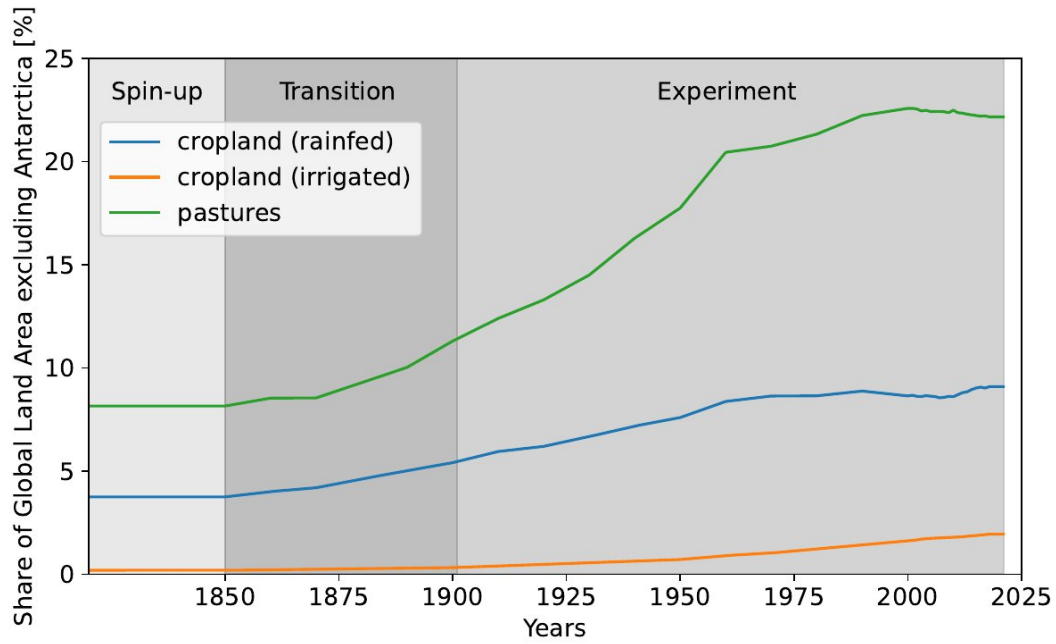
1137 As the disaggregation of GDP is not only based on population but also uses the NTL GDP per capita,
1138 it is not constant within different countries. Deriving the gridded GDP data from the gridded population
1139 data provided within ISIMIP3a ensures that the both data sets can be combined such that the associated
1140 GDP per capita does no longer show the artefacts that have been found in the ISIMIP2a GDP per capita
1141 (ISIMIP2a: suspicious gridded GDP per capita data; new functions in the isimip data repository; Forum
1142 on Scenarios for Climate and Societal Futures, 2023).

1143

1144

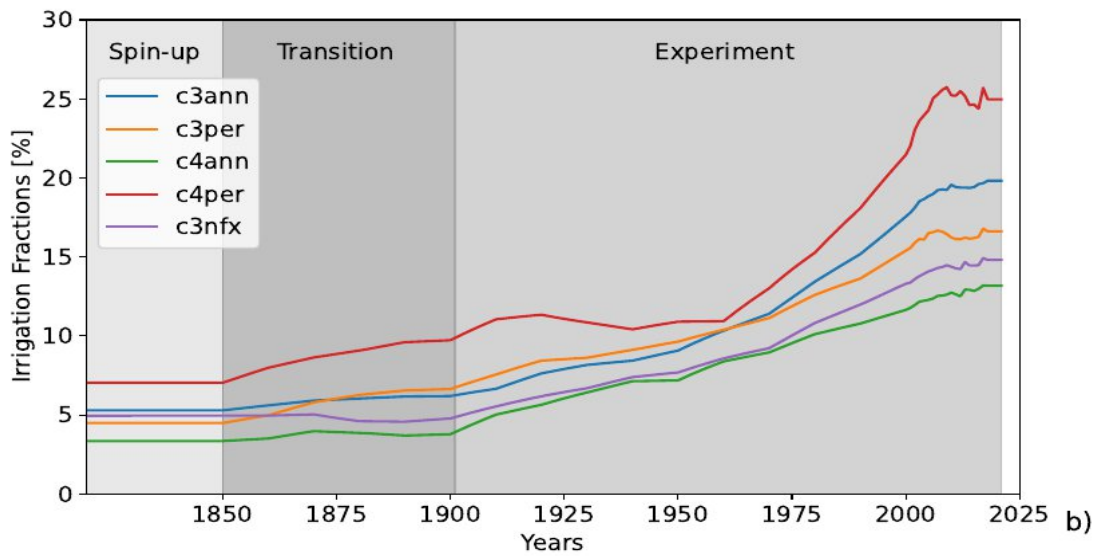
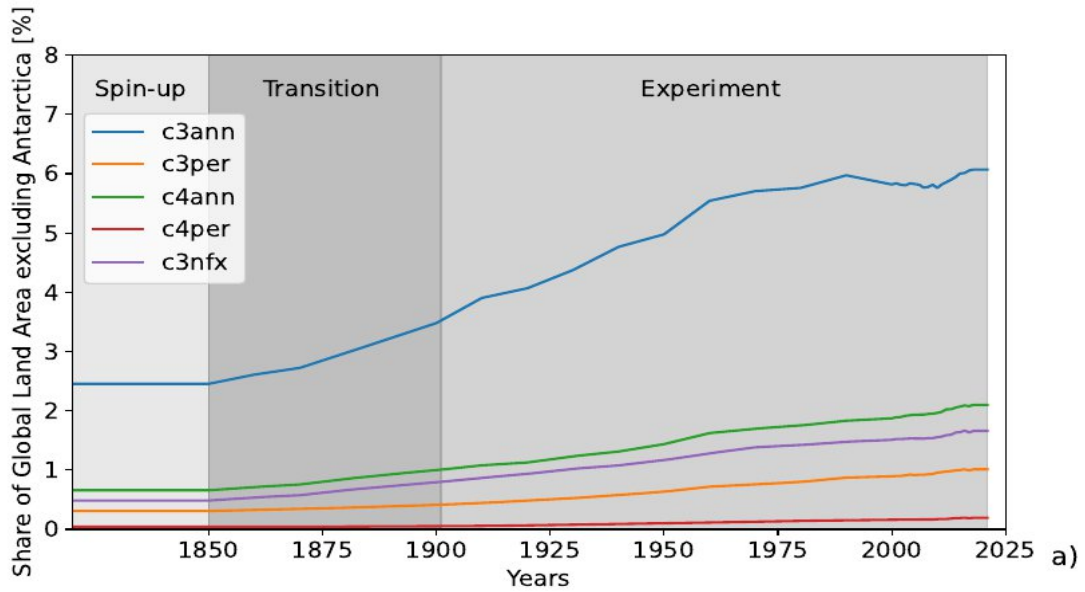
1145 **4.3 Land use and irrigation patterns**

1146



1147

1148 **Figure 6: Share of Global Land Area excluding Antarctica covered by rainfed cropland (green), irrigated**
1149 **cropland (blue), and pasture (orange) [%].** The information is from the LUH_v2 data set provided as direct human
1150 forcing for ISIMIP3a (see details below).
1151



1152
1153
1154
1155
1156
1157
1158
1159

Figure 7: Panel A: Share of Global Land Area excluding Antarctica covered by different groups of crops (C3 annual (blue), C3 perennial (orange), C4 annual (green), C4 perennial (red), C3 nitrogen fixing (purple)). Panel B: Fraction of irrigated land for the different groups of crops. The information is from the LUH v2 data set provided as direct human forcing for ISIMIP3a (see details on further [disaggregation of the LUH v2 groups](#) below).

Table 11: Historical land use and irrigation patterns provided as part of the ISIMIP3a direct human forcing.

Variable	Variable specifier	Unit	Resoluti on	Datasets

Total crop land, rainfed cropland, ⁷ irrigated cropland, ⁷ pastures	cropland_total, cropland_rainfed, cropland_irrigated, [¶] pastures	unitless (share of area in a grid cell)	0.5°×0.5°, annual	LUH2 v2 (Hurtt et al., 2020, Land use harmonization, 2023)
pastures [¶]	pastures [¶]	unitless (share of area in a grid cell) [¶]	0.5°×0.5°, annual [¶]	sum of 'managed_pastures' and 'rangeland' from HYDE 3.2 (see below) [¶]
Managed pastures [¶]	managed_pastures [¶]	1 (share of area in a grid cell) [¶]	0.5°×0.5°, annual [¶]	first subcategory of 'pastures' from HYDE 3.2 (see above) [¶]
rangeland [¶]	rangeland ^{¶¶}	1 (share of area in a grid cell) [¶]	0.5°×0.5°, annual [¶]	second subcategory of 'pastures' from HYDE 3.2, more extensive management than 'managed pastures' (see above) [¶]
C3 annual rainfed cropland, C3 annual irrigated cropland, ⁷	c3ann_irrigated, c3ann_rainfed	1 (share of area in a grid cell)	0.5°×0.5°, annual	LUH v2 , for the disaggregation we consider C3 annual to be: rapeseed, rice, temperate cereals, temperate roots, tropical roots, sunflower, others C3 annual (see below)

C3 perennial cropland	c3per_irrigated, c3per_rainfed	1 (share of area in a grid cell)	0.5°×0.5°, annual	LUH v2 (this variable appears in the file only distinguishing 5 land use types and in the file with the downscaled 15 land use types. The provided values are identical)
C3 nitrogen-fixing rainfed cropland, C3 nitrogen-fixing irrigated cropland	c3nfx_irrigated, c3nfx_rainfed	1 (share of area in a grid cell)	0.5°×0.5°, annual	LUH v2 for the disaggregation we consider 'C3 nitrogen-fixing' to be: groundnut, pulses, soybean, others C3 nitrogen-fixing (see below)
C4 annual rainfed cropland, C4 annual irrigated cropland	c4ann_irrigated, c4ann_rainfed	1 (share of area in a grid cell)	0.5°×0.5°, annual	LUH v2, for the disaggregation we consider 'C4 annual' to be: maize, tropical cereals (see below)
C4 perennial rainfed cropland, C4 perennial irrigated cropland	c4per_irrigated, c4per_rainfed	1 (share of area in a grid cell)	0.5°×0.5°, annual	LUH v2 (this variable appears in the file only distinguishing 5 land use types and in the file with the downscaled 15 land use types. The provided values are identical), in the file with the 15 crops 'C4 perennial' is considered to be

				sugarcane
Fraction of grid cell where maize is grown (rainfed and irrigated) Cropland downscaled to 15 crops, for both rainfed and irrigated land	maize_irrigated, maize_rainfed	1 (share of area in a grid cell)	0.5°×0.5° annual	downscaled from LUH_v2 data based on the crop distribution from (Monfreda et al., 2008). The method is described in (Frieler et al., 2017)
Fraction of grid cell where groundnut is grown (rainfed and irrigated)	oil_crops_groundnut_irrigated, oil_crops_groundnut_rainfed	1 (share of area in a grid cell)	0.5°×0.5° annual	downscaled from LUH v2 data based on the crop distribution from (Monfreda et al., 2008). The method is described in (Frieler et al., 2017)

Fraction of grid cell where rapeseed is grown (rainfed and irrigated) ☞	oil_crops_rapeseed_irrigated , oil_crops_rapeseed_rainfed ☞	1 (share of area in a grid cell)☞	0.5°×0.5°, annual☞	downscaled from LUH v2 data based on the crop distribution from (Monfreda et al., 2008). The method is described in (Frieler et al., 2017)☞
Fraction of grid cell where soybean is grown (rainfed and irrigated) ☞	oil_crops_soybean_irrigated , oil_crops_soybean_rainfed ☞	1 (share of area in a grid cell)☞	0.5°×0.5°, annual☞	downscaled from LUH v2 data based on the crop distribution from (Monfreda et al., 2008). The method is described in (Frieler et al., 2017)☞
Fraction of grid cell where sunflower is grown (rainfed and irrigated) ☞	oil_crops_sunflower_irrigated , oil_crops_sunflower_rainfed ☞	1 (share of area in a grid cell)☞	0.5°×0.5°, annual☞	downscaled from LUH v2 data based on the crop distribution from (Monfreda et al., 2008). The method is described in (Frieler et al., 2017)☞
Fraction of grid cell where pulses are grown (rainfed and irrigated) ☞	pulses_irrigated , ¶ pulses_rainfed ☞	1 (share of area in a grid cell)☞	0.5°×0.5°, annual☞	downscaled from LUH v2 data based on the crop distribution from (Monfreda et al., 2008). The method is described in (Frieler et al., 2017)☞
Fraction of grid cell where rice is grown (rainfed and irrigated) ☞	rice_irrigated , ¶ rice_rainfed ☞	1 (share of area in a	0.5°×0.5°, annual☞	downscaled from LUH v2 data based on the crop distribution from

		grid cell)☞		(Monfreda et al., 2008). The method is described in (Frieler et al., 2017)☞
Fraction of grid cell where temperate cereals are grown (rainfed and irrigated) ☞	temperate_cereals_irrigated , temperate_cereals_rainfed ☞	1 (share of area in a grid cell)☞	0.5°×0.5°, annual☞	downscaled from LUH v2 data based on the crop distribution from (Monfreda et al., 2008). The method is described in (Frieler et al., 2017)☞
Fraction of grid cell where temperate roots are grown (rainfed and irrigated) ☞	temperate_roots_irrigated , temperate_roots_rainfed ☞	1 (share of area in a grid cell)☞	0.5°×0.5°, annual☞	downscaled from LUH v2 data based on the crop distribution from (Monfreda et al., 2008). The method is described in (Frieler et al., 2017)☞
Fraction of grid cell where tropical cereals are grown (rainfed and irrigated) ☞	tropical_cereals_irrigated , tropical_cereals_rainfed ☞	1 (share of area in a grid cell)☞	0.5°×0.5°, annual☞	downscaled from LUH v2 data based on the crop distribution from (Monfreda et al., 2008). The method is described in (Frieler et al., 2017)☞
Fraction of grid cell where tropical roots are grown (rainfed and irrigated) ☞	tropical_roots_irrigated , tropical_roots_rainfed ☞☞	1 (share of area in a grid cell)☞	0.5°×0.5°, annual☞	downscaled from LUH v2 data based on the crop distribution from (Monfreda et al., 2008). The method is described in (Frieler et al., 2017)☞

Fraction of grid cell where C3 annual crops other than rapeseed , rice , temperate cereals , temperate roots , tropical roots , and sunflower are grown (rainfed and irrigated)	others_c3ann_irrigated , others_c3ann_rainfed	1 (share of area in a grid cell)	0.5°×0.5°, annual	downscaled from LUH v2 data based on the crop distribution from (Monfreda et al., 2008). The method is described in (Frieler et al., 2017)
Fraction of grid cell where nitrogen fixing C3 crops other than groundnut, pulses, and soybean are grown (rainfed and irrigated)	others_c3nfx_irrigated , others_c3nfx_rainfed	1 (share of area in a grid cell)	0.5°×0.5°, annual	downscaled from LUH v2 data based on the crop distribution from (Monfreda et al., 2008). The method is described in (Frieler et al., 2017)
Urban areas ☒	urbanareas ☒	1 (share of area in a grid cell)☒	0.5°×0.5°, annual☒	LUH v2☒
Urban areas ☒	urbanareas ☒	1 (share of area in a grid cell)☒	0.5°×0.5°, annual☒	LUH v2☒

1160

1161

1162 Historical land use and irrigation patterns for ISIMIP3a ~~and ISIMIP3b, group I and group II~~ simulations

1163 are taken from LUH v2 (Hurtt et al., 2020, Land use harmonization, 2023). The data set is, up to 2018,

1164 identical to the data provided with ISIMIP2b. The data are based on the HYDE 3.2 land use data set

1165 (Klein Goldewijk et al., 2017) and have been constantly extended up to 2021, i.e., by copying the 2018
1166 patterns into 2019, 2020, and 2021.

1167 The original HYDE 3.2 data distinguishes four categories of land use: rainfed and irrigated cropland,
1168 managed pastures, and more extensively managed rangelands (see **Table 11**). The latter two
1169 categories are combined to grazing lands (ISIMIP variable 'pastures', see [Figure 6](#)). In LUH_v2 the crop
1170 land information is further downscaled to five crop types: C3 annual plants, C3 perennial plants, C3
1171 nitrogen fixing plants, C4 annual plants and C4 perennial plants (see [global aggregates in Figure 7](#)). In
1172 the same vein as the HYDE case, the LUH_v2 data set distinguishes between rainfed and irrigated
1173 croplands. For the purpose of driving the ISIMIP impact models, the LUH_v2 data was interpolated from
1174 the original $0.25^\circ \times 0.25^\circ$ to the standard ISIMIP $0.5^\circ \times 0.5^\circ$ global grid. In a further downscaling step
1175 the 5 crops land use data has been downscaled even further to 15 crop types (see [global aggregates](#)
1176 [in Figure 7](#)). For this purpose the Monfreda land use dataset (Monfreda et al., 2008) has been used. It
1177 describes the crop land areas of 175 crops in the year 2000, and we use this to downscale the 5 crops
1178 categories into land use areas of 15 more specific crop types (maize, groundnut, rapeseed, soybeans,
1179 sunflower, rice, sugarcane, pulses, temperate cereals (including wheat), temperate roots, tropical
1180 cereals, tropical roots, others annual, others perennial, and others N-fixing). The ratios determined from
1181 the year 2000 numbers have then been applied to all years. For further details please refer to (Frieler
1182 et al., 2017).¶

1183 ¶

1184 [The areas outside of the specified agricultural and urban land is considered 'natural vegetation' and not](#)
1185 [prescribed further to not constrain the dynamical vegetation models.](#) ¶

1186 ¶

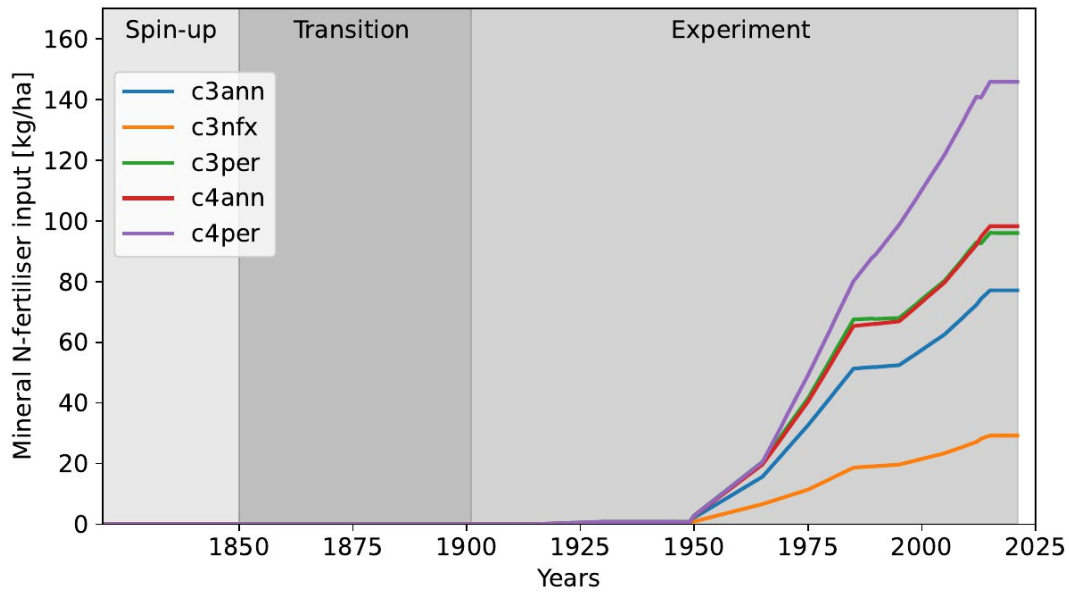
1187

1188

1189

1190 **4.4 Fertiliser input**

1191



1192

1193 **Figure 8: Mean mineral N-fertiliser input averaged across the land areas where the considered crop groups**
 1194 **are grown.**

1195

1196 **Table 12: Fertiliser inputs provided as part of the ISIMIP3a direct human forcing.**

Variable	Variable specifier	Unit	Resolution	Datasets
Mineral N-fertiliser input for annual 5-crop-types (C3 crops annual , C3 perennial , C4annual, C4 perennial, C3 nitrogen fixing)	fertl_c3ann , fertl_c3per , fertl_c4ann , fertl_c4per , fertl_c3nfx	kg ha-1 yr-1 (crop season)	0.5°×0.5°, annual	LUH_v2 (Hurtt et al., 2020)¶
Mineral N-fertiliser input for perennial C3 crops	fertl_c3per	kg ha-1 yr-1 (crop season)	0.5°×0.5°, annual	LUH v2 (Hurtt et al., 2020)¶

Mineral N-fertiliser input for annual C4 crops	fertl_c4ann	kg ha-1 yr-1 (crop season)	0.5°×0.5°, annual	LUH v2 (Hurtt et al., 2020) ¶
Mineral N-fertiliser input for perennial C4 crops	fertl_c4per	kg ha-1 yr-1 (crop season)	0.5°×0.5°, annual	LUH v2 (Hurtt et al., 2020) ¶
Mineral N-fertiliser input for nitrogen-fixing C3 crops	fertl_c3nfx	kg ha-1 yr-1 (crop season)	0.5°×0.5°, annual	LUH v2 (Hurtt et al., 2020) ¶

1197

1198 The LUH_v2 data set also includes national application rates of industrial nitrogen fertiliser (Hurtt et al.,
1199 2020). This does not include manure. The fertiliser data is not based on HYDE but was derived from
1200 other sources. The data for the years 1915–1960 are based on (Smil, 2001), 1961–2011 are based on
1201 a compilation by (Zhang et al., 2015) which in turn is based on FAOSTAT (FAO, 2016), and 2012–2015
1202 are based on a projection by the International Fertilizer Association (IFASTAT, 2015). For the pure crop
1203 runs within ISIMIP, where the considered crops are assumed to ~~to~~ be grown everywhere without a land
1204 use specification, the LUH_v2 national fertiliser inputs are assumed to be applied everywhere within the
1205 country. [To calculate crop production, the LUH2 v2 land use patterns are applied in post-processing, i.e. by multiplying the crop yields from the pure crop run with the land use patterns \(fraction of the grid cell where the crop has been grown\).](#)

1208

1209 4.5 Land transformation

1210

1211 **Table 13: Land transformation and wood harvest provided as part of the ISIMIP3a direct human forcing.**

Variable	Variable specifier	Unit	Resolution	Datasets
Wood harvest area from primary forest land	primf-harv	Fraction of the national land area, kg in case	Annual, national sum	Based on LUH_v2 (Hurtt et al., 2011, 2020; del Valle et al., 2022, Land use

		of biomass		harmonization, 2023)
Wood harvest area from primary non-forest land	primn-harv¶	Fraction of the national land area, kg in case of biomass	Annual national sum	Based on LUH v2 v2h (Hurtt et al., 2011, 2020; del Valle et al., 2022)
Wood harvest area from secondary mature forest land	secmf-harv	Fraction of the national land area, kg in case of biomass	Annual national sum	Based on LUH v2 v2h (Hurtt et al., 2011, 2020; del Valle et al., 2022)
Wood harvest area from secondary young forest land	secyf-harv	Fraction of the national land area, kg in case of biomass	Annual national sum	Based on LUH v2 v2h (Hurtt et al., 2011, 2020; del Valle et al., 2022)
Wood harvest area from secondary non-forest land	secnf-harv ¶	Fraction of the national land area, kg in case of biomass	Annual national sum	Based on LUH v2 v2h (Hurtt et al., 2011, 2020; del Valle et al., 2022)
Wood harvest biomass carbon from primary forest land	primf-bioh ¶	Fraction of the national land area, kg in case of biomass	Annual national sum	Based on LUH v2 v2h (Hurtt et al., 2011, 2020; del Valle et al., 2022)

Wood harvest biomass carbon from primary non-forest land	primn-bioh	Fraction of the national land area, kg in case of biomass	Annual national sum	Based on LUH v2 v2h (Hurtt et al., 2011, 2020; del Valle et al., 2022)
Wood harvest biomass carbon from secondary mature forest land	secmf-bioh	Fraction of the national land area, kg in case of biomass	Annual national sum	Based on LUH v2 v2h (Hurtt et al., 2011, 2020; del Valle et al., 2022)
Wood harvest biomass carbon from secondary young forest land	secyf-bioh	Fraction of the national land area, kg in case of biomass	Annual national sum	Based on LUH v2 v2h (Hurtt et al., 2011, 2020; del Valle et al., 2022)
Wood harvest biomass carbon from secondary non-forest land	secnf-bioh	Fraction of the national land area, kg in case of biomass	Annual national sum	Based on LUH v2 v2h (Hurtt et al., 2011, 2020; del Valle et al., 2022)
Not forest-related land transformations All transitions from one type of land use to another	<type 1>_to_<type 2> With type 1 and type 2 from the following list: secdf (potentially forested secondary land), secdn (potentially non-forested secondary land), urban (urban land), c3ann (C3 annual crops), c4ann (C4 annual crops), c3per (C3 perennial crops),	Fraction of the grid cell	Annual	Based on LUH2 v2h (Hurtt et al., 2011, 2020, Land use harmonization, 2023); Land is considered to be 'potentially forested' if the above ground biomass density (kg C m⁻²) of the potential vegetation

	c4per (C4 perennial crops), c3nfx (C3 nitrogen-fixing crops), pastr (managed pasture) range (rangeland)			as estimated by the Miami-LU model accounting for changes in cropland and grazing land is > 2 kg C m⁻² (Hurt et al., 2020)
--	--	--	--	--

1212

1213 These datasets are based on the LUH v2h Harmonization Data Set covering 850 to 2015 (Hurt et al.,
1214 2020, Land use harmonization, 2023). The wood harvest data were obtained by aggregating from the
1215 original LUH_v2 grid to the ISIMIP 0.5° × 0.5° grid (first-order conservative remapping) and then
1216 aggregating to the national sums. Wood harvesting data are used in the vegetation models to mimic
1217 wood removal as part of forest management and clearing, and has a strong influence on the carbon
1218 balance. National data are provided so that models can use their internal routines to distribute the
1219 harvesting within a country's forest area. The gridded land transformation data were obtained by
1220 aggregating from the original LUH_v2 grid to the ISIMIP 0.5° × 0.5° grid; these data always end a year
1221 earlier than all other land use data, because a year in these data sets actually describes the changes
1222 from the current to the next year. The data have been extended up to 2021 by copying the 2015 data
1223 into the following years (files end in 2020).

1224

1225

1226 **4.6 Nitrogen Deposition**

1227

1228 **Table 14: Nitrogen deposition provided as part of the ISIMIP3a direct human forcing.**

Variable	Variable specifier	Unit	Resolution	Datasets
Reduced nitrogen deposition	nhx	g N m ⁻² mon ⁻¹	monthly	based on simulations from (Tian et al., 2018)
Oxidised nitrogen deposition	noy	g N m ⁻² mon ⁻¹	monthly	based on simulations from (Tian et al., 2018)

1229

1230

1231 Reduced and oxidised nitrogen deposition (NH_x, NO_y) are based on simulations by the NCAR
 1232 Chemistry-Climate Model Initiative during 1850-2014 (Tian et al., 2018). Nitrogen deposition data was
 1233 interpolated to 0.5° by 0.5° using the nearest grid point method. Data in 2015-2021 are assumed to be
 1234 the same as that in 2014.

1235

1236 **4.7 Crop calendar**

1237

1238 **Table 15: Crop calendar provided as optional representation of agricultural management. [The information is](#)
 1239 [given for 18 crop types.](#)**

Variable	Variable specifier	Unit	Resolution	Datasets
Planting day, separated for rainfed and irrigated crops where applicable	planting_day	day of year	0.5°, time average, no variation in time	(Jägermeyr et al., 2021b)

Maturity day, separated for rainfed and irrigated crops where applicable	maturity_day	day of year	0.5°, time average, no variation in time	(Jägermeyr et al., 2021b)
--	---------------------	-------------	--	---------------------------

1240

1241 Unfortunately, there is no global data set describing changes in growing seasons across the historical
1242 period. Instead we provide a static crop calendar that has been developed within the AgMIP Global
1243 Gridded Crop Model Intercomparison GGCM and merges information from various observational data
1244 sources (Jägermeyr et al., 2021b). It provides planting and maturity days for 18 different crops at the
1245 ISIMIP standard 0.5° grid. Grid cells outside of currently cultivated areas are spatially extrapolated
1246 (details below). For wheat and rice two growing seasons are provided while for all other crops the
1247 calendar only specifies one main growing season. The reported growing seasons should not be
1248 considered the growing seasons for one specific year but as ‘representative growing season’ across
1249 the recent years. Within the crop models different crop varieties are represented by [different](#) heat
1250 units required to reach physiological maturity. The crop calendar should be implemented by adjusting
1251 the required heat units to the average of the annual sums of heat units between the specified planting
1252 and maturity date over all growing seasons between 1979 and 2010.

1253 If modellers use a temporal adjustment of cultivars by varying required heat units in response to socio-
1254 economic development or historical climate change this is certainly allowed within the ‘histsoc’ set-up.
1255 If cultivars are fixed according to the method described above this simulation will be considered a
1256 ‘2015soc’ simulation as long as other direct human drivers are also held constant at 2015 levels.
1257 However, if, e.g., fertiliser inputs are varied over time according to provided forcing data (see section
1258 **4.4**), the run will be considered a ‘histsoc’ run.

1259 GGCM is currently working on a temporally resolved global crop calendar at the same spatial resolution
1260 based on various new data sources including agricultural ministries, census reports, phenological data
1261 bases, experimental sites, etc. This data set will be published separately and could then be used to
1262 inform ‘histsoc’ simulations.

1263

1264 **4.8 Dams and reservoirs**

1265

1266 **Table 16: Information about dams and reservoirs**

Variable	Variable specifier	Unit	Resolution	Datasets
Unique ID for each point representing a dam and its associated	ID	unitless numbers: 1-7320 from	per dam	Global Reservoir and Dam Database

reservoir.		GRanD and J3-J26 from GeoDAR v1.2		(GRanDv1.3, data up to 2016; (Lehner et al., 2011a, b) and GeoDAR v1.2 (Wang et al., 2022) covering the period 2016-2020
Name of the dam structure	DAM_NAME	unitless	per dam	GRanDv1.3, GeoDARv1.2
Original longitudinal location of the dam	LON_ORIG	degree (°)	per dam	GRanDv1.3, GeoDARv1.2
Original longitudinal location of the dam	LAT_ORIG	degree (°)	per dam	GRanDv1.3, GeoDARv1.2
Longitude, adjusted to the ISIMIPddm30 0.5° grid cell centres	LON_DDM30	degree (°)	per dam	Adjustment of original GRanDv1.3, GeoDARv1.2 data
Latitude, adjusted to the ISIMIPddm30 0.5° grid cell centres	LAT_DDM30	degree (°)	per dam	Adjustment of original GRanDv1.3, GeoDARv1.2 data
Upstream area draining into the reservoir using ISIMIPddm30	CATCH_SKM_DDM30	km ²	per dam	Derived from dam location and the ISIMIPddm30 drainage map.
Upstream area draining into the reservoir acc. to GRanD [km ²]	CATCH_SKM_GRanD	km ²	per dam	GRanDv1.3
Representative	CAP_MCM	10 ⁶ m ³	per dam	GRanDv1.3,

maximum storage capacity of reservoir				GeoDARv1.2
Year of construction, completion, commissioning, etc. (not specified)	YEAR	year	per dam	GRanDv1.3, GeoDARv1.2 + complemented by internet research
Alternative year (may indicate multi-year construction, secondary dam, etc.)	ALT_YEAR	year	per dam	GRanD
Original, rounded location has been shifted with automatic mapping (FLAG_CORR=1) If visual check or manual re-location has been applied (FLAG_CORR=2)	FLAG_CORR	Unitless labels: 1 or 2	per dam	Introduced when adjusting the locations to the ISIMIPddm30 0.5° grid
Name of the river which the dam impounds	RIVER	unitless	per dam	GeoDARv1.2. For GRanD records, it can be found in the GRanD database
Country where the dam is located	COUNTRY	unitless	per dam	GeoDARv1.2. For GRanD records, it can be found in the GRanD database
Height of the dam. If multiple heights are available, the	D_Hght_m	m	per dam	GeoDARv1.2. For GRanD records, it can be found in the

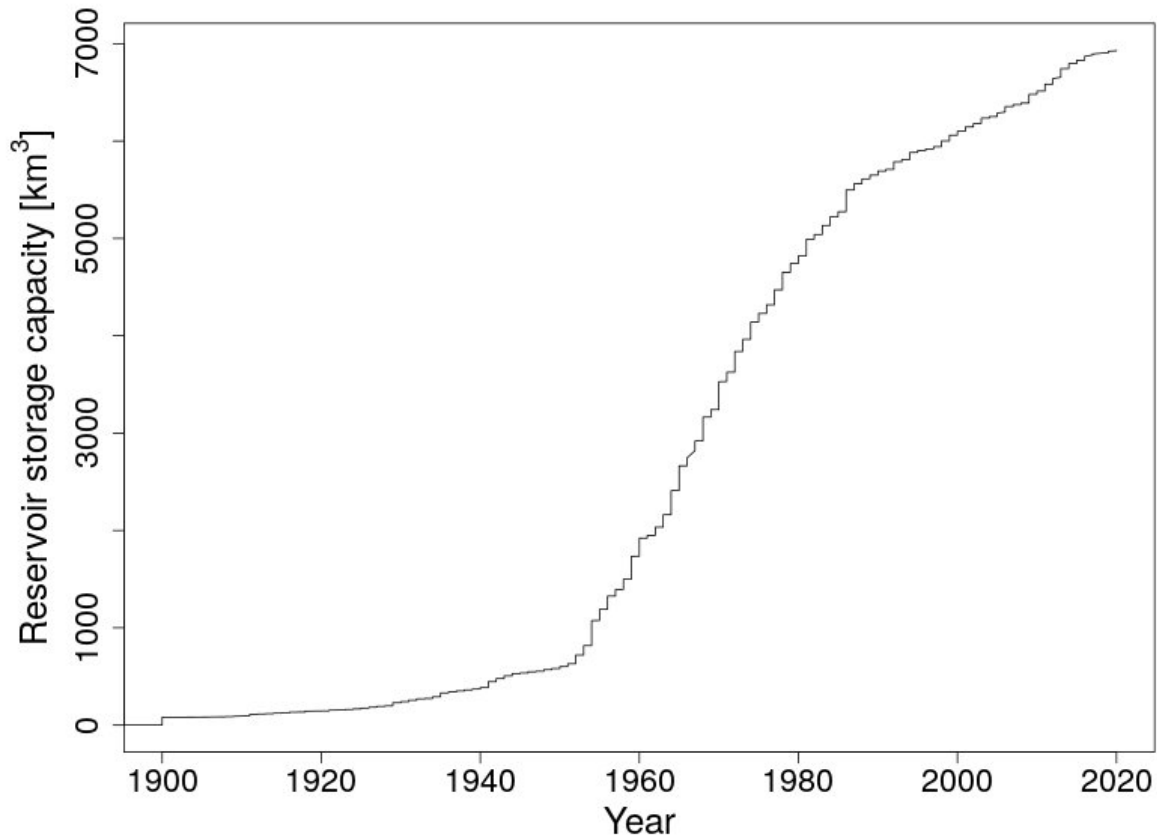
foundation height was used.				GRanD database
Maximum inundation area of the reservoir	R_Area_km2	km ²	per dam	GeoDARv1.2. For GRanD records, it can be found in the GRanD database
Maximum inundation length of the reservoir	R_Lgth_km	km	per dam	GeoDARv1.2. For GRanD records, it can be found in the GRanD database
Main purpose(s) of the dam	PURPOSE	no units	per dam	GeoDARv1.2. For GRanD records, it can be found in the GRanD database
Sources used to collect this dam's information	SOURCE	no units	per dam	GeoDARv1.2. For GRanD records, it can be found in the GRanD database. If filled out for GeoDAR records, it corresponds to the source for the year of construction/

				commissioning
Other notes related to the mapping or re-location of dams to ISIMIPddm30	COMMENTS	no units	per dam	

1267

1268 In order to offer a consistent and common source of information about reservoirs and associated dams
1269 for climate impact modellers (see **Table 16**), we joined the Global Reservoir and Dam Database of the
1270 Global Water System Project (GRanD v1.3; (Lehner et al., 2011a, b) with a subset of the Georeferenced
1271 global Dams And Reservoirs (GeoDAR v1.2) database (Wang et al., 2022), developed at Kansas State
1272 University (KSU), and provided by Jida Wang ahead of publication, [so that it could be provided when](#)
1273 [launching ISIMIP3 in 2020](#). These additional dams have construction or projected finalisation dates
1274 between 2016 and 2025, while GRanD v1.3 includes dams constructed up until 2017. In total, the
1275 combined database now includes 7331 dams whose construction [will be](#) finished by 2025. It
1276 includes dams that were constructed before [the simulation period](#), but still ~~in existence during the~~
1277 ~~simulation period~~ (the first reported dam was finished in the year 286). ~~In total the reported dams have~~
1278 ~~a global cumulative storage capacity of approximately 6932 km³ (Figure 92).~~ For the simulations
1279 described here, dams with (projected) construction dates after 2020 are not considered; these will
1280 become relevant in the ISIMIP3b ~~group III~~ simulations, with exception of the Grand Ethiopian
1281 Renaissance Dam, which we decided to include since its reservoir reached a first stage of filling of 4.9
1282 km³ in July 2020 (BBC news: Nile dam row, 2020; Tractebel: Filling of the reservoir of the Grand
1283 Renaissance Dam, 2020).

1284



1285
1286
1287
1288
1289

Figure 9: Cumulative reservoir storage capacity between 1900 and 2020. Reservoirs that are active before the year 1901 have been assigned to the year 1900. Horizontal axis shows year of construction, completion, or commissioning, reflecting ambiguity in available data.

1290 The original GRanDv1.3 dam locations were mapped to the global 30-min drainage direction map
1291 (ISIMIPddm30, (Müller Schmied, 2022) based on DDM30 (Döll and Lehner, 2002), by applying the
1292 following algorithm:

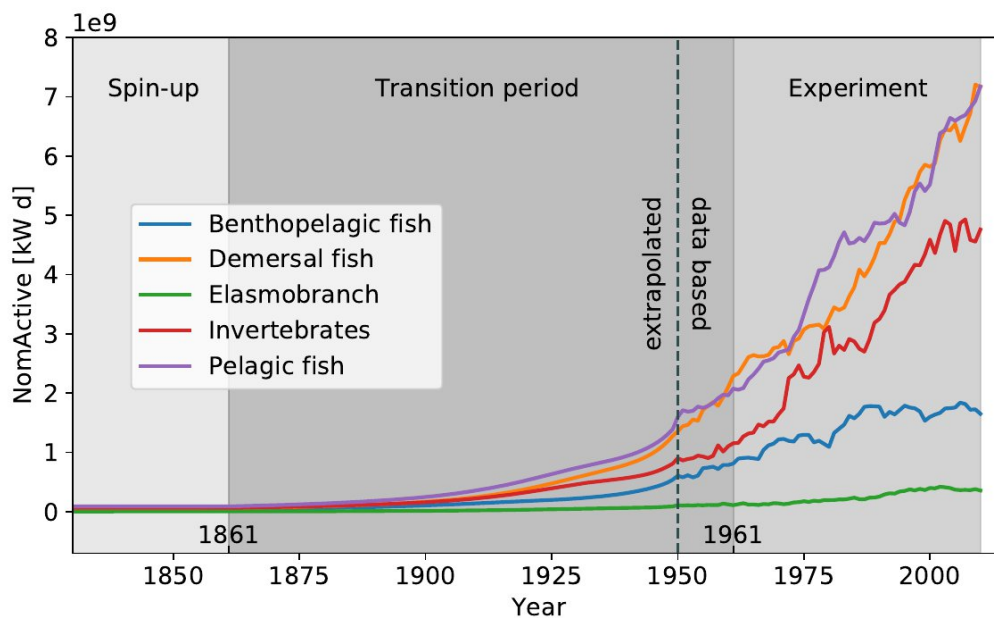
1293 Firstly, the locations have been rounded to the closest 0.5° grid cell centre. Then, the area of the
1294 upstream catchment draining into the GRanD reservoirs (previous version of GRanDv1.3) in the
1295 ISIMIPddm30 map have been calculated and compared against the ones reported in GRanD. All dams
1296 with an upstream area bigger than 10000 km² in GRanD and more than 50% deviation from the GRanD
1297 upstream area have been shifted to the 8 possible neighbouring cells. If any of these shifts resulted in
1298 a smaller deviation from the GRanD upstream areas, the dam was moved to the grid cell resulting in
1299 the smallest deviation in the upstream area.

1300 Additionally, a visual validation and, where appropriate, manual relocation were applied with the aim to
1301 find the best fitting grid cell from a hydrological perspective. [Due to the low resolution of the model grid,](#)
1302 [reservoirs might get wrongly assigned to e.g. the main stream \(either before or after the confluence of](#)
1303 [two rivers\), even though the dam is located in a particular tributary according to the database.](#)

1304 In those cases, and based on visual GIS inspection, the best location was searched, e.g. by moving the
1305 dam location one cell upstream to preserve the routing order and to avoid a different or much deviating
1306 river basin in the ISIMIPddm30 stream network. In case a dam is not assigned to any river basin in the
1307 ISIMIPddm30 (which can happen due to the difference in spatial resolution), the most suited location

1308 according to the observed upstream area was selected. Because of limited capacity, this visual
 1309 validation procedure was applied only for dams present in the earlier GranDv1.1 version that have a
 1310 maximum storage capacity greater than 0.5 km³ (1108 dams), as well as for all the 458 additional dams
 1311 in GRanDv1.3 and the 11 dams (excluding post-2020 dams) added from GeoDAR v1.2, and not for
 1312 several thousand smaller dams present in GranDv1.1. [In total the reported dams have a global
 1313 cumulative storage capacity of approximately 6932 km³ \(Figure 9\).](#)

1314
 1315 **4.9 Fishing intensities**



1316
 1317 **Figure 10: Evolution of historical nominal active fishing effort (NomActive) as provided for the spin-up,**
 1318 **transition period, and ‘obsclim + histoc, default’ ISIMIP3a experiment, separated by target functional group.** The
 1319 **groups represent an aggregation of 29 even finer categories covered by the data set (see Table 17).**

1320
 1321 **Table 17: Information about historical fishing intensities provided as DHF within ISIMIP3a.** For the spin-up
 1322 **+ transition period required by models within the *marine ecosystems and fisheries* sector the forcing is provided**
 1323 **for 1841-2010 although the ‘obsclim + histoc, default’ experiment only starts in 1961.**

Variable	Variable specifier	Unit	Resolution	Datasets
Total nominal active fishing effort (i.e., accounting for total power of the fleet but not including changes in the efficiency of fishing technology) separated by fishing sector, fleet, and target	NomActive	kW d (kilowatts of fleet power times days at sea)	annual data spatially grouped by Exclusive Economic Zones (EEZ), (Sea Around Us Area Parameters and Definitions) and nested within Large Marine Ecosystems. Masks for the latter	Reconstruction based on historical yearbook and FAO compilations ((Rousseau et al., 2022) based on (Rousseau et al., submitted 2023). The reconstructions have

functional groups.			are provided as static geographic information (see Table 1).	been extended backwards to 1841 by constant 1861 values to cover the 120 years of spin-up required for the marine ecosystems and fisheries models
--------------------	--	--	--	---

1324

1325 The data set of reconstructed historical fishing efforts (Rousseau et al., 2022) serves as the DHF for
 1326 the *marine ecosystems and fisheries* sector. The efforts are quantified for 'artisanal' and 'industrial'
 1327 fishing (sector), 66 Large Marine Ecosystems (LME), 187 national Exclusive Economic Zones (EEZ)
 1328 and 'high seas', 244 country identifiers from the Sea Around Us Project (SAUP), 16 different categories
 1329 of applied gears (e.g. bottom trawls, longlines and purse seines), 29 target functional groups ([see](#)
 1330 [nominal active fishing effort for 5 aggregated categories in Figure 10](#)), separately.

1331 The original annual time series spanning 1950-2015 were further extrapolated into the past to 1861
 1332 using generalised additive models (Rousseau et al., submitted 2023; see **Figure 10**). To cover the
 1333 'spin-up + transition' period from 1841-1960 the data set has been extended backwards by 1861 values.
 1334 Forcing with this dataset allows for a comparison of simulated catches against the congruent (Watson,
 1335 2019) reconstruction of historical fisheries catches (spanning the period 1869-2015; (Watson and Tidd,
 1336 2018). To permit integration into marine ecosystem models that capture different fishing sectors, fleets,
 1337 and functional groups these data include nominal active fishing effort disaggregated by location
 1338 (Exclusive Economic Zone/High Seas and Large Marine Ecosystem), fishing country, fishing gear,
 1339 targeted functional group, and fishing sector (coastal artisanal and industrial). Impact modellers are
 1340 allowed to distribute this effort across space, time, and target organisms in any method compatible with
 1341 their models' structure. The fishing effort data does not include any information about changes in the
 1342 efficiency of fishing technology over time (technological creep). Assumptions about these efficiencies
 1343 are left to the individual modellers and usually determined in model calibration.

1344

1345 **4.10 Forest management for *regional forest sector***

1346

1347 **Table 18:** Information about historical forest management provided as DHF for the *regional forest sector* within
 1348 ISIMIP3a

Variable	Variable specifier	Unit	Resolution	Datasets
Silvicultural system	sysi	na	stand	(Reyer et al., 2023)
Tree species	species	na	stand	(Reyer et al.,

				2023)
Harvest type	harvtype	na	stand	(Reyer et al., 2023)
Thinning type	thintype	% of basal area	stand	(Reyer et al., 2023)
Rotation length	rotlength	year	stand	(Reyer et al., 2023)
Thinning frequency	thinfrequ	year	stand	(Reyer et al., 2023)
Year of Management intervention	manyear	year	stand	(Reyer et al., 2023)
Type of management intervention	mantype	na	stand	(Reyer et al., 2023)
Regeneration species	regen	na	stand	(Reyer et al., 2023)
Planting density	plantdens	na	stand	(Reyer et al., 2023)
Planting age	plantage	year	stand	(Reyer et al., 2023)
Planting seedling height	planthei	m	stand	(Reyer et al., 2023)
Planting diameter at breast height	plantdbh	cm	stand	(Reyer et al., 2023)
Age when diameter at breast height is reached	dbhage	year	stand	(Reyer et al., 2023)
Stem number	stemno	na	stand	(Reyer et al., 2020a) based on (Reyer et al., 2020b)

1349

1350 For the *regional forest* sector, forest management is defined for nine forest sites in Europe, four in
1351 Germany (Peitz, KROOF, Solling-beech, Solling-spruce) as well in Czech Republic (Bily Kriz), Denmark
1352 (Sorø), France (Le Bray), Italy (Collelongo) and Finland (Hyytiälä) (Reyer et al., 2020b). ~~For the~~
1353 ~~historical period, observed stem numbers and forest thinning types are provided in the same ways as~~
1354 ~~in ISIMIP2b from the PROFOUND Database (Reyer et al., 2020b) so that modellers can mimic the~~
1355 ~~exact management that has happened at the site and perform the histsoc runs as close to reality as~~
1356 ~~possible (for further information about the ISIMIP2 simulation round see introduction).~~ Additionally, a
1357 set of forest site-specific forest management rules and planting numbers based on historical standard
1358 management practices of the area where the forest sites are located are defined and spelled out in
1359 concrete management schedules to enable modellers to simulate '2015soc' conditions (Reyer et al.,
1360 2023). ~~The regional forest management data has not been harmonised to the global gridded wood~~
1361 ~~harvest data provided for the biomes sector, because the data is very site-specific and the variation not~~
1362 ~~resolved in the global data set.~~

1363

1364 **5 ConclusionDiscussion**

1365 ~~The first part of the third simulation round of the Inter-sectoral Impact Model Intercomparison Project~~
1366 ~~ISIMIP (ISIMIP3a) is intended to facilitate impact model evaluation and impact attribution experiments~~
1367 ~~to significantly move forward our understanding of observed changes in natural and human systems~~
1368 ~~and their respective drivers. Impact models as participating in ISIMIP encode our process knowledge~~
1369 ~~on how several drivers (climate-related ones as well as direct human influences) come together to~~
1370 ~~generate observed changes. As such, they are ideal tools for this task. The new ISIMIP3a simulation~~
1371 ~~framework including the provision of the relevant forcing data is intended to unleash the power of a wide~~
1372 ~~range of models from different sectors to quantify the contribution of observed changes in climate-~~
1373 ~~related systems to observed environmental or societal changes. ¶~~

1374 ~~As a first step towards impact attribution, the~~ ISIMIP3a evaluation experiments will help to clarify how
1375 well the current generation of impact models can explain observed changes in impacted systems based
1376 on provided information about the different forcings. ~~The performance of the models in reproducing~~
1377 ~~observed variations and long-term changes in the impacted systems, certainly does not only depend~~
1378 ~~on the models themselves but also on the availability and uncertainties associated with the climate-~~
1379 ~~related and direct human forcings (see Table 1). We capture part of this uncertainty by providing four~~
1380 ~~different observational atmospheric climate forcing data and associated counterfactual forcings (see~~
1381 ~~section 2.1) and TC windfields derived from two different modelling approaches (see section 3.2).~~
1382 ~~Uncertainties in the direct human forcings are represented to the degree that the forcing data sets~~
1383 ~~considered as 'optional' vary from model to model. In addition, the multi-model framework of ISIMIP~~
1384 ~~allows for testing to what degree different process-representations may be better suitable to explain the~~
1385 ~~observations than others. ¶~~

1386 ~~High explanatory power is then a prerequisite then allows~~ for impact attribution through the ISIMIP3a
1387 attribution experiments ~~based on counterfactual climate-related forcings~~ following the IPCC definition
1388 (O'Neill et al., 2022), ~~disentangling changes in climate-related forcings from other drivers of change. ¶~~

1389 ¶

1390 The setup is the first that allows to easily and broadly address impact attribution across many impact
1391 categories. This will fill an important gap as only few process-based impact models have been used in
1392 this field despite their general suitability. [The presented](#) work can thus lay the ground for urgently
1393 necessary works to inform climate litigation (Burger et al., 2020; Burger and Tigre, 2023), the loss and
1394 damage debate (Mechler et al., 2018; Wyns, 2023), and last but not least also decisions about short
1395 term adaptation measures. It will ultimately help to carve out the sensitivity of our ecosystems and
1396 human societies to historical climate change, which is a precondition for robustly projecting future
1397 climate impacts.

1398 This paper aims to give an overview of the ISIMIP3a experiments and the provided climate-related and
1399 direct human forcing data sets. It is intended to work as a catalogue where modellers can find all
1400 relevant information about the data sets they need for the impact model simulations within ISIMIP3a.
1401 As a community-driven initiative across multiple disciplines the selection of the best available forcing
1402 data for ISIMIP builds on the expertise within the different sectoral communities.

1403 We would like to improve or complement these data sets in a continuous process wherever possible.
1404 So this paper can also be read as a call for contributing additional data that could i) be provided within
1405 the current round (ISIMIP3) as optional data (see explanation in the introduction) that is not harmonised
1406 within or across sectors or ii) as mandatory forcing for an upcoming simulation round. In particular, we
1407 aim for temporally resolved historical growing seasons that have been shown to be critical to reproduce
1408 observed crop yields (Jägermeyr and Frieler, 2018), counterfactual oceanic climate-related forcings,
1409 counterfactual TC-related precipitation (Risser and Wehner, 2017; van Oldenborgh et al., 2017; Wang
1410 et al., 2018; Patricola and Wehner, 2018), temporally resolved lightning data for the full set of considered
1411 climate model simulations, and temporally resolved human drainage and restoration activities in
1412 peatlands as one of the key controls over global peatland greenhouse gas emissions (Loisel et al.,
1413 2020).

1414

1415

1416 **Author contribution:** KF lead the project and developed the concept with contributions from JS, MM,
1417 CO, CPOR, JLB, CSH, CMP, TDE, KOC, CN, RH, DT, OM, JJ, GL, SC, EB, AGS, NS, JC, SH, CB, AG,
1418 FL, SNG, HMS, FH, TH, RM, DP, WT, DMB, MB. JV supported the data generation [and harmonisation](#)
1419 [of the protocol across all sectors](#). SL provided atmospheric climate forcing data. MM provided coastal
1420 water level data and atmospheric forcing data. MdRRL, JW and FY provided dam data. CO and IJS
1421 provided GDP data. CPOR provided forest management data. DNK and JTM provided high resolution
1422 climate forcing data. ST provided coastal water levels and counterfactual climate forcing data. YR
1423 provided data on fishing efforts. CS and XL provided ocean forcing data. TV provided TC data. TW and
1424 FS provided gridded GDP data. IV provided lake data. JJ provided growing seasons. CM provided soil
1425 data. KF prepared the manuscript with contributions from all co-authors.

1426

1427 **Code and data availability:** All input data described is available for participating modelers with a
1428 respective account at the DKRZ server. Data will be made publicly available, and most data is already
1429 publicly available at <https://data.isimip.org/>. Availability is documented on www.isimip.org where the

1430 way of accessing the data is described, as well. Model output is already partly available at
1431 <https://data.isimip.org/>.

1432 The ISIMIP Repository fulfills the Archive standards as stated in the "GMD code and data policy". The
1433 Repository is hosted and maintained by the Potsdam Institute for Climate Impact Research (PIK). Data
1434 can only be published or removed from the repository by the ISIMIP data team, that is monitored by the
1435 ISIMIP steering committee according to the organisational structure of ISIMIP (ISIMIP organigram,
1436 2020). DOI are used to refer to datasets in a persistent way. Whenever a dataset is replaced for any
1437 reason a copy is kept on tape, and a new DOI is issued, while the old DOI is kept online with information
1438 on how to retrieve the archived data. Detailed information can be found in the ISIMIP terms of use
1439 (ISIMIP terms of use, 2023).

1440

1441 **Competing interests:** At least one of the (co-)authors is a member of the editorial board of
1442 Geoscientific Model Development.

1443

1444 **Acknowledgements**

1445 This article is based upon work from COST Action CA19139 PROCLIAS (PROcess-based models for
1446 CLimate Impact Attribution across Sectors), supported by COST (European Cooperation in Science
1447 and Technology; <https://www.cost.eu>). Funding from the EU Horizon 2020 research and innovation
1448 program under grant agreement 821010 (CASCADES) supported the work of C.P.O.R., J.V. and
1449 I.D.VdV., and the provisioning of the high resolution climate data, and supported the work of ST under
1450 grant agreement No 820712 (RECEIPT). SL received funding from the German Research Foundation
1451 (DFG, project number 427397136). The German Federal Ministry of Education and Research
1452 (BMBF) supported the work under the research projects ISIAccess (16QK05), SLICE (01LA1829A),
1453 QUIDIC (01LP1907A), CHIPS (01LS1904A), ISlpedia (01LS1711A). FL received funding from the
1454 National Key Research and Development Program of China (project number 2022YFE0106500). JC
1455 received funding from the National Key Research and Development Program of China (project number
1456 2022YFF0801904). MB acknowledges funding from the Research Foundation—Flanders (FWO,
1457 G095720N). SC and NS were supported by the National Environmental Research Council (NERC)
1458 grant NE/R015791/1. SC, AGS, MB and NS acknowledge funding through NERC NE/V01854X/1
1459 (MOTHERSHIP). CB was supported by the Newton Fund through the Met Office. The research by DNK
1460 was funded through the 2019-2020 BiodivERsA joint call for research proposals, under the BiodivClim
1461 ERA-Net COFUND program, and with the funding organisations Swiss National Science Foundation
1462 SNF (project: FeedBaCks, 193907), and the Swiss National Science Foundation SNF (project: Adohris,
1463 205530). RM was supported by the Alter-C project (PID2020-114024GB-C32/AEI
1464 /10.13039/501100011033). CSH was supported by Open Philanthropy, NSF award 2218777, and
1465 NOAA CPO.

1466

1467

1468 **References**

- 1469 Anon: World development indicators, World Bank Publications, Washington, D.C., DC, 2008.
- 1470 Land use harmonization: <https://luh.umd.edu>, last access: 9 January 2023.
- 1471 Outcomes of the ISIMIP Strategy Group Meeting: <https://www.isimip.org/news/outcome-isimip-strategy-group-meeting-2018/>, last access: 14 January 2023.
- 1472
- 1473 Protocol - TRENDY: <https://blogs.exeter.ac.uk/trendy/protocol/>, last access: 18 October 2023.
- 1474 ISIMIP2a: suspicious gridded GDP per capita data; new functions in the isimip data repository; Forum
1475 on Scenarios for Climate and Societal Futures: <https://www.isimip.org/newsletter/simip2a-suspicious-gridded-gdp-capita-data-new-functions-isimip-data-repository-forum-scenarios-climate-and-societal-futures/>, last access: 10 February 2023.
- 1476
- 1477
- 1478 ISIMIP Output Data Table: <https://www.isimip.org/outputdata/>, last access: 19 October 2023.
- 1479 ISIMIP terms of use: <https://www.isimip.org/gettingstarted/terms-of-use/>, last access: 14 January
1480 2023.
- 1481 ISIMIP3 simulation protocol: <https://protocol.isimip.org/>, last access: 14 January 2023.
- 1482 WOCE Atlas: <http://woceatlas.ucsd.edu>, last access: 11 January 2023.
- 1483 Arujo, E., Bodirsky, B. L., Crawford, M. S., Leip, D., and Dietrich, J.: MissingIslands dataset for filling
1484 in data gaps from the WDI datasets, <https://doi.org/10.5281/zenodo.4421504>, 2021.
- 1485 Badger, J., Bauwens, I., Casso, P., Davis, N., Hahmann, A., Hansen, S. B. K., Hansen, B. O.,
1486 Heathfield, D., Knight, O. J., Lacave, O., Lizcano, G., Mas, A. B. i., Mortensen, N. G., Olsen, B. T.,
1487 Onninen, M., Van Loon, A. P., and Volker, P.: Global Wind Atlas, n.d.
- 1488 Bloemendaal, N., de Moel, H., Mol, J. M., Bosma, P. R. M., Polen, A. N., and Collins, J. M.:
1489 Adequately reflecting the severity of tropical cyclones using the new Tropical Cyclone Severity Scale,
1490 *Environ. Res. Lett.*, 16, 014048, 2021.
- 1491 Brun, P., Zimmermann, N. E., Hari, C., Pellissier, L., and Karger, D. N.: CHELSA-BIOCLIM+ A novel
1492 set of global climate-related predictors at kilometre-resolution, <https://doi.org/10.16904/envidat.332>,
1493 2022a.
- 1494 Brun, P., Zimmermann, N. E., Hari, C., Pellissier, L., and Karger, D. N.: Global climate-related
1495 predictors at kilometre resolution for the past and future, , <https://doi.org/10.5194/essd-2022-212>,
1496 2022b.
- 1497 Büchner, M. and Reyer, C.: ISIMIP3a atmospheric composition input data,
1498 <https://doi.org/10.48364/ISIMIP.664235.2>, 2022.
- 1499 Burger, M. and Tigre, M. A.: Global Climate Litigation Report: 2023 Status Review, 2023.
- 1500 Burger, M., Wentz, J., and Horton, R.: The Law and Science of Climate Change Attribution, 1, 45,
1501 <https://doi.org/10.7916/cjel.v45i1.4730>, 2020.
- 1502 Caron, L., Ivins, E. R., Larour, E., Adhikari, S., Nilsson, J., and Blewitt, G.: GIA model statistics for
1503 GRACE hydrology, cryosphere, and ocean science, *Geophys. Res. Lett.*, 45, 2203–2212, 2018.
- 1504 Cecil, D.: LIS/OTD 0.5 Degree High Resolution Monthly Climatology (HRMC),
1505 <https://doi.org/10.5067/LIS/LIS-OTD/DATA303>, 2006.
- 1506 Chavas, D. R. and Lin, N.: A Model for the Complete Radial Structure of the Tropical Cyclone Wind
1507 Field. Part II: Wind Field Variability, *J. Atmos. Sci.*, 73, 3093–3113, 2016.
- 1508 Compo, G. P., Whitaker, J. S., Sardeshmukh, P. D., Matsui, N., Allan, R. J., Yin, X., Gleason, B. E.,
1509 Vose, R. S., Rutledge, G., Bessemoulin, P., Brönnimann, S., Brunet, M., Crouthamel, R. I., Grant, A.

- 1510 N., Groisman, P. Y., Jones, P. D., Kruk, M. C., Kruger, A. C., Marshall, G. J., Maugeri, M., Mok, H. Y.,
 1511 Nordli, Ø., Ross, T. F., Trigo, R. M., Wang, X. L., Woodruff, S. D., and Worley, S. J.: The twentieth
 1512 century reanalysis project, *Quart. J. Roy. Meteor. Soc.*, 137, 1–28, 2011.
- 1513 Cramer, W., Yohe, G. W., Auffhammer, M., Huggel, C., Molau, U., da Silva Dias, M. A. F., Solow, A.,
 1514 Stone, D. A., and Tibig, L.: Detection and Attribution of Observed Impacts: Climate Change 2014:
 1515 Impacts Adaptation and Vulnerability, Contribution of Working Group II to the Fifth Assessment Report
 1516 of the Intergovernmental Panel on Climate Change, in: *Climate Change 2014: Impacts Adaptation and*
 1517 *Vulnerability, Contribution of Working Group II to the Fifth Assessment Report of the*
 1518 *Intergovernmental Panel on Climate Change*, Cambridge University Press, 2014.
- 1519 Cucchi, M., Weedon, G. P., Amici, A., Bellouin, N., Lange, S., Müller Schmied, H., Hersbach, H., and
 1520 Buontempo, C.: WFDE5: bias-adjusted ERA5 reanalysis data for impact studies, *Earth Syst. Sci.*
 1521 *Data*, 12, 2097–2120, 2020.
- 1522 Dangendorf, S., Hay, C., Calafat, F. M., Marcos, M., Piecuch, C. G., Berk, K., and Jensen, J.:
 1523 Persistent acceleration in global sea-level rise since the 1960s, *Nat. Clim. Chang.*, 9, 705–710, 2019.
- 1524 Danielson, J. J. and Gesch, D. B.: Global multi-resolution terrain elevation data 2010 (GMTED2010),
 1525 U.S. Geological Survey, <https://doi.org/10.3133/ofr20111073>, 2011.
- 1526 Dirmeyer, P. A., Gao, X., Zhao, M., Guo, Z., Oki, T., and Hanasaki, N.: GSWP-2: Multimodel Analysis
 1527 and Implications for Our Perception of the Land Surface, *Bull. Am. Meteorol. Soc.*, 87, 1381–1398,
 1528 2006.
- 1529 Döll, P. and Lehner, B.: Validation of a new global 30-min drainage direction map, *J. Hydrol.*, 258,
 1530 214–231, 2002.
- 1531 Eberenz, S., Stocker, D., Rösli, T., and Bresch, D. N.: LitPop: Global Exposure Data for Disaster
 1532 Risk Assessment, 2019.
- 1533 Eberenz, S., Lüthi, S., and Bresch, D. N.: Regional tropical cyclone impact functions for globally
 1534 consistent risk assessments, *Nat. Hazards Earth Syst. Sci.*, 21, 393–415, 2021.
- 1535 Elvidge, C. D., Baugh, K., Zhizhin, M., Hsu, F. C., and Ghosh, T.: VIIRS night-time lights, *Int. J.*
 1536 *Remote Sens.*, 38, 5860–5879, 2017.
- 1537 Emanuel, K. and Rotunno, R.: Self-Stratification of Tropical Cyclone Outflow. Part I: Implications for
 1538 Storm Structure, *J. Atmos. Sci.*, 68, 2236–2249, 2011.
- 1539 Fagnant, C., Gori, A., Sebastian, A., Bedient, P. B., and Ensor, K. B.: Characterizing spatiotemporal
 1540 trends in extreme precipitation in Southeast Texas, *Nat. Hazards*, 104, 1597–1621, 2020.
- 1541 FAO: Faostat: FAO Statistical Databases, 2016.
- 1542 Feenstra, R. C., Inklaar, R., Timmer, M., and Woltjer, P.: Penn World Table 10.0,
 1543 <https://doi.org/10.15141/S5Q94M>, 2015.
- 1544 Feldmann, M., Emanuel, K., Zhu, L., and Lohmann, U.: Estimation of Atlantic Tropical Cyclone
 1545 Rainfall Frequency in the United States, *J. Appl. Meteorol. Climatol.*, 58, 1853–1866, 2019.
- 1546 Fiddes, J. and Gruber, S.: TopoSCALE v.1.0: downscaling gridded climate data in complex terrain,
 1547 *Geosci. Model Dev.*, 7, 387–405, 2014.
- 1548 Friedlingstein, P., O'Sullivan, M., Jones, M. W., Andrew, R. M., Gregor, L., Hauck, J., Le Quéré, C.,
 1549 Lujikx, I. T., Olsen, A., Peters, G. P., Peters, W., Pongratz, J., Schwingshackl, C., Sitch, S., Canadell,
 1550 J. G., Ciais, P., Jackson, R. B., Alin, S. R., Alkama, R., Arneeth, A., Arora, V. K., Bates, N. R., Becker,
 1551 M., Bellouin, N., Bittig, H. C., Bopp, L., Chevallier, F., Chini, L. P., Cronin, M., Evans, W., Falk, S.,
 1552 Feely, R. A., Gasser, T., Gehlen, M., Gkritzalis, T., Gloege, L., Grassi, G., Gruber, N., Gürses, Ö.,
 1553 Harris, I., Hefner, M., Houghton, R. A., Hurtt, G. C., Iida, Y., Ilyina, T., Jain, A. K., Jersild, A., Kadono,
 1554 K., Kato, E., Kennedy, D., Klein Goldewijk, K., Knauer, J., Korsbakken, J. I., Landschützer, P.,
 1555 Lefèvre, N., Lindsay, K., Liu, J., Liu, Z., Marland, G., Mayot, N., McGrath, M. J., Metz, N., Monacci, N.

- 1556 M., Munro, D. R., Nakaoka, S.-I., Niwa, Y., O'Brien, K., Ono, T., Palmer, P. I., Pan, N., Pierrot, D.,
 1557 Pocock, K., Poulter, B., Resplandy, L., Robertson, E., Rödenbeck, C., Rodriguez, C., Rosan, T. M.,
 1558 Schwinger, J., Séférian, R., Shutler, J. D., Skjelvan, I., Steinhoff, T., Sun, Q., Sutton, A. J., Sweeney,
 1559 C., Takao, S., Tanhua, T., Tans, P. P., Tian, X., Tian, H., Tilbrook, B., Tsujino, H., Tubiello, F., van der
 1560 Werf, G. R., Walker, A. P., Wanninkhof, R., Whitehead, C., Willstrand Wranne, A., et al.: Global
 1561 carbon budget 2022, *Earth Syst. Sci. Data*, 14, 4811–4900, 2022.
- 1562 Frieler, K.: Scenario Set-up and the new CMIP6-based climate-related forcings provided within the
 1563 third round of the Inter-Sectoral Model Intercomparison Project (ISIMIP3b, group I and II),
 1564 Geoscientific Model Development, submitted 2023.
- 1565 Frieler, K., Lange, S., Piontek, F., Reyer, C. P. O., Schewe, J., Warszawski, L., Zhao, F., Chini, L.,
 1566 Denvil, S., Emanuel, K., Geiger, T., Halladay, K., Hurtt, G., Mengel, M., Murakami, D., Ostberg, S.,
 1567 Popp, A., Riva, R., Stevanovic, M., Suzuki, T., Volkholz, J., Burke, E., Ciais, P., Ebi, K., Eddy, T. D.,
 1568 Elliott, J., Galbraith, E., Gosling, S. N., Hattermann, F., Hickler, T., Hinkel, J., Hof, C., Huber, V.,
 1569 Jägermeyr, J., Krysanova, V., Marcé, R., Müller Schmied, H., Mouratiadou, I., Pierson, D., Tittensor,
 1570 D. P., Vautard, R., van Vliet, M., Biber, M. F., Betts, R. A., Bodirsky, B. L., Deryng, D., Frohking, S.,
 1571 Jones, C. D., Lotze, H. K., Lotze-Campen, H., Sahajpal, R., Thonicke, K., Tian, H., and Yamagata, Y.:
 1572 Assessing the impacts of 1.5 °C global warming – simulation protocol of the Inter-Sectoral Impact
 1573 Model Intercomparison Project (ISIMIP2b), *Geosci. Model Dev.*, 10, 4321–4345, 2017.
- 1574 Geiger, T., Frieler, K., and Bresch, D. N.: A global historical data set of tropical cyclone exposure
 1575 (TCE-DAT), *Earth System Science Data*, 10, 185–194, 2018.
- 1576 Gillett, N. P., Shiogama, H., Funke, B., Hegerl, G., Knutti, R., Matthes, K., Santer, B. D., Stone, D.,
 1577 and Tebaldi, C.: The Detection and Attribution Model Intercomparison Project (DAMIP v1.0)
 1578 contribution to CMIP6, *Geoscientific Model Development*, 9, 3685–3697, 2016.
- 1579 Golub, M., Thiery, W., Marcé, R., Pierson, D., Vanderkelen, I., Mercado-Bettin, D., Woolway, R. I.,
 1580 Grant, L., Jennings, E., Kraemer, B. M., Schewe, J., Zhao, F., Frieler, K., Mengel, M., Bogomolov, V.
 1581 Y., Bouffard, D., Côté, M., Couture, R.-M., Debolskiy, A. V., Droppers, B., Gal, G., Guo, M., Janssen,
 1582 A. B. G., Kirillin, G., Ladwig, R., Magee, M., Moore, T., Perroud, M., Piccolroaz, S., Raaman Vinnua,
 1583 L., Schmid, M., Shatwell, T., Stepanenko, V. M., Tan, Z., Woodward, B., Yao, H., Adrian, R., Allan, M.,
 1584 Anneville, O., Arvola, L., Atkins, K., Boegman, L., Carey, C., Christianson, K., de Eyto, E., DeGasperi,
 1585 C., Grechushnikova, M., Hejzlar, J., Joehnk, K., Jones, I. D., Laas, A., Mackay, E. B., Mammarella, I.,
 1586 Markensten, H., McBride, C., Özkundakci, D., Potes, M., Rinke, K., Robertson, D., Rusak, J. A.,
 1587 Salgado, R., van der Linden, L., Verburg, P., Wain, D., Ward, N. K., Wollrab, S., and Zdrovennova,
 1588 G.: A framework for ensemble modelling of climate change impacts on lakes worldwide: the ISIMIP
 1589 Lake Sector, *Geosci. Model Dev.*, 15, 4597–4623, 2022.
- 1590 Gori, A., Lin, N., and Smith, J.: Assessing compound flooding from landfalling tropical cyclones on the
 1591 North Carolina coast, *Water Resour. Res.*, 56, <https://doi.org/10.1029/2019wr026788>, 2020.
- 1592 Gori, A., Lin, N., Xi, D., and Emanuel, K.: Tropical cyclone climatology change greatly exacerbates US
 1593 extreme rainfall–surge hazard, *Nat. Clim. Chang.*, 12, 171–178, 2022.
- 1594 Hansen, G., Stone, D., Auffhammer, M., Huggel, C., and Cramer, W.: Linking local impacts to
 1595 changes in climate: a guide to attribution, *Regional Environ. Change*, 16, 527–541, 2016.
- 1596 Hersbach, H., Bell, B., Berrisford, P., Hirahara, S., Horányi, A., Muñoz-Sabater, J., Nicolas, J.,
 1597 Peubey, C., Radu, R., Schepers, D., Simmons, A., Soci, C., Abdalla, S., Abellan, X., Balsamo, G.,
 1598 Bechtold, P., Biavati, G., Bidlot, J., Bonavita, M., Chiara, G., Dahlgren, P., Dee, D., Diamantakis, M.,
 1599 Dragani, R., Flemming, J., Forbes, R., Fuentes, M., Geer, A., Haimberger, L., Healy, S., Hogan, R. J.,
 1600 Hólm, E., Janisková, M., Keeley, S., Laloyaux, P., Lopez, P., Lupu, C., Radnoti, G., Rosnay, P.,
 1601 Rozum, I., Vamborg, F., Villaume, S., and Jean-Noël Thépaut: The ERA5 global reanalysis, *Quart. J.*
 1602 *Roy. Meteor. Soc.*, 146, 1999–2049, 2020.
- 1603 Holland, G.: A Revised Hurricane Pressure–Wind Model, *Mon. Weather Rev.*, 136, 3432–3445, 2008.
- 1604 Holland, G. J.: An Analytic Model of the Wind and Pressure Profiles in Hurricanes, *Mon. Weather*
 1605 *Rev.*, 108, 1212–1218, 1980.

- 1606 Hope, P., Cramer, W., van Aalst, M., Flato, G., Frieler, K., Gillett, N., Huggel, C., Minx, J., Otto, F.,
 1607 Parmesan, C., Rogelj, J., Rojas, M., Seneviratne, S. I., Slangen, A., Stone, D., Terray, L., Vautard, R.,
 1608 and Zhang, X.: Cross-Working Group Box ATTRIBUTION | Attribution in the IPCC Sixth Assessment
 1609 Report, in: *Climate Change 2022 – Impacts, Adaptation and Vulnerability: Working Group II*
 1610 *Contribution to the Sixth Assessment Report of the Intergovernmental Panel on Climate Change*,
 1611 edited by: Pörtner, H.-O., Roberts, D. C., Tignor, M., Poloczanska, E. S., Mintenbeck, K., Alegría, A.,
 1612 Craig, M., Langsdorf, S., Löschke, S., Möller, V., Okem, A., and Rama, B., Cambridge University
 1613 Press, 121–196, 2022.
- 1614 van den Hurk, B., Kim, H., Krinner, G., Seneviratne, S. I., Derksen, C., Oki, T., Douville, H., Colin, J.,
 1615 Ducharne, A., Cheruy, F., Viovy, N., Puma, M. J., Wada, Y., Li, W., Jia, B., Alessandri, A., Lawrence,
 1616 D. M., Weedon, G. P., Ellis, R., Hagemann, S., Mao, J., Flanner, M. G., Zampieri, M., Matera, S.,
 1617 Law, R. M., and Sheffield, J.: LS3MIP (v1.0) contribution to CMIP6: the Land Surface, Snow and Soil
 1618 moisture Model Intercomparison Project – aims, setup and expected outcome, *Geosci. Model Dev.*, 9,
 1619 2809–2832, 2016.
- 1620 Hurtt, G. C., Chini, L. P., Frohking, S., Betts, R. A., Feddema, J., Fischer, G., Fisk, J. P., Hibbard, K.,
 1621 Houghton, R. A., Janetos, A., Jones, C. D., Kindermann, G., Kinoshita, T., Klein Goldewijk, K., Riahi,
 1622 K., Shevliakova, E., Smith, S., Stehfest, E., Thomson, A., Thornton, P., van Vuuren, D. P., and Wang,
 1623 Y. P.: Harmonization of land-use scenarios for the period 1500–2100: 600 years of global gridded
 1624 annual land-use transitions, wood harvest, and resulting secondary lands, *Clim. Change*, 109, 117,
 1625 2011.
- 1626 Hurtt, G. C., Chini, L., Sahajpal, R., Frohking, S., Bodirsky, B. L., Calvin, K., Doelman, J. C., Fisk, J.,
 1627 Fujimori, S., Klein Goldewijk, K., Hasegawa, T., Havlik, P., Heinemann, A., Humpenöder, F.,
 1628 Jungclaus, J., Kaplan, J. O., Kennedy, J., Krisztin, T., Lawrence, D., Lawrence, P., Ma, L., Mertz, O.,
 1629 Pongratz, J., Popp, A., Poulter, B., Riahi, K., Shevliakova, E., Stehfest, E., Thornton, P., Tubiello, F.
 1630 N., van Vuuren, D. P., and Zhang, X.: Harmonization of global land use change and management for
 1631 the period 850–2100 (LUH2) for CMIP6, *Geosci. Model Dev.*, 13, 5425–5464, 2020.
- 1632 IFASTAT: <https://www.ifastat.org>, last access: 21 January 2015.
- 1633 International Monetary Fund: *World economic outlook*, 2021.
- 1634 IPCC: Annex II: Glossary [Mach, K.J., S. Planton and C. von Stechow (eds.)], in: *Climate Change*
 1635 *2014: Synthesis Report. Contribution of Working Groups I, II and III to the Fifth Assessment Report of*
 1636 *the Intergovernmental Panel on Climate Change*, edited by: Core Writing Team, R. K. Pachauri and L.
 1637 A. Meyer, Geneva, Switzerland, 117–130, 2014.
- 1638 ISIMIP Coordination Team, Sectoral Coordinators, Scientific Advisory Board: *The Inter-Sectoral*
 1639 *Impact Model Intercomparison Project (ISIMIP), Mission & Implementation Document*,
 1640 https://www.isimip.org/documents/646/MissionAndImplementation_12Sep2018_5Hlvj2N.pdf, 2018.
- 1641 Jägermeyr, J. and Frieler, K.: Spatial variations in crop growing seasons pivotal to reproduce global
 1642 fluctuations in maize and wheat yields, *Sci Adv*, 4, eaat4517, 2018.
- 1643 Jägermeyr, J., Müller, C., Ruane, A. C., Elliott, J., Balkovic, J., Castillo, O., Faye, B., Foster, I.,
 1644 Folberth, C., Franke, J. A., Fuchs, K., Guarin, J. R., Heinke, J., Hoogenboom, G., Iizumi, T., Jain, A.
 1645 K., Kelly, D., Khabarov, N., Lange, S., Lin, T.-S., Liu, W., Mialyk, O., Minoli, S., Moyer, E. J., Okada,
 1646 M., Phillips, M., Porter, C., Rabin, S. S., Scheer, C., Schneider, J. M., Schyns, J. F., Skalsky, R.,
 1647 Smerald, A., Stella, T., Stephens, H., Webber, H., Zabel, F., and Rosenzweig, C.: Climate impacts on
 1648 global agriculture emerge earlier in new generation of climate and crop models, *Nature Food*, 2,
 1649 873–885, 2021a.
- 1650 Jägermeyr, J., Müller, C., Minoli, S., Ray, D., and Siebert, S.: GGCM Phase 3 crop calendar,
 1651 <https://doi.org/10.5281/ZENODO.5062513>, 2021b.
- 1652 Karger, D. N., Conrad, O., Böhner, J., Kawohl, T., Kreft, H., Soria-Auza, R. W., Zimmermann, N. E.,
 1653 Linder, H. P., and Kessler, M.: Climatologies at high resolution for the earth's land surface areas, *Sci*
 1654 *Data*, 4, 170122, 2017.
- 1655 Karger, D. N., Wilson, A. M., Mahony, C., Zimmermann, N. E., and Jetz, W.: Global daily 1 km land

- 1656 surface precipitation based on cloud cover-informed downscaling, *Sci Data*, 8, 307, 2021.
- 1657 Karger, D. N., Lange, S., Hari, C., Reyer, C. P. O., Conrad, O., Zimmermann, N. E., and Frieler, K.:
 1658 CHELSA-W5E5: Daily 1 km meteorological forcing data for climate impact studies, *Earth System*
 1659 *Science Data Discussions*, <https://doi.org/10.5194/essd-2022-367>, 2022a.
- 1660 Karger, D. N., Lange, S., Hari, C., Reyer, C. P. O., and Zimmermann, N. E.: CHELSA-W5E5 v1.0:
 1661 W5E5 v1.0 downscaled with CHELSA v2.0, <https://doi.org/10.48364/ISIMIP.836809.3>, 2022b.
- 1662 Khazaei, B., Read, L. K., Casali, M., Sampson, K. M., and Yates, D. N.: GLOBathy, the global lakes
 1663 bathymetry dataset, *Sci. Data*, 9, 36, 2022.
- 1664 Global soil wetness project phase 3 — GSWP3 documentation: <http://hydro.iis.u-tokyo.ac.jp/GSWP3/>,
 1665 last access: 9 January 2023.
- 1666 Kim, H.: Global Soil Wetness Project Phase 3 Atmospheric Boundary Conditions (Experiment 1),
 1667 <https://doi.org/10.20783/DIAS.501>, 2017.
- 1668 Klein Goldewijk, K., 2022.
- 1669 Klein Goldewijk, K., Beusen, A., Doelman, J., and Stehfest, E.: Anthropogenic land use estimates for
 1670 the Holocene – HYDE 3.2, *Earth Syst. Sci. Data*, 9, 927–953, 2017.
- 1671 Knapp, K. R. and Kruk, M. C.: Quantifying Interagency Differences in Tropical Cyclone Best-Track
 1672 Wind Speed Estimates, *Mon. Weather Rev.*, 138, 1459–1473, 2010.
- 1673 Knapp, K. R., Kruk, M. C., Levinson, D. H., Diamond, H. J., and Neumann, C. J.: The International
 1674 Best Track Archive for Climate Stewardship (IBTrACS): Unifying Tropical Cyclone Data, *Bull. Am.*
 1675 *Meteorol. Soc.*, 91, 363–376, 2010.
- 1676 Koch, J. and Leimbach, M.: SSP economic growth projections: Major changes of key drivers in
 1677 integrated assessment modelling, *Ecol. Econ.*, 206, 107751, 2023.
- 1678 Konzelmann, T., van de Wal, R. S. W., Greuell, W., Bintanja, R., Henneken, E. A. C., and Abe-Ouchi,
 1679 A.: Parameterization of global and longwave incoming radiation for the Greenland Ice Sheet, *Glob.*
 1680 *Planet. Change*, 9, 143–164, 1994.
- 1681 Krien, Y., Dudon, B., Roger, J., Arnaud, G., and Zahibo, N.: Assessing storm surge hazard and impact
 1682 of sea level rise in the Lesser Antilles case study of Martinique, *Nat. Hazards Earth Syst. Sci.*, 17,
 1683 1559–1571, 2017.
- 1684 Lange, S.: Trend-preserving bias adjustment and statistical downscaling with ISIMIP3BASD (v1.0),
 1685 *Geosci. Model Dev.*, 12, 3055–3070, 2019.
- 1686 Lange, S.: ISIMIP3BASD, <https://doi.org/10.5281/zenodo.4686991>, 2021.
- 1687 Lange, S. and Büchner, M.: ISIMIP3 land-sea masks, <https://doi.org/10.48364/ISIMIP.822294>, 2020.
- 1688 Lange, S., Menz, C., Gleixner, S., Cucchi, M., Weedon, G. P., Amici, A., Bellouin, N., Schmied, H. M.,
 1689 Hersbach, H., Buontempo, C., and Cagnazzo, C.: WFDE5 over land merged with ERA5 over the
 1690 ocean (W5E5 v2.0), <https://doi.org/10.48364/ISIMIP.342217>, 2021.
- 1691 Lan, X., Tans, P., and Thoning, K. W.: Trends in globally-averaged CO₂ determined from NOAA
 1692 Global Monitoring Laboratory measurements. Version 2023-01 NOAA/GML, 2023.
- 1693 Large, W. G. and Yeager, S. G.: The global climatology of an interannually varying air–sea flux data
 1694 set, *Clim. Dyn.*, 33, 341–364, 2009.
- 1695 Lawrence, D. M., Hurtt, G. C., Arneeth, A., Brovkin, V., Calvin, K. V., Jones, A. D., Jones, C. D.,
 1696 Lawrence, P. J., de Noblet-Ducoudré, N., Pongratz, J., Seneviratne, S. I., and Shevliakova, E.: The
 1697 Land Use Model Intercomparison Project (LUMIP) contribution to CMIP6: rationale and experimental
 1698 design, *Geosci. Model Dev.*, 9, 2973–2998, 2016.

- 1699 Lee, M., Shevliakova, E., Stock, C. A., Malyshev, S., and Milly, P. C. D.: Prominence of the tropics in
1700 the recent rise of global nitrogen pollution, *Nat. Commun.*, 10, 1437, 2019.
- 1701 Lehner, B., Reidy Liermann, C., Revenga, C., Vorosmarty, C., Fekete, B., Crouzet, P., Doll, P.,
1702 Endejan, M., Frenken, K., Magome, J., Nilsson, C., Robertson, J. C., Rodel, R., and Sindorf, N.:
1703 Global Reservoir and Dam Database, Version 1 (GRanDv1): Dams, Revision 01,
1704 <https://doi.org/10.7927/H4N877QK>, 2011a.
- 1705 Lehner, B., Liermann, C. R., Revenga, C., Vörösmarty, C., Fekete, B., Crouzet, P., Döll, P., Endejan,
1706 M., Frenken, K., Magome, J., Nilsson, C., Robertson, J. C., Rödel, R., Sindorf, N., and Wisser, D.:
1707 High-resolution mapping of the world's reservoirs and dams for sustainable river-flow management,
1708 *Front. Ecol. Environ.*, 9, 494–502, 2011b.
- 1709 Lejeune, Q., Maskell, G., Menke, I., and Pleeck, S.: Stakeholder Survey Report,
1710 https://www.isimip.org/documents/376/ISllopedia_survey_result_report_w47NU6L.pdf, 2018.
- 1711 Liu, X., Stock, C. A., Dunne, J. P., Lee, M., Shevliakova, E., Malyshev, S., and Milly, P. C. D.:
1712 Simulated global coastal ecosystem responses to a half-century increase in river nitrogen loads,
1713 *Geophys. Res. Lett.*, 48, <https://doi.org/10.1029/2021gl094367>, 2021.
- 1714 Loisel, J., Gallego-Sala, A. V., Amesbury, M. J., Magnan, G., Anshari, G., Beilman, D. W., Benavides,
1715 J. C., Blewett, J., Camill, P., Charman, D. J., Chawchai, S., Hedgpeth, A., Kleinen, T., Korhola, A.,
1716 Large, D., Mansilla, C. A., Müller, J., van Bellen, S., West, J. B., Yu, Z., Bubier, J. L., Garneau, M.,
1717 Moore, T., Sannel, A. B. K., Page, S., Väiliranta, M., Bechtold, M., Brovkin, V., Cole, L. E. S., Chanton,
1718 J. P., Christensen, T. R., Davies, M. A., De Vleeschouwer, F., Finkelstein, S. A., Frolking, S., Gałka,
1719 M., Gandois, L., Girkin, N., Harris, L. I., Heinemeyer, A., Hoyt, A. M., Jones, M. C., Joos, F., Juutinen,
1720 S., Kaiser, K., Lacourse, T., Lamentowicz, M., Larmola, T., Leifeld, J., Lohila, A., Milner, A. M.,
1721 Minkinen, K., Moss, P., Naafs, B. D. A., Nichols, J., O'Donnell, J., Payne, R., Philben, M., Piilo, S.,
1722 Quillet, A., Ratnayake, A. S., Roland, T. P., Sjögersten, S., Sonnentag, O., Swindles, G. T., Swinnen,
1723 W., Talbot, J., Treat, C., Valach, A. C., and Wu, J.: Expert assessment of future vulnerability of the
1724 global peatland carbon sink, *Nat. Clim. Chang.*, 11, 70–77, 2020.
- 1725 Lu, P., Lin, N., Emanuel, K., Chavas, D., and Smith, J.: Assessing Hurricane Rainfall Mechanisms
1726 Using a Physics-Based Model: Hurricanes Isabel (2003) and Irene (2011), *J. Atmos. Sci.*, 75,
1727 2337–2358, 2018.
- 1728 Marsooli, R., Lin, N., Emanuel, K., and Feng, K.: Climate change exacerbates hurricane flood hazards
1729 along US Atlantic and Gulf Coasts in spatially varying patterns, *Nat. Commun.*, 10, 3785, 2019.
- 1730 Matthews, J. B. R., Möller, V., van Diemen, R., Fuglestvedt, J. S., Masson-Delmotte, V., Méndez, C.,
1731 Semenov, S., and Reisinger, A.: Annex VII: Glossary, in: *Climate Change 2021: The Physical Science
1732 Basis. Contribution of Working Group I to the Sixth Assessment Report of the Intergovernmental
1733 Panel on Climate Change*, edited by: Masson-Delmotte, V., Zhai, P., Pirani, A., Connors, S. L., Péan,
1734 C., Berger, S., Caud, N., Chen, Y., Goldfarb, L., Gomis, M. I., Huang, M., Leitzell, K., Lonnoy, E.,
1735 Matthews, J. B. R., Maycock, T. K., Waterfield, T., Yelekçi, O., Yu, R., and Zhou, B., Cambridge,
1736 United Kingdom and New York, NY, USA, 2215–2256, 2021.
- 1737 Mechler, R., Bouwer, L. M., Schinko, T., Surminski, S., and Linnerooth-Bayer, J.: Loss and damage
1738 from climate change: Concepts, methods and policy options, 1st ed., edited by: Mechler, R., Bouwer,
1739 L. M., Schinko, T., Surminski, S., and Linnerooth-Bayer, J., Springer International Publishing, Cham,
1740 Switzerland, 557 pp., 2018.
- 1741 Meinshausen, M., Smith, S. J., Calvin, K., Daniel, J. S., Kainuma, M. L. T., Lamarque, J.-F.,
1742 Matsumoto, K., Montzka, S. A., Raper, S. C. B., Riahi, K., Thomson, A., Velders, G. J. M., and van
1743 Vuuren, D. P. P.: The RCP greenhouse gas concentrations and their extensions from 1765 to 2300,
1744 *Clim. Change*, 109, 213, 2011.
- 1745 Meinshausen, M., Vogel, E., Nauels, A., Lorbacher, K., Meinshausen, N., Etheridge, D. M., Fraser, P.
1746 J., Montzka, S. A., Rayner, P. J., Trudinger, C. M., Krummel, P. B., Beyerle, U., Canadell, J. G.,
1747 Daniel, J. S., Enting, I. G., Law, R. M., Lunder, C. R., O'Doherty, S., Prinn, R. G., Reimann, S.,
1748 Rubino, M., Velders, G. J. M., Vollmer, M. K., Wang, R. H. J., and Weiss, R.: Historical greenhouse
1749 gas concentrations for climate modelling (CMIP6), *Geoscientific Model Development*, 10, 2057–2116,

- 1750 2017.
- 1751 Mengel, M., Treu, S., Lange, S., and Frieler, K.: ATTRICI v1.1 – counterfactual climate for impact
1752 attribution, *Geosci. Model Dev.*, 14, 5269–5284, 2021.
- 1753 Messenger, M. L., Lehner, B., Grill, G., Nedeva, I., and Schmitt, O.: Estimating the volume and age of
1754 water stored in global lakes using a geo-statistical approach, *Nat. Commun.*, 7, 13603, 2016.
- 1755 Monfreda, C., Ramankutty, N., and Foley, J. A.: Farming the planet: 2. Geographic distribution of crop
1756 areas, yields, physiological types, and net primary production in the year 2000, *Global Biogeochem.*
1757 *Cycles*, 22, <https://doi.org/10.1029/2007gb002947>, 2008.
- 1758 Cyclone Database Manager:
1759 [https://citeseerx.ist.psu.edu/document?repid=rep1&type=pdf&doi=b80049f3add16c6c4b8937c8f6b80](https://citeseerx.ist.psu.edu/document?repid=rep1&type=pdf&doi=b80049f3add16c6c4b8937c8f6b804071dd110b3)
1760 [4071dd110b3](https://citeseerx.ist.psu.edu/document?repid=rep1&type=pdf&doi=b80049f3add16c6c4b8937c8f6b804071dd110b3), last access: 18 October 2023.
- 1761 Muis, S., Apecechea, M. I., Dullaart, J., de Lima Rego, J., Madsen, K. S., Su, J., Yan, K., and Verlaan,
1762 M.: A high-resolution global dataset of extreme sea levels, tides, and storm surges, including future
1763 projections, *Front. Mar. Sci.*, 7, <https://doi.org/10.3389/fmars.2020.00263>, 2020.
- 1764 Müller Schmied, H.: DDM30 river routing network for ISIMIP3,
1765 <https://doi.org/10.48364/ISIMIP.865475>, 2022.
- 1766 Earth observation group - defense meteorological satellite program, boulder:
1767 <https://www.ngdc.noaa.gov/eog/dmsp/downloadV4composites.html>.
- 1768 van Oldenborgh, G. J., van der Wiel, K., Sebastian, A., Singh, R., Arrighi, J., Otto, F., Haustein, K., Li,
1769 S., Vecchi, G., and Cullen, H.: Attribution of extreme rainfall from Hurricane Harvey, August 2017,
1770 *Environ. Res. Lett.*, 12, 124009, 2017.
- 1771 O'Neill, B., van Aalst, M., Z., Z. I., Berrang Ford, L., Bhadwal, S., Buhaug, H., Diaz, D., Frieler, K.,
1772 Garschagen, M., Magnan, A., Midgley, G., Mirzabaev, A., Thomas, A., and Warren, R.: Climate
1773 Change 2022: Impacts, Adaptation and Vulnerability. Key Risks Across Sectors and Regions, in:
1774 Contribution of Working Group II to the Sixth Assessment Report of the Intergovernmental Panel on
1775 Climate Change, edited by: Pörtner, H.-O., Roberts, D. C., Tignor, M., Poloczanska, E. S.,
1776 Mintenbeck, K., Alegría, A., Craig, M., Langsdorf, S., Löschke, S., Möller, V., Okem, A., and Rama,
1777 B., Cambridge University Press, Cambridge, UK and New York, NY, USA, 2411–2538, 2022.
- 1778 Patricola, C. M. and Wehner, M. F.: Anthropogenic influences on major tropical cyclone events,
1779 *Nature*, 563, 339–346, 2018.
- 1780 Peduzzi, P., Chatenoux, B., Dao, H., De Bono, A., Herold, C., Kossin, J., Mouton, F., and Nordbeck,
1781 O.: Global trends in tropical cyclone risk, *Nat. Clim. Chang.*, 2, 289–294, 2012.
- 1782 Portmann, F. T., Siebert, S., and Döll, P.: MIRCA2000-Global monthly irrigated and rainfed crop areas
1783 around the year 2000: A new high-resolution data set for agricultural and hydrological modeling,
1784 *Global Biogeochem. Cycles*, 24, <https://doi.org/10.1029/2008gb003435>, 2010.
- 1785 Reyer, C., Silveyra Gonzalez, R., Dolos, K., Hartig, F., Hauf, Y., Noack, M., Lasch-Born, P., Rötzer,
1786 T., Pretzsch, H., Meesenburg, H., Fleck, S., Wagner, M., Bolte, A., Sanders, T., Kolari, P., Mäkelä, A.,
1787 Vesala, T., Mammarella, I., Pumpanen, J., Matteucci, G., Collalti, A., D'Andrea, E., Foltýnová, L.,
1788 Krejza, J., Ibrom, A., Pilegaard, K., Loustau, D., Bonnefond, J.-M., Berbigier, P., Picart, D., Lafont, S.,
1789 Dietze, M., Cameron, D., Vieno, M., Tian, H., Palacios-Orueta, A., Cicuendez, V., Recuero, L., Wiese,
1790 K., Büchner, M., Lange, S., Volkholz, J., Kim, H., Weedon, G., Sheffield, J., Vega del Valle, I.,
1791 Suckow, F., Horemans, J., Martel, S., Bohn, F., Steinkamp, J., Chikalanov, A., Mahnken, M., Gutsch,
1792 M., Trotta, C., Babst, F., and Frieler, K.: The PROFOUND database for evaluating vegetation models
1793 and simulating climate impacts on European forests. V. 0.3. GFZ Data Services,
1794 <https://doi.org/10.5880/PIK.2020.006>, 2020a.
- 1795 Reyer, C. P. O., Silveyra Gonzalez, R., Dolos, K., Hartig, F., Hauf, Y., Noack, M., Lasch-Born, P.,
1796 Rötzer, T., Pretzsch, H., Meesenburg, H., Fleck, S., Wagner, M., Bolte, A., Sanders, T. G. M., Kolari,
1797 P., Mäkelä, A., Vesala, T., Mammarella, I., Pumpanen, J., Collalti, A., Trotta, C., Matteucci, G.,

- 1798 D'Andrea, E., Foltýnová, L., Krejza, J., Ibrom, A., Pilegaard, K., Loustau, D., Bonnefond, J.-M.,
1799 Berbigier, P., Picart, D., Lafont, S., Dietze, M., Cameron, D., Vieno, M., Tian, H., Palacios-Orueta, A.,
1800 Cicuendez, V., Recuero, L., Wiese, K., Büchner, M., Lange, S., Volkholz, J., Kim, H., Horemans, J. A.,
1801 Bohn, F., Steinkamp, J., Chikalanov, A., Weedon, G. P., Sheffield, J., Babst, F., Vega del Valle, I.,
1802 Suckow, F., Martel, S., Mahnken, M., Gutsch, M., and Frieler, K.: The PROFOUND Database for
1803 evaluating vegetation models and simulating climate impacts on European forests, *Earth Syst. Sci.*
1804 *Data*, 12, 1295–1320, 2020b.
- 1805 Reyer, C. P. O., Schelhaas, M.-J., Mäkelä, A., Peltoniemi, M., Gutsch, M., Mahnken, M., Loustau, D.,
1806 Martel, S., Merganič, J., Merganičová, K., Meesenburg, H., Rötzer, T., Heym, M., Collalti, A.,
1807 D'Andrea, E., Matteucci, G., Ibrom, A., and Kvist Johannsen, V.: Current Site-specific management
1808 guidelines and schedules for the 9 PROFOUND forest sites of the regional forest sector in ISIMIP,
1809 <https://doi.org/10.5281/zenodo.7622027>, 2023.
- 1810 Risser, M. D. and Wehner, M. F.: Attributable human-induced changes in the likelihood and
1811 magnitude of the observed extreme precipitation during hurricane Harvey, *Geophys. Res. Lett.*, 44,
1812 12,457–12,464, 2017.
- 1813 Rousseau, Y., Blanchard, J., Novaglio, C., Pinnell, K., Tittensor, D., Watson, R., and Ye, Y.: A data
1814 base of mapped global fishing activity, 1950-2017, *Scientific Data*, submitted 2023.
- 1815 Rousseau, Y., Blanchard, J., Novaglio, C., Kirsty, P., Tittensor, D., Watson, R., and Ye, Y.: Global
1816 Fishing Effort, <https://doi.org/10.25959/MNGY-0Q43>, 2022.
- 1817 Rust, H. W., Kruschke, T., Dobler, A., Fischer, M., and Ulbrich, U.: Discontinuous Daily Temperatures
1818 in the WATCH Forcing Datasets, *J. Hydrometeorol.*, 16, 465–472, 2015.
- 1819 Sarmiento, J. L. and Gruber, N.: Ocean Biogeochemical Dynamics, *Geol. Mag.*, 144, 1034–1034,
1820 2006.
- 1821 Seitzinger, S., Harrison, J. A., Böhlke, J. K., Bouwman, A. F., Lowrance, R., Peterson, B., Tobias, C.,
1822 and Van Dreht, G.: Denitrification across landscapes and waterscapes: a synthesis, *Ecol. Appl.*, 16,
1823 2064–2090, 2006.
- 1824 Sherman, K.: Large Marine Ecosystems, in: *Encyclopedia of Ocean Sciences*, Elsevier, 709–723,
1825 2017.
- 1826 Sitch, S., Friedlingstein, P., Gruber, N., Jones, S. D., Murray-Tortarolo, G., Ahlström, A., Doney, S. C.,
1827 Graven, H., Heinze, C., Huntingford, C., Levis, S., Levy, P. E., Lomas, M., Poulter, B., Viovy, N.,
1828 Zaehle, S., Zeng, N., Arneeth, A., Bonan, G., Bopp, L., Canadell, J. G., Chevallier, F., Ciais, P., Ellis,
1829 R., Gloor, M., Peylin, P., Piao, S. L., Le Quéré, C., Smith, B., Zhu, Z., and Myneni, R.: Recent trends
1830 and drivers of regional sources and sinks of carbon dioxide, *Biogeosciences*, 12, 653–679, 2015.
- 1831 Slivinski, L. C., Compo, G. P., Whitaker, J. S., Sardeshmukh, P. D., Giese, B. S., McColl, C., Allan, R.,
1832 Yin, X., Vose, R., Titchner, H., Kennedy, J., Spencer, L. J., Ashcroft, L., Brönnimann, S., Brunet, M.,
1833 Camuffo, D., Cornes, R., Cram, T. A., Crouthamel, R., Domínguez-Castro, F., Freeman, J. E., Gergis,
1834 J., Hawkins, E., Jones, P. D., Jourdain, S., Kaplan, A., Kubota, H., Blancq, F. L., Lee, T.-C., Lorrey,
1835 A., Luterbacher, J., Maugeri, M., Mock, C. J., Moore, G. W. K., Przybylak, R., Pudmenzky, C.,
1836 Reason, C., Slonosky, V. C., Smith, C. A., Tinz, B., Trewin, B., Valente, M. A., Wang, X. L., Wilkinson,
1837 C., Wood, K., and Wyszyński, P.: Towards a more reliable historical reanalysis: Improvements for
1838 version 3 of the Twentieth Century Reanalysis system, *Quart. J. Roy. Meteor. Soc.*, 145, 2876–2908,
1839 2019.
- 1840 Slivinski, L. C., Compo, G. P., Sardeshmukh, P. D., Whitaker, J. S., McColl, C., Allan, R. J., Brohan,
1841 P., Yin, X., Smith, C. A., Spencer, L. J., Vose, R. S., Rohrer, M., Conroy, R. P., Schuster, D. C.,
1842 Kennedy, J. J., Ashcroft, L., Brönnimann, S., Brunet, M., Camuffo, D., Cornes, R., Cram, T. A.,
1843 Domínguez-Castro, F., Freeman, J. E., Gergis, J., Hawkins, E., Jones, P. D., Kubota, H., Lee, T. C.,
1844 Lorrey, A. M., Luterbacher, J., Mock, C. J., Przybylak, R. K., Pudmenzky, C., Slonosky, V. C., Tinz, B.,
1845 Trewin, B., Wang, X. L., Wilkinson, C., Wood, K., and Wyszyński, P.: An Evaluation of the
1846 Performance of the Twentieth Century Reanalysis Version 3, *J. Clim.*, 34, 1417–1438, 2021.
- 1847 Smil, V.: *Enriching the Earth: Fritz Haber, Carl Bosch and the Transformation of World Food*

- 1848 Production, MIT Press, 2001.
- 1849 Stock, C. A., Dunne, J. P., and John, J. G.: Global-scale carbon and energy flows through the marine
1850 planktonic food web: An analysis with a coupled physical–biological model, *Prog. Oceanogr.*, 120,
1851 1–28, 2014.
- 1852 Tian, H., Yang, J., Lu, C., Xu, R., Canadell, J. G., Jackson, R. B., Arneeth, A., Chang, J., Chen, G.,
1853 Ciais, P., Gerber, S., Ito, A., Huang, Y., Joos, F., Lienert, S., Messina, P., Olin, S., Pan, S., Peng, C.,
1854 Saikawa, E., Thompson, R. L., Vuichard, N., Winiwarter, W., Zaehle, S., Zhang, B., Zhang, K., and
1855 Zhu, Q.: The Global N₂O Model Intercomparison Project, *Bull. Am. Meteorol. Soc.*, 99, 1231–1251,
1856 2018.
- 1857 Tittensor, D. P., Eddy, T. D., Lotze, H. K., Galbraith, E. D., Cheung, W., Barange, M., Blanchard, J. L.,
1858 Bopp, L., Bryndum-Buchholz, A., Büchner, M., Bulman, C., Carozza, D. A., Christensen, V., Coll, M.,
1859 Dunne, J. P., Fernandes, J. A., Fulton, E. A., Hobday, A. J., Huber, V., Jennings, S., Jones, M.,
1860 Lehodey, P., Link, J. S., Mackinson, S., Maury, O., Niiranen, S., Oliveros-Ramos, R., Roy, T.,
1861 Schewe, J., Shin, Y.-J., Silva, T., Stock, C. A., Steenbeek, J., Underwood, P. J., Volkholz, J., Watson,
1862 J. R., and Walker, N. D.: A protocol for the intercomparison of marine fishery and ecosystem models:
1863 Fish-MIP v1.0, *Geoscientific Model Development*, 11, 1421–1442, 2018.
- 1864 Treu, S., Muis, S., Dangendorf, S., Wahl, S., Heinicke, S., Frieler, K., and M., M.: [Reconstruction of](https://doi.org/10.5194/essd-2023-112)
1865 [hourly coastal water levels and counterfactuals without sea level rise for impact attribution](https://doi.org/10.5194/essd-2023-112), *Earth*
1866 *System Science Data Discussions*, 1-23, <https://doi.org/10.5194/essd-2023-112>, 2023. ~~Hourly coastal~~
1867 ~~water levels with long term trends for impact attribution: the HLT Dataset~~, *Earth System Science Data*,
1868 ~~submitted 2023~~.
- 1869 Tsujino, H., Urakawa, S., Nakano, H., Small, R. J., Kim, W. M., Yeager, S. G., Danabasoglu, G.,
1870 Suzuki, T., Bamber, J. L., Bentsen, M., Böning, C. W., Bozec, A., Chassignet, E. P., Curchitser, E.,
1871 Boeira Dias, F., Durack, P. J., Griffies, S. M., Harada, Y., Ilıcak, M., Josey, S. A., Kobayashi, C.,
1872 Kobayashi, S., Komuro, Y., Large, W. G., Le Sommer, J., Marsland, S. J., Masina, S., Scheinert, M.,
1873 Tomita, H., Valdivieso, M., and Yamazaki, D.: JRA-55 based surface dataset for driving ocean–sea-
1874 ice models (JRA55-do), *Ocean Model.*, 130, 79–139, 2018.
- 1875 del Valle, I. V., Reyer, C., and Perrette, M.: ISIMIP3a wood harvesting input data,
1876 <https://doi.org/10.48364/ISIMIP.482888.1>, 2022.
- 1877 Wada, Y., Lo, M.-H., Yeh, P. J.-F., Reager, J. T., Famiglietti, J. S., Wu, R.-J., and Tseng, Y.-H.: Fate
1878 of water pumped from underground and contributions to sea-level rise, *Nat. Clim. Chang.*, 6, 777–780,
1879 2016a.
- 1880 Wada, Y., Flörke, M., Hanasaki, N., Eisner, S., Fischer, G., Tramberend, S., Satoh, Y., van Vliet, M. T.
1881 H., Yillia, P., Ringler, C., Burek, P., and Wiberg, D.: Modeling global water use for the 21st century:
1882 the Water Futures and Solutions (WFaS) initiative and its approaches, *Geoscientific Model*
1883 *Development*, 9, 175–222, 2016b.
- 1884 Wang, J., Walter, B. A., Yao, F., Song, C., Ding, M., Maroof, A. S., Zhu, J., Fan, C., McAlister, J. M.,
1885 Sikder, S., Sheng, Y., Allen, G. H., Crétaux, J.-F., and Wada, Y.: GeoDAR: georeferenced global
1886 dams and reservoirs dataset for bridging attributes and geolocations, *Earth Syst. Sci. Data*, 14,
1887 1869–1899, 2022.
- 1888 Wang, S.-Y. S., Zhao, L., Yoon, J.-H., Klotzbach, P., and Gillies, R. R.: Quantitative attribution of
1889 climate effects on Hurricane Harvey’s extreme rainfall in Texas, *Environ. Res. Lett.*, 13, 054014, 2018.
- 1890 Wang, T. and Sun, F.: Global gridded GDP data set consistent with the shared socioeconomic
1891 pathways, *Sci Data*, 9, 221, 2022.
- 1892 Watson, R.: Global Fisheries Landings V4.0, <https://doi.org/10.25959/5C522CADBEA37>, 2019.
- 1893 Watson, R. A. and Tidd, A.: Mapping nearly a century and a half of global marine fishing: 1869–2015,
1894 *Mar. Policy*, 93, 171–177, 2018.
- 1895 Whitehouse, P. L.: Glacial isostatic adjustment modelling: historical perspectives, recent advances,

- 1896 and future directions, *Earth Surf. Dyn.*, 6, 401–429, 2018.
- 1897 Wöppelmann, G. and Marcos, M.: Vertical land motion as a key to understanding sea level change
1898 and variability, *Rev. Geophys.*, 54, 64–92, 2016.
- 1899 Wyns, A.: COP27 establishes loss and damage fund to respond to human cost of climate change,
1900 *Lancet Planet Health*, 7, e21–e22, 2023.
- 1901 Xi, D., Lin, N., and Smith, J.: Evaluation of a Physics-Based Tropical Cyclone Rainfall Model for Risk
1902 Assessment, *J. Hydrometeorol.*, 21, 2197–2218, 2020.
- 1903 Yang, J. and Tian, H.: ISIMIP3a N-deposition input data, <https://doi.org/10.48364/ISIMIP.759077.1>,
1904 2020.
- 1905 Yang, J., Yan, F., and Chen, M.: Effects of sea level rise on storm surges in the south Yellow Sea: A
1906 case study of Typhoon Muifa (2011), *Cont. Shelf Res.*, 215, 104346, 2021.
- 1907 Sea Around Us Area Parameters and Definitions: <https://www.seaaroundus.org/sea-around-us-area-parameters-and-definitions/>.
1908
- 1909 Zhang, X., Davidson, E. A., Mauzerall, D. L., Searchinger, T. D., Dumas, P., and Shen, Y.: Managing
1910 nitrogen for sustainable development, *Nature*, 528, 51–59, 2015.
- 1911 Zhao, N., Liu, Y., Cao, G., Samson, E. L., and Zhang, J.: Forecasting China’s GDP at the pixel level
1912 using nighttime lights time series and population images, *GISci. Remote Sens.*, 54, 407–425, 2017.
- 1913 Zhu, L., Quiring, S. M., and Emanuel, K. A.: Estimating tropical cyclone precipitation risk in Texas,
1914 *Geophys. Res. Lett.*, 40, 6225–6230, 2013.
- 1915
- 1916 GSWP3 soil texture map: <http://hydro.iis.u-tokyo.ac.jp/~sujan/research/gswp3/soil-texture-map.html>,
1917 upscaling method A., last access 28 April 2022
- 1918
- 1919 GGCM-HWSD: https://github.com/AgMIP-GGCM/processing_hwsd_for_GGCM, last access: 9
1920 February 2023
- 1921
- 1922 Tractebel: Filling of the reservoir of the Grand Renaissance Dam: [https://tractebel-
1923 engie.com/en/news/2020/ethiopia-first-stage-of-the-filling-of-the-reservoir-of-the-grand-renaissance-
1924 dam](https://tractebel-engie.com/en/news/2020/ethiopia-first-stage-of-the-filling-of-the-reservoir-of-the-grand-renaissance-dam), September 2020, last access: 10 February 2023.
- 1925
- 1926 UN 2019 World Population Prospects (WPP) Database 2019: <https://population.un.org/wpp/>, last
1927 access: 15 February 2023
- 1928 Malle, Johanna. 2023. w5e5_downscale. Github. https://github.com/johanna-malle/w5e5_downscale.
- 1929 IFASTAT: Statistics, International Fertilizer Association, IFASTAT Database [data set], available at:
1930 <https://www.ifastat.org>, last access: 21 January 2015.
- 1931
- 1932 ISIMIP organigram: <https://www.isimip.org/about/#organisational-structure>, last access: 7 March, 2023
- 1933 Technical University of Denmark (DTU): Global Wind Atlas 3.0, released in partnership with World
1934 Bank Group, utilising data provided by Vortex, using funding provided by Energy Sector Management
1935 Assistance Program (ESMAP) [data set], available at: <https://globalwindatlas.info>, 2023.
- 1936 United Nations, Department of Economic and Social Affairs: Population Division (2019), World
1937 Population Prospects 2019, archive [data set],
1938 <https://population.un.org/wpp/Download/Archive/Standard/>, 2019.
- 1939